VOLTAGE CONTROL AND OPTIMIZATION OF ENERGY CONSUMPTION IN A MICROGRID

Teză destinată obţinerii
titlului ştiinţific de doctor inginer
la
Universitatea "Politehnica" din Timişoara
în domeniul INGINERIA SISTEMELOR
de către

Ing. Cosmin Koch-Ciobotaru

Conducător ştiinţific:	prof.univ.dr.ing. Octavian Proştean
Referenţi ştiinţifici:	prof.univ.dr.ing. Mihail Abrudean
	prof.univ.dr.ing. Dumitru Popescu
	prof.univ.dr.ing. Ioan Filip

Ziua susţinerii tezei: 16.11.2012

Seriile Teze de doctorat ale UPT sunt:

1. Automatică
2. Chimie
3. Energetică
4. Ingineria Chimică
5. Inginerie Civilă
6. Inginerie Electrică
7. Inginerie Electronică şi Telecomunicaţii
8. Inginerie Industrială
9. Inginerie Mecanică
10. Ştiinţa Calculatoarelor
11. Ştiinţa şi Ingineria Materialelor

Universitatea „Politehnica” din Timişoara a iniţiat seriile de mai sus în scopul diseminării expertizei, cunoştinţelor şi rezultatelor cercetărilor întreprinse în cadrul şcolii doctorale a universităţii. Seriile conţin, potrivit H.B.Ex.S Nr. 14 / 14.07.2006, tezele de doctorat susţinute în universitate începând cu 1 octombrie 2006.

România, 300159 Timişoara, Bd. Republicii 9,
tel. 0256 403823, fax. 0256 403221
e-mail: editura@edipol.upt.ro

Acknowledgement

I wish to thank my supervisor, prof. Octavian Proştean, for providing academic guidance and support during the project. Many thanks to prof. Ioan Filip for his availability and help in various stages of my PhD. Things learned in this group will be a consistent help for me in the future.

I wish to thank prof. Nicolae Muntean and his research group from the Faculty of Electrical Engineering at "Politehnica" University from Timişoara for contributing to my engineering education. I will remember and cherish the dynamic and fruitful working environment that I found there as an aspiration for the future.

Also I wish to thank assoc. prof. Lucian Mihet-Popa for his help in choosing my internship at RISØ DTU.

I would like to express my deep gratitude to senior scientist Henrik Bindner and the group at RISØ research laboratory from Denmark Technical University for providing the opportunity to perform, at their facility, most part of my PhD research. For all their warm welcome and lovely working environment, I am grateful. I would especially like to thank Fridrik Isleifsson and Oliver Gehrke for their helpful insight on power systems and Jacopo Parvizi for the ideas born from our discussions on model predictive control.

During my PhD I had enjoyed the constant support from very good friends, both on a technical and on a personal level; they each had their important part for me. I wish to express my special gratitude to Raluca Rotar, Alexandru Codrean, Gelu Frese, Adi Lifa, Bogdan Rădac and, certainly not least, to Sergiu Spătaru.

And firstly, I may say, my deepest and warmest gratitude to my mother, for her unconditioned and endless support, for her influence and for providing me an example of a beautiful personality. I owe much of my technical interest and professional development to my uncle, Alexandru Herbei, who was a true professional and a mentor. I hope that I inherited a fraction of their dedication and tenacity. This thesis is dedicated to them.

The PhD thesis was partially supported by the strategic grant POSDRU/88/1.5/S/50783, Project ID50783 (2009), co-financed by European Social Fund "Invest in people" within the Sectoral Operational Programme Human Resources Development 2007-2013.

Timişoara, November 2012 Cosmin Koch-Ciobotaru

Koch-Ciobotaru, Cosmin

VOLTAGE CONTROL AND OPTIMIZATION OF ENERGY CONSUMPTION IN A MICROGRID

Teze de doctorat ale UPT, Seria 12, Nr. 6, Editura Politehnica, 2012, 174 pagini, 98 figuri, 12 tabele.

ISSN: 2068-7990

ISBN: 978-606-554-560-1

Cuvinte cheie:

Renewable energy, distributed energy resources integration, model predictive control, finite state machine, energy optimization

Rezumat,
The PhD thesis deals with two issues concerning the integration of renewable energy sources in a microgrid: the voltage control and the optimization of the energy consumption. It is presented the development of mathematical models for a photovoltaic system, a battery and a thermodynamic model of a building, which are validated based on experimental measurements on the actual microgrid components. The models' implementation is performed in specialized software like Matlab and PowerFactory. Algorithms for driving the heating system of the building and the battery in order avoid surges that occur due to the injection of power into the grid photovoltaic system, are being developed. Optimizing energy consumption is achieved by using model predictive control by defining two objectives: minimizing the cost of operating the building's heating system when using only energy from the grid and the second, maximizing the consumption of locally produced energy from the photovoltaic system. The developed algorithms are validated by experiments and simulations in many operating conditions that allow comparison of the results obtained with other methods of control, which highlight the opportunity of using the proposed algorithm.

Table of contents

Notations and Abbreviations

$\bar{\Phi}$	– Performance cost index
A	– Aria of the photovoltaic cells
A_w	– Windows area
C_G	– Cost of grid energy
C_{G2H}	– Cost of the grid energy consumed by the electrical heaters
$C_{G2HnoPV}$	– Cost of the grid energy consumed by the electrical heaters with no PV panel installation
C_i, C_m, C_h	– Heat capacity of the inside of the house, heat capacity of the interior walls, and the heat capacity of the heaters
C_{PV}	– Cost of produced PV energy
C_{PV2H}	– Cost of the PV energy consumed by the electrical heaters
DER	– Distributed energy resources
d_k	– Disturbance vector
E_{batt}	– The battery's capacity available during operation
E_{G2H}	– Amount of PV energy consumed by the electrical heaters
E_H	– Amount of energy consumed by the heaters
E_{input}	– Input energy
E_{output}	– Output energy
E_{PV2G}	– Amount of PV energy injected into the grid
EqofTime	– Equation of time
E_T	– Total capacity of the battery
FF	– Fill factor, defined as the ratio of the maximum power that can be delivered to the load and the product of Isc and Voc for a PV cell
FlexHouse	– Intelligent building with configurable loads from SYSLAB
G_a	– Solar irradiance incident on the PV cell
G_{aNOCT}	– Solar irradiance incident on the PV cell under NOCT conditions
G_{cell}	– Solar irradiance considering the tilt angle and the orientation of the PV panels
G_p	– Solar irradiance over the prediction horizon
G_{panel}	– Solar irradiance considering the tilt angle of the PV panels
I_0	– Dark saturation current of a photovoltaic cell
I_D	– Diode current of a photovoltaic cell model
I_{max}	– Electric current at the maximum output power point of a PV cell
I_{mpp}	– Nominal current of a PV cell
I_{ph}	– Photo-generated current of a photovoltaic cell
I_{sc}, V_{oc}	– Short circuit current and open circuit voltage of a photovoltaic cell
I_{sc25}	– Short circuit current under STC of a PV cell
K_B	– Boltzmann constant $1.3806503 \times 10^{-23}$ JK^{-1}
M_1, M_3	– One state space model and the three states space model
MPC	– Model predictive control
MPPT	– Maximum power point tracking
n	– Calendar day number of the current day
NOCT	– Normal operating cell temperature, under which the PV cell parameters are measured
n_{ps}	– Number of PV panels connected in series
n_s	– Number of PV cells connected in series on a PV panel
n_{sp}	– Number of PV panels connected in parallel
OF	– Optimization function
P_{ac}	– ac power

P_{dc}	– dc power
P_{EMF}	– Electromotive power changed at the cells stack terminal
P_{Grid}	– Amount of power consumed from the grid
PH	– The heaters' output power
P_h	– Electric heaters' output power
Pi	– Last iteration heaters' output power
P_{max}	– Maximum electric output power of a PV cell
P_{max25}	– Maximum electric output power of a PV cell under STC conditions
P_{mpp}	– Rated output power of a PV cell
P_{PV}	– Amount of power produced by the PV installation
PV	– Photovoltaic installation
q	– The charge of electron $1.602176565\times10^{-19}$ C
Q	– Weight factor for the reference error term of the OF
q	– elementary charge 1.602×10^{-19} Coulombs
Q_{cost}	– Weight factor for the grid energy price term of the optimization function
RES	– Renewable energy sources
R_i	– Internal resistance of a battery
R_{ia}, R_{im}, R_{ih}	– Thermal resistance of the inside of the building, the interior walls, and of the electric heaters
r_k	– The reference at step k
R_s	– Series resistance value of the PV cell mathematical model
R_{sh}	– Shunt resistance value of the PV cell mathematical model
S	– Weight factor for the command variation term of the OF
S_{horiz}	– Solar irradiance on a horizontal surface
SOC	– State of charge of a battery
S_{panel}	– Solar irradiance on the PV panel surface
STC	– Standard test condition, under which the PV cell parameters are measured
SYSLAB	– Test facility at Denmark Technical University, Elektro Department at RISØ campus, consisting of a low voltage configurable microgrid
Ta	– Ambient air temperature
T_{aNOCT}	– Ambient air temperature under NOCT conditions
T_{ap}	– Ambient air temperature over the prediction horizon
T_c	– Photovoltaic panel cell temperature
$T_{control}$	– Temperature control state of the finite state machine
T_i, T_m, T_h	– Temperatures of the inside of the house, interior walls, and of the heaters
T_{inside}	– Inside temperature of the house
T_{max}	– Maximum temperature of the thermal comfort interval in the house
T_{min}	– The minimum temperature of the thermal comfort interval in the house
Toe	– Tons of oil equivalent
T_s	– Simulation time of the finite state machine
U	– Amount of power consumed by the electric heaters
u_k	– Command vector
uk	– The value of the manipulated variable at step k
u_{max}	– Upper limit of the manipulated variable
u_{min}	– Lower limit of the manipulated variable
V_{bus}	– Bus voltage value
V_{EMF}	– Open circuit voltage under the effect of electromotive force of the

VRB's cell stack

V_{max} – Voltage at the maximum output power point of a PV cell
$V_{maxHigh}$ – Maximum voltage deadband upper value
V_{maxLow} – Maximum voltage deadband lower value
$V_{minHigh}$ – Minimum voltage deadband upper value
V_{minLow} – Minimum voltage deadband lower value
V_{mpp} – Nominal voltage of a PV cell
V_{oc25} – Open circuit voltage under STC conditions of a PV cell
$V_{Over\ control}$ – Over voltage control state of the finite state machine
VRB – Vanadium redox flow battery
V_T – Thermal voltage of a photovoltaic cell
$V_{under\ control}$ – Under voltage control state of the finite state machine
W_{sh} – Horizontal wind speed
x_0 – Initial state of the thermodynamic system
x_k – State variable vector
z – Predicted process output at step k, for the prediction horizon based on the current available data
z_k – The thermodynamic model output for step k
z_k – The value of the controlled variable at step k
z_{max} – Upper limit of the controlled variable
z_{min} – Lower limit of the controlled variable
α – Temperature coefficient for change in P_{mpp}
α – Weight factor for the virtual energy price
β – Temperature coefficient for change in I_{sc}
β – PV panels tilt angle
δ – Temperature coefficient for change in I_{mpp}
δ – Declination angle
Δu_k – Manipulated variable's variation at step k
$\Delta u_{k,max}$ – Maximum value of the manipulated variable's variance at step k
$\Delta u_{k,min}$ – Minimum value of the manipulated variable's variance at step k
ε – Temperature coefficient for change in U_{mpp}
η – Maximum efficiency of a photovoltaic cell defined as the ratio between the maximum power and the incident light power
η_{acdc} – The efficiency of the VRB's ac-dc converter
η_{batt} – The overall efficiency of the VRB over a full cycle
η_{conv} – The power convertor efficiency
φ – PV location latitude
Φ_{O0} – Performance cost index for MPC formulation without the observer
Φ_{O1} – Performance cost index for MPC formulation with state observer
χ – Temperature coefficient for change in U_{oc}
ω – Mounting coefficient

List of tables

List of figures

1. Introduction

1.1. Motivations and objectives of the thesis

It is expected that the renewable energy resources (RES) to increase their penetration into the low voltage distribution grid due to the economic advantages that they represent for the end consumer: accessible installation costs and the return of the investment in a few years. They also bring the energetic independence for the user whose electric bill will not depend on the national power grid prices.

So far, the consumers were stimulated to install such renewable energy sources, especially photovoltaic (PV), in the proximity of their houses by government subsidies.

Another factor of PV penetration is that in the past few years, it is the architecture and construction companies that are designing and constructing buildings with integrated PVs on their façade [Roberts2005].

As the number of installed RES increased, a problem aroused: the consumers were becoming energy producers and in the case of PVs, a large number of households were turning into energy producers at the same time, during sunny days. As the grid was designed to transport the energy from the power plants to the end consumer, having the voltage profile similar to an inclined slope, the renewable energy sources production is altering the voltage profile along the low voltage feeders by injecting power at the coupling points, making possible the appearance of over voltages.

As an effect of the over voltages at the coupling point between the household with the installed PVs on one side and the low voltage grid on the other side, the safety mechanisms are decoupling the PVs, as well as other appliances equipped with such safety measures, during high PV power production which is the most likely moment that these over voltages occur.

As a preliminary remark, it is important to mention that this work does not try to develop new components or algorithms for controlling the power electronics (converters) of individual microgrid components in order to track the maximum power point or to synchronize with the grid.

The present work is concerned on the integration of existing renewable energy resources components, developed by companies with many years of experience, into a microgrid, and the interaction between renewable energy sources, energy storage devices, and controllable loads from a power system perspective. To this purpose, the models are developed for running on time samples of one second and above, disregarding transient regimes, and the operation variables are average (RMS) values of power, current and voltage and not instantaneous values.

The first objective of the work is to develop simulation models of existing microgrid components validated by electric measurements taken from a test facility.

For this work, the algorithms were implemented for the case study of the SYSLAB microgrid, from Denmark Technical University (DTU), Elektro department at RISØ campus. The SYSLAB infrastructure is presented in Appendix A.

The second objective is to test different methods and algorithms for dealing with over voltage problems that may appear in the low voltage distribution grid when renewable energy resources are present: as RES inject power into the grid, the voltage profile along the feeder is influenced and this can translate to over voltages at some coupling points.

The third objective is to optimize the power consumption by minimizing the energy cost needed to run the heating system of a household.

The fourth objective is to develop an algorithm that maximizes the consumption of local RES produced power by shifting the loads to time intervals with high RES production.

1.2. Thesis organization

Chapter 2 presents the development stages of simulation models for specific distributed energy resources (DER) components. These models are validated through measurements on the real components at the test facility of DTU at RISØ campus.

Chapter 3 presents several case studies on voltage control for a considered microgrid configuration based on the SYSLAB setup. The subject of control is the voltage at the consumer's, or household, bus bar which during operation fluctuates due to PV power production. Several control techniques are developed and tested through simulations and experiment: load shifting by using a proposed thermostatic control with voltage regulation states, defined as a finite state space machine, control of storage device, the modelled vanadium redox battery (VRB) in overvoltage mode and schedule mode to store the excess produced power that may cause an overvoltage at the coupling point.

In **Chapter 4** is presented an advanced control algorithm for controlling the inside temperature in the house, based on the modelled building from SYSLAB. The control algorithm is a model predictive control (MPC) designed in order to achieve offset free operation in the presence of model errors, unknown disturbances, and white noise at the process level. The algorithm is tested through simulations and experiment; also comparative results of using different control algorithms in various operation scenarios are presented.

In **Chapter 5** an economic model predictive control algorithm is designed in order to optimize the operation cost of the heating system of the house by minimizing the cost of the consumed grid energy. In addition, a new virtual price is proposed and defined: it considers the grid energy price, the available power from the local PV installation and the current power needed by the heating system; this virtual price is further used to optimize the heating system operation to maximize the consumption of local produced PV power, which has implications on the voltage profile as discussed in chapter 4.

Chapter 6 presents the overall conclusions and discussions as well as future research directions.

Each chapter has an introductive section that presents the preliminary considerations regarding the approached subject

At the end of the thesis are added three appendixes:

- **Appendix 1** – describes the SYSLAB facility at Denmark Technical University at RISØ Campus, which consists the subject of modelling, simulations, and experiments developed during the work towards this thesis
- **Appendix 2** – presents the mathematical explanation of the Kalman filter
- **Appendix 3** – presents the Matlab functions used in chapter 4 and 5 for designing the MPC controller; this code was used both in simulations and experiments

2. Distributed Energy Resources Models

As stated in the introduction, the purpose of this work is the study of algorithms for the integration of renewable energy sources (RES) in the low voltage microgrid with minimal disturbances on the power system.

The mathematical models of different components are developed from this power system perspective and implemented in specialized software in order to be used in simulations and experiments. These algorithms are presented in future chapters and are concerning voltage control along the feeder (presented in chapter 3) and load management and optimizing the use of locally produced energy (the subject of chapter 4 and chapter 5).

This chapter presents the development, implementation, and validation through experiments of mathematical models for

- Photovoltaic plant,
- Vanadium redox battery, and
- Thermal model of a building.

The models are implemented first in Matlab [Magrab2010], a software which contains numerous specialized toolboxes used in this thesis: Simulink – used to develop line diagram models and simulations, graphical user interface designer toolbox – used to add interfaces to the models, an optimization toolbox – used in chapter 4 and 5 for model predictive control implementation, and the state flow toolbox – in which the finite state machine controlling the inside temperature from chapter 3 was implemented. Another important feature of Matlab and also a critical reason for using this software is its ability to use java written functions in order to implement real-time control, using the developed models and communicating with the real microgrid components.

The second software used for the model implementation is PowerFactory from DigSILENT [PowerFactory]. This software is specialized in power system simulations, power flow and voltage control being accurate simulated by very precise reproduction of the real power system configuration due to the numerous configuration parameters needed to run the simulation. However, the software does not have control oriented toolboxes and real-time simulation lacks the versatility of Matlab and was not used in running real-time experiments and simulations testing complex control algorithms. Simulations in PowerFactory were used to study the voltage profile along the feeder of a considered microgrid when using controllers described in chapter 3.

2.1. Photovoltaic model

2.1.1. Introduction

This subchapter presents the development and implementation, in dedicated software like Matlab and PowerFactory, of equivalent photovoltaic (PV) panel mathematical models, design to be used in power flow and voltage control simulations deferring an existing microgrid. The models have the solar irradiance and temperature on the PV panel surface as inputs and the power generated by the

PV as output and will be used in simulations that run on time samples of a few seconds.

The models were validated through experiments by comparison with the electrical measurements taken from the real PV installation seen in figure 2.1.

An ambient data correction module is proposed, developed and validated in order to estimate the solar irradiance and temperature on the PV surface given the measurements from the local weather station.

2.1.2. General overview

The design problem is to develop a mathematical model that calculates the electrical output power of a PV setup given two input values: the solar irradiance on the PV cell and the PV cell temperature. These developed PV models are used to study problems regarding low voltage distribution grids like power flow problems, predictions of PV availability, and the study and control of the voltage profile along the feeder in a microgrid with PV penetration.

The models disregard the transient regimes and consider the maximum power point tracking (MPPT) algorithm included in the model, in the sense that the model considers that this maximum is always, instantaneous, achieved and the PV always extracts the maximum amount of power from the available weather conditions. This assumption can be justified by the fact that in the case of a PV panel, the MPPT is very fast, the tracking algorithm having a strictly electrical character, with no inertial masses, unlike the MPPT used for wind turbine control, where large rotating masses are involved.

In the literature numerous mathematical models are presented that describe PV panels, by developing relation between the current, voltage and the photovoltaic cell's temperature and surface solar irradiance.

The first approach is the electrical circuit equivalent model, where the PV cell is modelled as an electrical circuit, the parameters of which are to be estimated. The simplest model is the one diode equivalent circuit, as presented in [Lopes2003] [Koch2012c] [Mihet2012a][Mihet2012b] represented by a current source and a diode. A more complex model is achieved by considering a series and a parallel resistance, as shown in [Park2004], [Campbell2007] and [Petreus2009].

For a more accurate model, the two diode equivalent circuit model was developed and studied [Chan1987][Jungsangsri2010]. This model is more accurate for low output power as explained in [Sera2009].

The second approach on modelling the PV panels was the development of empirical models, described in [Petcut2012] and [Petreus2009] and consists in experimental determination of parameters for estimating exponential and logarithmic mathematical relations for describing the current-voltage characteristic of the panels.

The third approach is represented by the interpolative models, consisting of empirical determination of a set of characteristics through measurement and experiments. The testing standard ASTM-E 1036-96 implies measuring 36 sets of current-voltage characteristics for 6 different cell temperature and solar irradiance values. Work has been made for developing methods of characterization of PV panels based on a reduced number of experimental current-voltage characteristics measurements. The work of [Marion2004] and [Tsuno2009] can be mentioned in this context.

2.1.3. Problem statement

The mathematical models developed in this chapter are useful in simulating different configurations of the distribution grid using many distributed energy resources (DER), loads and energy storage devices. Further on, the models are used in developing controllers for maintaining voltage quality on the low voltage distribution level due to the renewable energy sources (RES) penetration and for controlling the power flow in order to optimize energy consumption and cost.

In order to be used in such simulations, the models had to be developed in Matlab and PowerFactory. As stated in the first chapter, these software are specialized in controller development and in power system simulations and studies.

The developed models were tested on the SYSLAB infrastructure using the particularities of the site, nominal data from the PV panels, inclination angle of the panels, orientation, and ambient data measured from a local weather station. These ambient data consist of solar irradiance, ambient temperature and wind speed values that were fed into the model as inputs and the simulation results were compared to the electrical measurements taken from the PV inverter for validation.

The PV array setup from the SYSLAB facility which was used to validate the models consists of three solar panel strings: two strings of 18 Schuko 165-SP panels each (PV1 and PV2) and one string of 12 SOLEL SE100x panels (PV3) as seen in figure 2.1.

A Sunny Tripower 10000TL inverter from SMA Solar Technology is used to control the operation of PV panels; this inverter enables the connection of two different types of solar panels on each of its two inputs. Each input has its own maximum power point tracking (MPPT) algorithm. The inverter also presents a data logger for the electrical measurements that were later used for comparison.

For adapting the ambient data read from the weather station to the values on the PV panels, an additional module was developed that takes into account the declination angle and the orientation of the PV panels, as well as the cooling effect of the wind on the PV cells.

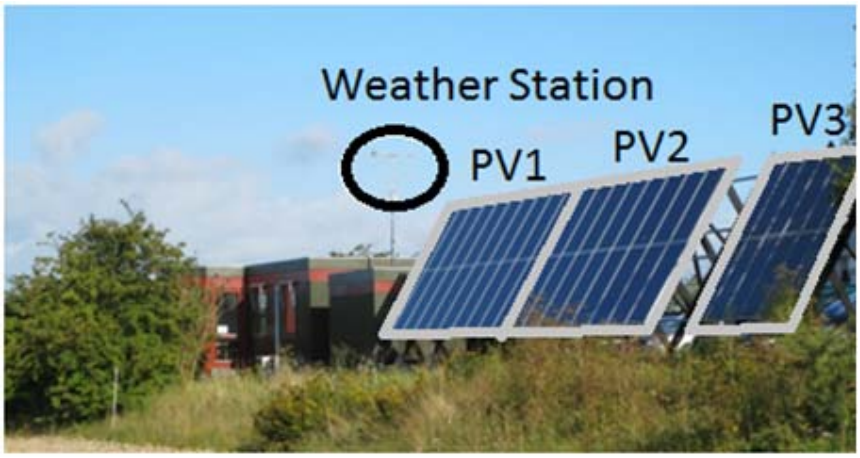

Fig. 2.1. PV panel configuration at SYSLAB.

The design problem and SYSLAB setup described above are presented in Fig. 2.2.

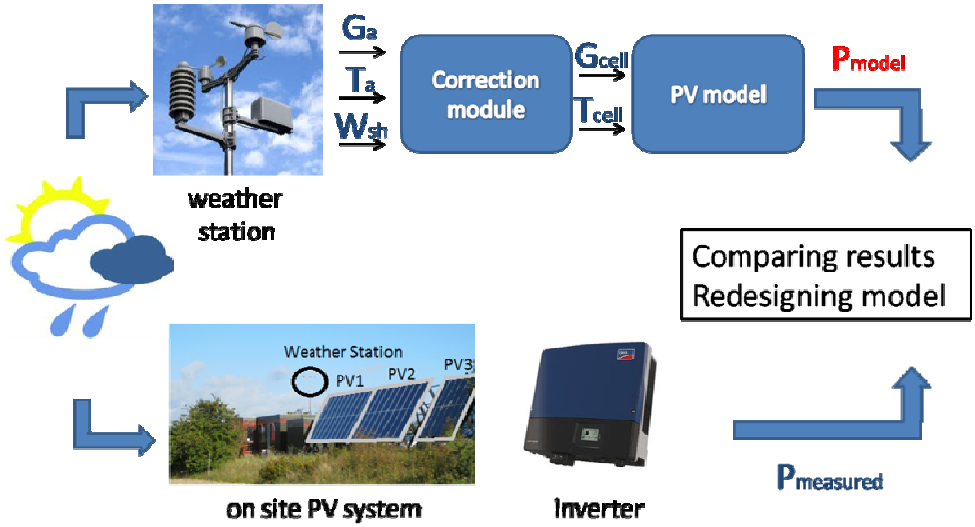

Fig. 2.2. PV panel modelling problem overview.

Two approaches were taken, and two types of models were developed:

- an equivalent circuit of the single diode model, which implies solving a transcendent equation
- a model based on the parameters provided by the manufacturer's technical datasheet, which uses basic arithmetic operations

2.1.4. General PV parameters and characteristics

The PV panels are obtained by connecting solar cells in series. Then the panels are connected in series and parallel to form strings that are connected to inverters that operate at a desired nominal voltage and between current limits.

The fundamental parameters used in defining the operation regime and characteristics of a PV cell are presented in Fig. 2.3 and discussed in the following [RISO2000]:

(a) Maximum power point is the operating point A(V_{max}, I_{max}) in Fig. 2.3, at which the power dissipated in the resistive load is maximum: $P_{max}=I_{max}U_{max}$

(b) Short circuit current: $I_{ph}=I_{sc}$. It is the greatest value of the current generated by a cell. It is produced under short circuit conditions: *V=0.*

(c) Open circuit voltage corresponds to the voltage drop across the diode (p-n junction), when it is traversed by the photocurrent I_{ph} ($I_D=I_{ph}$), namely when the generated current is I=0. It reflects the voltage of the cell in the night and it can be mathematically expressed as:

$$V_{oc} = \frac{K_B T_c A}{q} ln\left(\frac{I_{ph}}{I_0}\right) = V_T ln\left(\frac{I_{ph}}{I_0}\right) \quad (2.1)$$

where $V_T = \frac{K_B \cdot T_c \cdot A}{q}$ is known as thermal voltage and T_c is the absolute cell temperature.

(d) Maximum efficiency is the ratio between the maximum power and the incident light power:

$$\eta = \frac{P_{max}}{P_{in}} = \frac{I_{max} V_{max}}{A G_a} \quad (2.2)$$

(e) Fill factor is the ratio of the maximum power that can be delivered to the load and the product of I_{sc} and V_{oc}:

$$FF = \frac{P_{max}}{V_{oc} I_{sc}} = \frac{V_{max} I_{max}}{V_{oc} I_{sc}} \quad (2.3)$$

The fill factor is a measure of the real current-voltage characteristic. It is considered that for values higher than 0.7, the cell has a good quality. The increase in temperature of the PV cell has the effect of lowering the fill factor, and decreasing the energy conversion efficiency [Hansen2000].

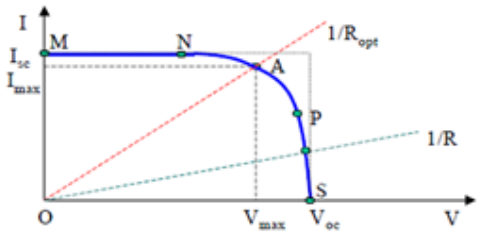

Fig. 2.3. Current-voltage characteristic of a solar cell.

Each PV manufacturing company is compelled to give a datasheet with measured values on Standard Test Conditions (STC) and Normal Operating Cell Temperature (NOCT):

STC is considered as having the following characteristics:

- solar irradiance (G_a) = 1000W/m^2,
- cell temperature(T_c) = 25°C, and
- wind speed = 1m/s

NOCT is defined by the following values:

- solar irradiance(G_{aNOCT}) = 800W/m^2,
- ambient air temperature(T_{aNOCT}) = 20°C, and
- wind speed = 1m/s

The list of available parameters provided by the manufacturer is presented in Table 2.1:

Table 2.1. PV Parameters provided by the manufacturer.

Parameter name	Measurement unit	Description
for STC		
P_{mpp}	W	Rated output power
V_{mpp}	V	Nominal voltage
I_{mpp}	A	Nominal current
V_{oc25}	V	Open circuit voltage
I_{sc25}	A	Short circuit current
α (P_{mpp})	%/°C	Temperature coefficient for change of P_{mpp}
β (I_{sc})	%/°C	Temperature coefficient for change of I_{sc}
χ (V_{oc})	%/°C	Temperature coefficient for change of U_{oc}
δ (I_{mpp})	%/°C	Temperature coefficient for change of I_{mpp}
ε (V_{mpp})	%/°C	Temperature coefficient for change of U_{mpp}
for NOCT		
NOCT	°C	Cell temperature on the above mentioned conditions

The influence of solar irradiance at the PV panel level and cell temperature on the I-V characteristic of the PV panel is presented in Fig. 2.4:

The irradiance dependence is affecting only the short-circuit current of the PV:

$$I_{SC} = I_{SC25}\frac{G_a}{1000} \tag{2.4}$$

The temperature dependence of I_{SC} and V_{OC} are:

$$I_{SC} = I_{SC25}(1 + \beta\,\Delta T) \tag{2.5}$$

$$V_{OC} = V_{OC25}(1 + \chi\Delta T) \tag{2.6}$$

$$\Delta T = T^C(℃) - 25° \tag{2.7}$$

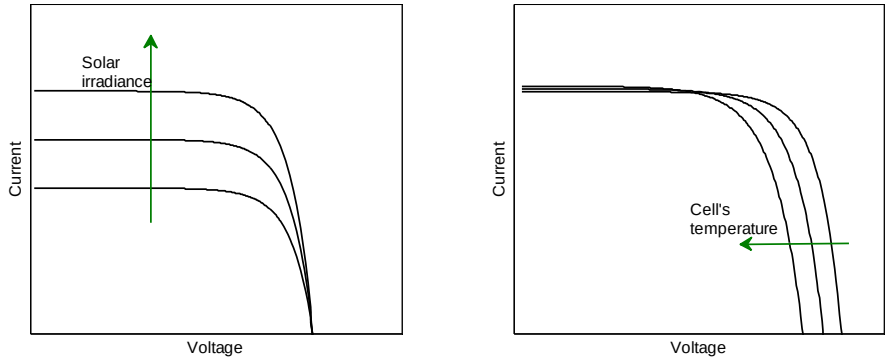

Fig. 2.4. Influence of the cell solar irradiance and cell temperature.

2.1.5. Single diode circuit model

The first model used in this work is the so called equivalent single diode circuit model. From this equivalent circuit, presented in Fig. 2.5, a four parameters model can be considered – having I_{ph}, I_0, R_s and A as electrical parameters, or the five parameters, having R_{sh} in addition.

The parameters have the following meaning:

I_{ph} – photo-generated current (A)

I_0 – dark saturation current (A)

A – diode ideality factor

R_s – panel series resistance (Ω)

R_{sh} – panel parallel (shunt) resistance (Ω)

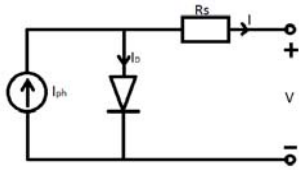

Fig. 2.5. Single diode equivalent circuit.

The double diode model is considered by many authors to be more accurate than the single diode model; the latter one is blamed for being imprecise particularly at low irradiance levels. However, it has been found out that when used for modelling the behaviour of many interconnected modules, the single diode model is preferred by many of the authors in the literature. [Sera2000]

The general current-voltage (i-v) characteristic of a PV panel based on the single diode model is represented by a transcendent function:

$$i = I_{ph} - I_0\left(e^{\frac{v+iR_s}{nsV_t}} - 1\right) - \frac{v + iR_s}{R_{sh}} \tag{2.8}$$

Equation (2.8) can be written for the three key points of the i-v characteristic: the short-circuit point, the maximum power point, and the open-circuit point, in order to develop additional relations using the data from the PV panels' data sheet.

Using the short circuit point and the open circuit point, expressions for the I_{ph} and I_0 can be determined:

$$I_{ph} = I_0 e^{\frac{V_{oc}}{nsV_t}} + \frac{V_{oc}}{R_{sh}} \tag{2.9}$$

$$I_0 = \left(I_{sc} - \frac{V_{oc} - I_{sc}R_s}{R_{sh}}\right) e^{-\frac{V_{oc}}{nsV_t}} \tag{2.10}$$

The i-v characteristic for a solar panel string, depending on the irradiance G_a and temperature T_c, for a four parameters model, considering R_{sh} to be infinite and neglecting the term $e^{-\frac{V_{oc}}{nsV_t}}$, has the following expressions:

$$v = n_{ps}V_{OC} + n_{ps}n_s V_T ln\left(1 - \frac{i}{n_{sp}I_{SC25}\frac{G_a}{1000}}\right) \quad (2.11)$$

$$i = n_{sp}I_{sc}\left(1 - e^{\frac{v - n_{ps}V_{OC} + R_s i}{n_{ps}n_s V_T}}\right) \quad (2.12)$$

Where:
n_s – no. of cells in series in one panel
n_{ps} – no. of panels in series
n_{sp} – no. of strings in parallel

$$V_T = \frac{K_B \cdot T_c \cdot A}{q} \quad (2.13)$$

K_B – the Boltzmann's constant
q – the charge of the electron
T_c – cell temperature

As stated in section 2.2, this model always considers the output power as being the maximum power point on the characteristic, given a certain operation condition. For obtaining the maximum power of the panel, the condition (2.14) is used:

$$\frac{dP}{dV} = 0 \quad (2.14)$$

Which translate into:

$$\frac{dP}{dV} = n_{sp}I_{SC}\left[1 - e^{\frac{v - n_{ps}V_{OC} + R_s i}{n_{ps}n_s V_T}} - \frac{v}{n_{ps}n_s V_T}e^{\frac{v - n_{ps}V_{OC} + R_s i}{n_{ps}n_s V_T}}\right] = 0 \quad (2.15)$$

The Matlab implementation of the mathematical model from equation 2.15 used to obtain the static characteristics of the PV panels is depicted in fig. 2.6. The model has as inputs: the solar irradiance, the cell temperature and it sweeps the voltage range of the PV panel in order to calculate the corresponding current and power. Function blocks were used to implement the I_{sc} and V_{oc} values, from equation 2.4, 2.5, and 2.6, and also for calculating the output current i, equation 2.12.

The mathematical equation 2.15 presents an algebraic loop: to calculate the variables in this loop, the variable values themselves are needed. The "algebraic constraint" block from Matlab/Simulink has been used during implementation in order to solve this equation.

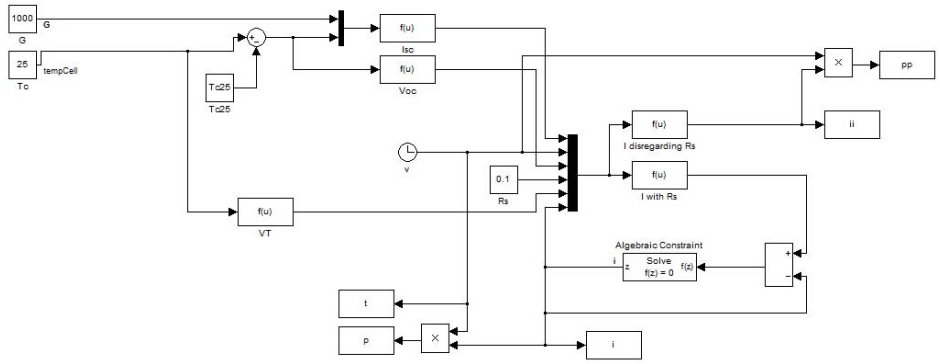

Fig. 2.6. Matlab block diagram used to model the static characteristic of the PV panels.

The parameters from the technical data sheet of the two types of panels used at SYSLAB facility are gathered in Table 2.2

The i-v and p-v characteristic, the temperature dependence and irradiance dependence of the short-circuit current, the open circuit voltage and the maximum power of the model and of the PV panels are compared in fig. 2.7. These characteristics are computed for specific cell temperature and solar irradiance, under STC.

Table 2.2 PV panel parameters from data sheet

Parameter name [unit]	**Schuco S 165-SP Photovoltaic module**	**SOLEL SE100x Photovoltaic module**
for STC – solar irradiance (G_a)=1000W/m^2, cell temperature(T_c)=25°C, wind speed 1m/s		
P_{mpp} [W]	165	100
V_{mpp} [V]	24.20	16.90
I_{mpp} [A]	6.83	6.13
V_{oc} [V]	30.40	21.10
I_{sc} [A]	7.36	6.60
α (P_{mpp}) [%/°C]	-0.478	
β (I_{sc}) [%/°C]	+0.057	
χ (V_{oc}) [%/°C]	-0.346	
δ (I_{mpp}) [%/°C]	-0.004	
ε (V_{mpp}) [%/°C]	-0.474	
Number of cells	50	70
for NOCT – solar irradiance(G_{aNOCT})=800W/m^2, ambient air temperature(T_{aNOCT})=20°C, wind speed 1m/s		
NOCT [°C]	46.2	

The simulation results using the developed PV model are compared with the characteristics presented in the data sheet from the Schuko panels.

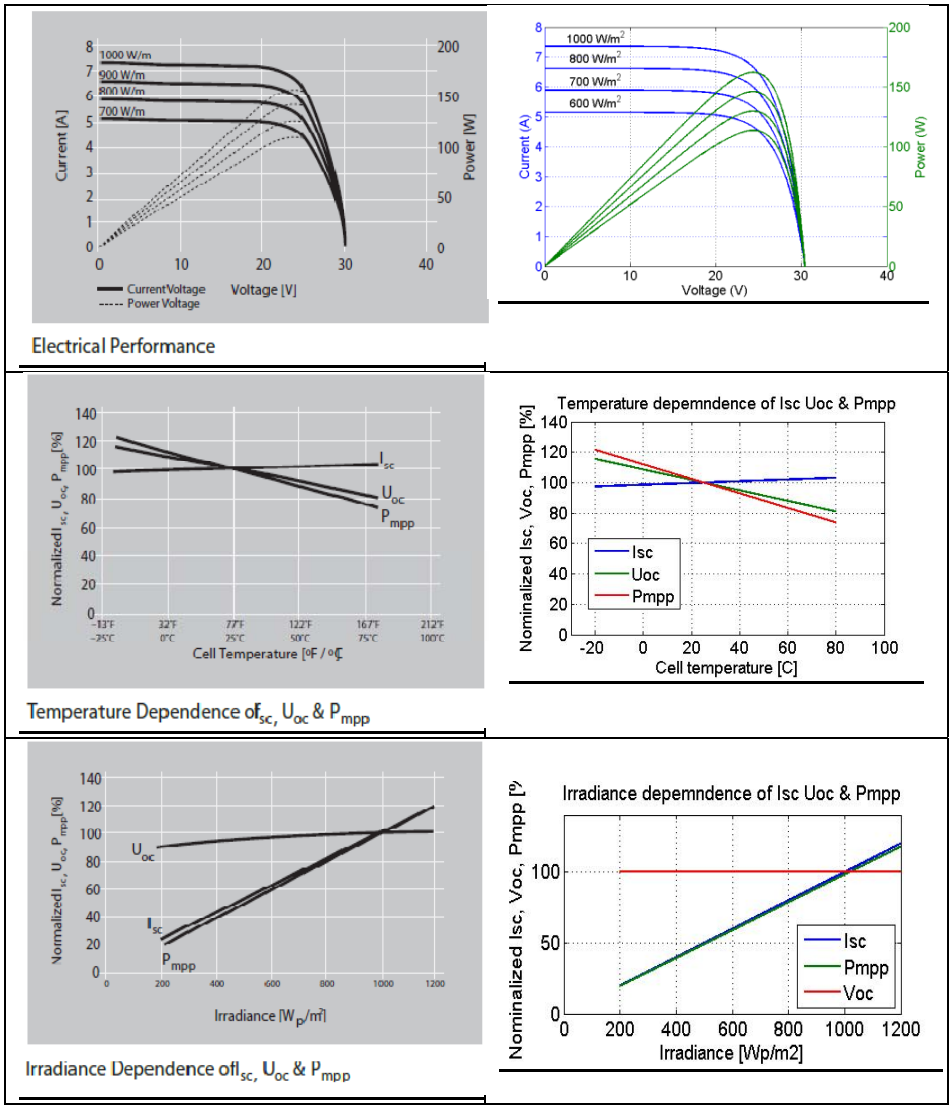

Fig. 2.7. Compared results between datasheet characteristics and simulation results.

2.1.5.1. Simulation model

As stated in paragraph 2.2, the goal of this research was the development of a simulation model that reproduces the electrical values of a three string PV plant, given ambient measurements from the local weather station.

Although for the following use of this model as a power source only the computed output power of the model is necessary, in this development stage, by computing the model's values of DC current and voltage, additional calibration could

be made, by comparing these obtained values to the measured real values taken from the solar inverter for each of the three PV strings.

The PV panels' model is based on the equation 2.15. Solving this equation determines the maximum power point, which the inverter should track precisely. Because in the PV systems there are no mechanical parts involved, and thus, the time constants are very small, being all electrical in nature (compared to Wind turbine systems), it is accurate to say the MPP value obtained from equation 2.15 is rapidly tracked by the inverter in real operation.

The schematic of the PV panel model is presented in Fig. 2.8.

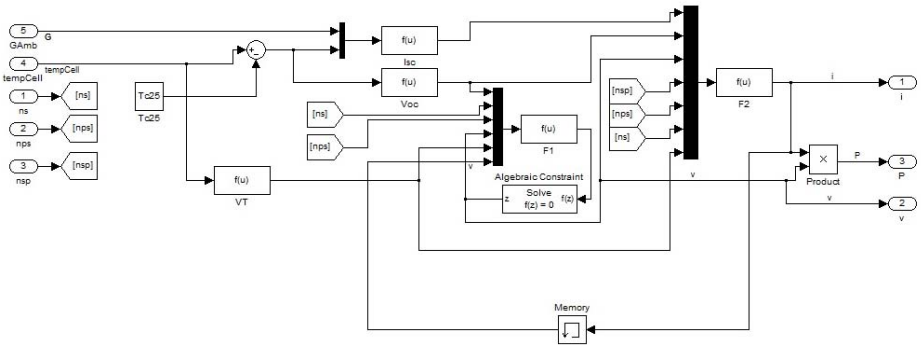

Fig. 2.8. One PV panel string block diagram.

Like in the previous model, used to plot the operation characteristics of the PV, shown in Fig. 2.6, the "Algebraic Constraints" block was used in this case for computing the voltage value "v" of the panel array from equation 2.15.

An additional assumption was made in this case: because the equation also requires the current value, which is computed from the voltage value, in order to break the algebraic loop, the current value is taken from the last simulation step. This assumption relies on the fact that the electric measurements have a time period of 1 second and the environment measurements have a resolution of 10 seconds; thus the system changes states each 10 seconds, and only for the first second in this 10 seconds interval the model takes the current value from the previous state. Since the model does not have dynamics (integrators or derivatives) and the simulation is running with a discrete time solver, this assumption is considered accurate.

2.1.6. Power model

As the purpose of the developed model is to calculate only the output power of the PV panels, a simpler model can be used, the so called power model. In order that sufficient parameters are provided by the manufacturers, as the case for new PV panels, this model can be accurately used.

The needed parameters are: I_{SC25}, V_{OC25}, P_{max25}, α, β, and χ, which were explained in Section 2.1.4.

Like in the case of the model presented in Section 2.1.5, the power model has two inputs:

T_{cell} - the cell temperature and

G_{cell} - the solar irradiance on the PV panels' surface.

The short circuit current for the present weather conditions is affected by the two model inputs as presented in the following relations:

By the temperature $\Delta T = 25 - T_{cell}$

$$I_{SC} = I_{SC25}(1 + \beta\,\Delta T) \tag{2.16}$$

By the solar irradiance

$$I_{SC} = I_{SC25}\frac{G_{cell}}{1000} \tag{2.17}$$

where
I_{sc25} is the short circuit current at STC.

The open circuit voltage is affected by temperature variations as:

$$V_{OC} = V_{OC25}(1 + \chi\Delta T) \tag{2.18}$$

The PV fill factor, taken from the PV data sheet, as described in section 2.4:

$$FF = \frac{P_{max25}}{I_{SC25}V_{OC25}} \tag{2.19}$$

Equations (2.16) to (2.19) are used to calculate, with a first order equation, the maximum power given the present weather conditions:

$$P_{MAX} = FFI_{SC}V_{OC}(1+\propto \Delta T) \tag{2.20}$$

As for the I_{SC} and V_{OC}, the output power is affected by temperature variations.

This model can be easily implemented in PowerFactory and further used in power system studies and simulations.

The developed PV panel's model in PowerFactory calculates only the dc output power, since the inverter used to connect it to the grid is an existing PowerFactory block.

As stated in Section 2.1.2, PowerFactory is a software dedicated to power system simulation, power flow and power quality analysis. In order to be used, each component has to be connected in a valid form to the specific simulation. Since the purpose is to run simulations as close as possible to the physical available microgrid, in the case of PV panels, the developed model will reproduce the DC output power and will connect to an existing model for the inverter.

From this perspective, where only the output power is of interest, the PV panels of the same type were considered to be part of the same string, e.g. string 1 and string 2 considered in Matlab as separate strings, in the PowerFactory model are considered together, as presented in Fig. 2.9.

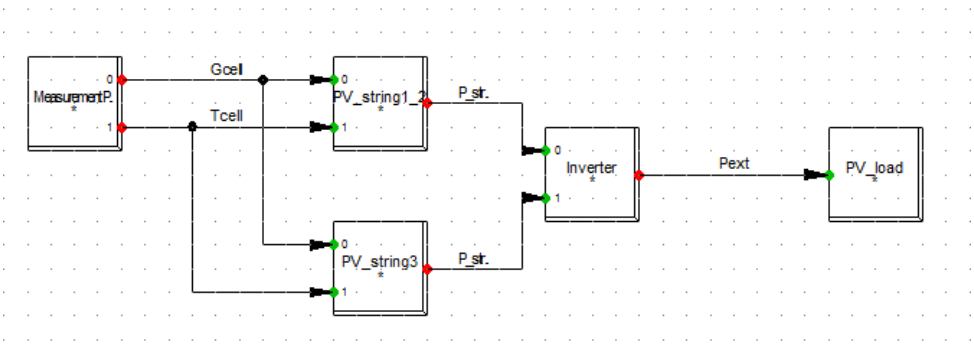

Fig. 2.9. Block diagram of PV panels in PowerFactory.

The PV mathematical model implemented in PowerFactory uses the equations 2.16 to 2.20. For simulating the output power for each PV string, the equations are grouped in a block diagram as shown in Fig. 2.10. This block is used for each of the two different types of PV panels grouped in a string (PV_string1_2 and PV_string3 from fig. 2.9) considering the parameters taken from Table 2.2.

In fig. 2.11 are shown comparative results between the measured output power (green) from the PV inverter and the model output (red) for PV1+PV2 and PV3, the setup being presented in fig. 2.1. The model was fed the ambient measurements from the weather station estimated for the PV panels surface with the correction module described in Section 2.1.7.

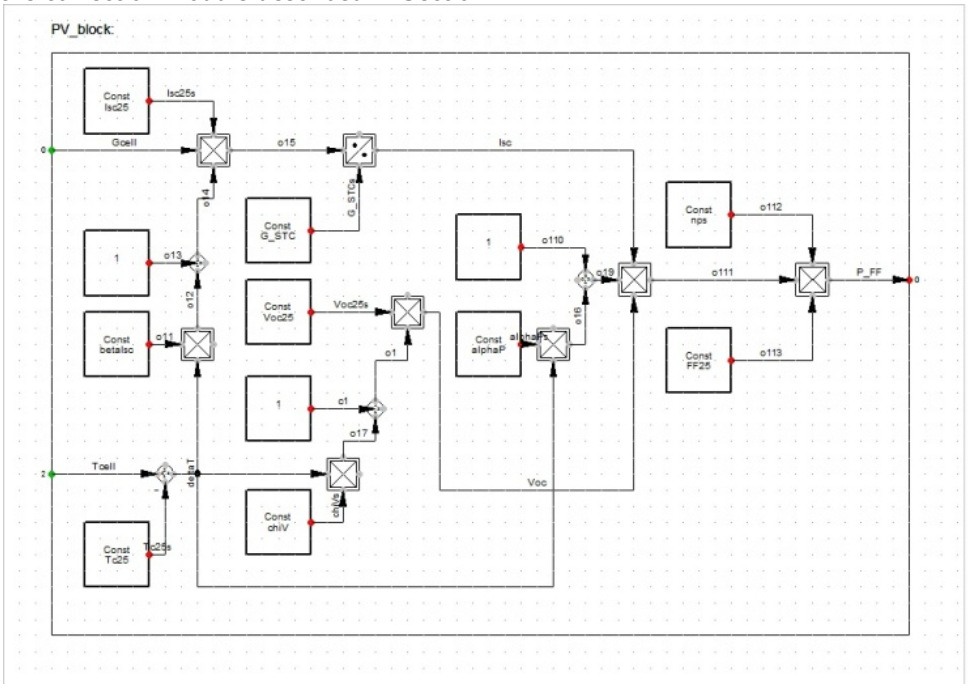

Fig. 2.10. Block diagram of PV string model in PowerFactory.

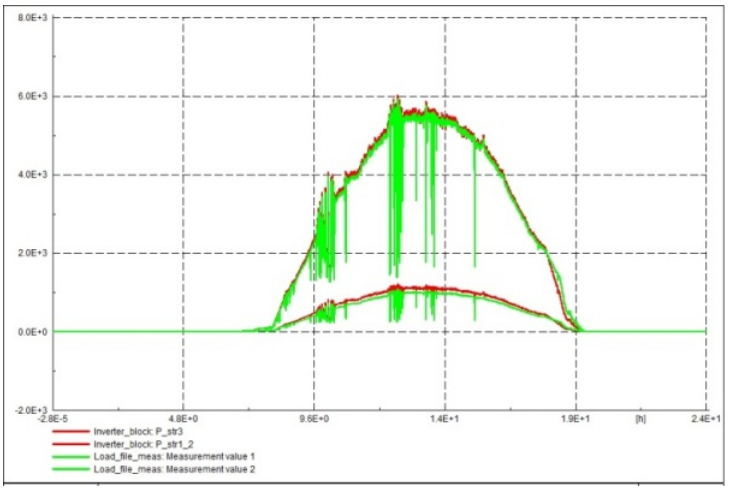

Fig. 2.11. Compared results between measured and simulation results.

2.1.7. Correction module

The ambient values, of temperature and solar irradiance, measured from the weather station can be very different from the values on the PV panels:

- the cell temperature is affected by the ambient temperature, but also by the solar irradiance – which has a heating effect and by the wind – which has a cooling effect on the panels
- the solar irradiance on the cell surface has a different value on the 60 degrees tilted PV panels as for the solar irradiance at the weather station which is measured on a horizontal plane

At SYSLAB research facility there are several PV plants mounted at different tilt angles and orientations, and there is no temperature or solar irradiance measurement devices on the actual panels but only the ambient data measured from the local weather station. This configuration makes it imperative to develop a module that corrects the data read from the station and estimates the values on the PV panels.

2.1.7.1. The cell temperature:

The cell temperature can be very different from the ambient temperature and it depends on the solar irradiation (Ga), ambient temperature (Ta) and also on the wind speed (Ws). Factors like solar irradiation act on increasing Tcell and factors like the Ws have a cooling effect (which can be seen in Fig. 2.12).

The simplest relation for the steady state operating cell temperature (Tc) and the ambient temperature (Ta), considering the influence of the solar irradiance (Ga) is:

$$T_c = T_a + kG_a \tag{2.21}$$

In this linear expression, which does not consider the wind, the constant k, known as the Ross coefficient [skoplaki08], expresses the temperature dependence on the solar flux:

$$k = \frac{T_c - T_a}{G_a} \tag{2.22}$$

The values for k are usually in the range of 0.02-0.04. The value for this coefficient can be obtained from the data sheet, considering the NOCT values:

$$k = \frac{NOCT - T_{aNOCT}}{G_{aNOCT}} \tag{2.23}$$

Usually, in low speed wind areas, the effect of the wind on the PV cells is negligible, the free convection and the radiation term having very small values [Goswami2000] [Eicker2003].

If the PV panels are mounted in regions with high wind potential, the wind speed must be considered because it has a large influence.[Skoplaki2008]. The forced (wind) convection is large for high wind speeds and the cell temperature function takes the following form:

$$T_c = T_a + \omega\left(\frac{0.32}{8.91 + 2\frac{W_{sh}}{0.67}}\right)G_a \tag{2.24}$$

where:

ω is the mounting coefficient, which depends on the mounting conditions of the PV panels; some values are given in Table 2.3.

W_{sh} is the wind speed measured on horizontal

The wind that produces the cooling effect through forced convection is the wind parallel to the panel surface; that is why the transformation $W_{sparallel} = W_{sh}/0.67$ is used.

Table 2.3. Values of the mounting coefficient.

PV array mounting type	ω
Free standing	1.0
Flat roof	1.2
Sloped roof	1.8 (1.0-2.7)
Facade integrated	2.4 (2.2-2.6)

For a better understanding on the influence of solar irradiance and wind speed on the cell temperature, a graphical representation of these values is depicted in fig. 2.12. For all the model simulations, the effect of both solar irradiance and wind speed are considered.

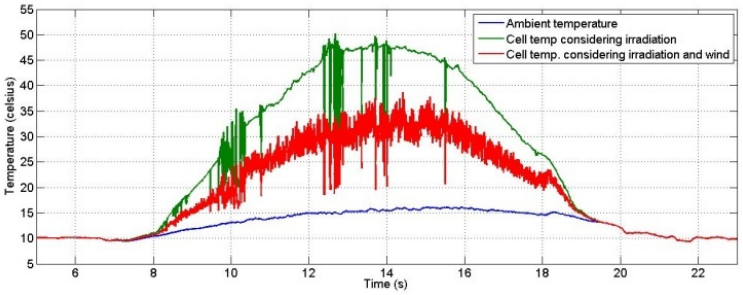

(a) cell temperature under different conditions

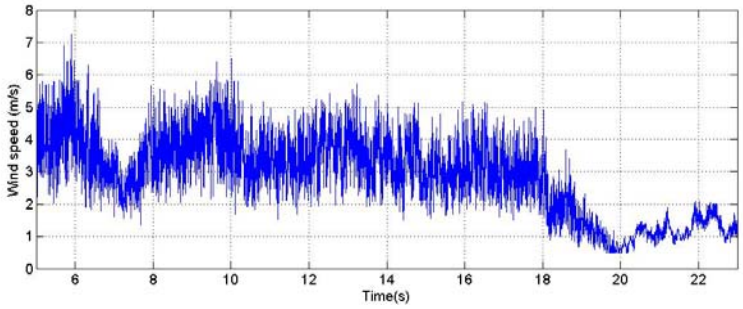

(b) Wind speed

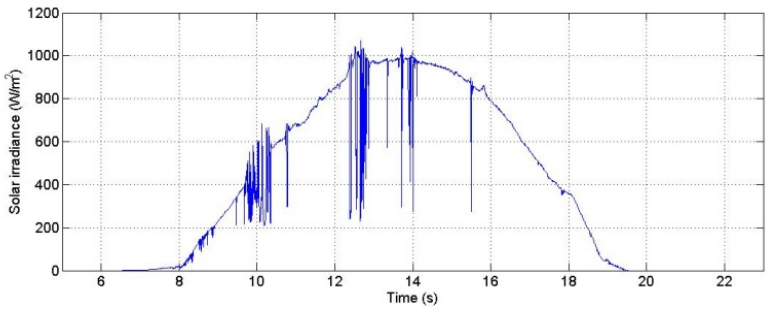

(c) Solar irradiance on the PV panel

Fig. 2.12. Ambient factors influence on the cell temperature of measurements taken on 2011.09.16.

The first plot from fig. 2.12 represents the PV cell temperature under three different considerations:

- when the cell temperature is considered to be equal to the ambient air temperature,
- the heating influence of the solar irradiance, represented in fig.2.12c, as defined in equation 2.21, and
- the combined effect of the solar irradiance and the cooling effect of the wind speed, represented in fig.2.12b.

2.1.7.2. The cell solar irradiance

If the measurements taken from the weather station are considered to be the same as on the PV panels, and used as inputs to the developed PV model, the simulated output power has a different profile as the actual output power measured at the PV installation, see Fig. 2.17.

In the case when the measurements are not on the actual panels and most often are taken from a weather station, like in the case of SYSLAB installations, the solar irradiance is measured on the horizontal plane, in order to be more general and could be used for different applications and purposes.

The solar irradiance on each surface has three components:

- direct irradiance – the amount of solar irradiance that travels in strait line from the sun
- diffuse irradiance – the amount of solar irradiance reflected by the air and dust particles in the atmosphere
- reflected irradiance – the amount of solar irradiance reflected from the ground, vegetation and buildings at the earth's level

The values of these three components vary on the location of the PV panels, the tilt angle, and the orientation and for an accurate model they should be considered specifically for each mounting location.

First of all, a relation was needed in order to translate the measured horizontal solar irradiance available from the local weather station onto the tilted PV panel surface. For this, some new parameters had to be introduced into the model:

The *declination angle* is the angular position of the sun at solar noon with respect to the plane of the equator. Its value is given by:

$$\delta = 23.45 \sin\left(360 \frac{284 + n}{365.25}\right) \tag{2.25}$$

where 23.45 represents the Tropic of Cancer latitude.

For this equation, the days are numbered from the spring equinox (day 81) and using the fact that sin is a periodic function, 365-81=284

The relation between solar irradiance on a tilted panel and the solar irradiance on a horizontal plane, facing south is:

$$S_{panel} = \frac{S_{horiz} \sin(\alpha + \beta)}{\sin \alpha} \tag{2.26}$$

where:

α – 90-φ+δ

β – panel tilt angle

φ – location latitude.

From this equation it is clear that the ratio between the solar irradiance on the PV panel and the one on the horizontal changes during the year, as the earth orbits the sun, and the declination angle changes with every day.

The Matlab/Simulink block that models this correction is shown in Fig. 2.13.

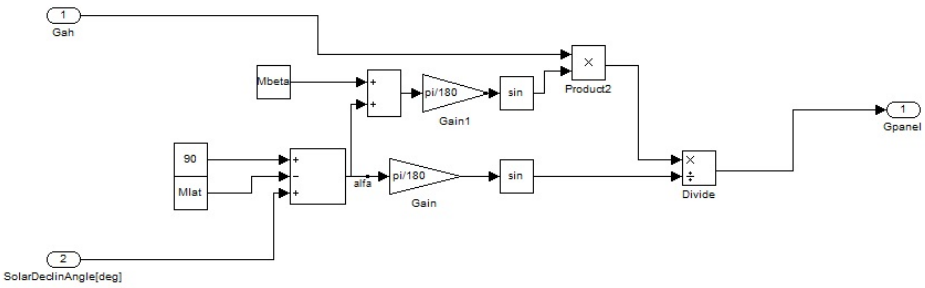

Fig. 2.13. Correction of solar irradiance values from horizontal to a tilted plane.

There is an influence on the output power and on the output power evolution during the day regarding the orientation of the PV panels. If they are mounted on the E-W axis, facing directly south, the maximum output power will be at precisely solar noon, when the direct solar beam radiation is at its peak, and the solar azimuth angle is zero. As the PV panels from SYSLAB are deviated from the E-W axis, the output power presents a time characteristic shifted from the time representation of the solar irradiance measured on a horizontal or facing south PV panel, as seen in figure 2.18.

The two curves present different sunrises, different sunsets and different solar noon. Those points, however, have the same lag in time. For example, if the panel deviation from the E-W axis is of 15° to west, on the deviated panel the sunrise, noon, and sunset will be one hour late that on the one facing south. [Goswami1999] [Seme2011]. This phenomenon is clear when the data from the electrical measurements are compared with the results from the model, considering the PV panels on the E-W axis as shown in Fig. 2.18.

The events that appear in this figure, like shadows that translate in drop of current (and power) are synchronized both in the measurement and in the simulation. However the response in amplitude has a different wave form, the one from the simulation has a delay in time of around 50 minutes.

This is due to the deviation of the PV panels from SYSLAB with around 14 degrees to the west, as shown in Fig. 2.14, in the capture taken from National Oceanic&Atmospheric Administration, U.S. Department of Commerce [NOAA]

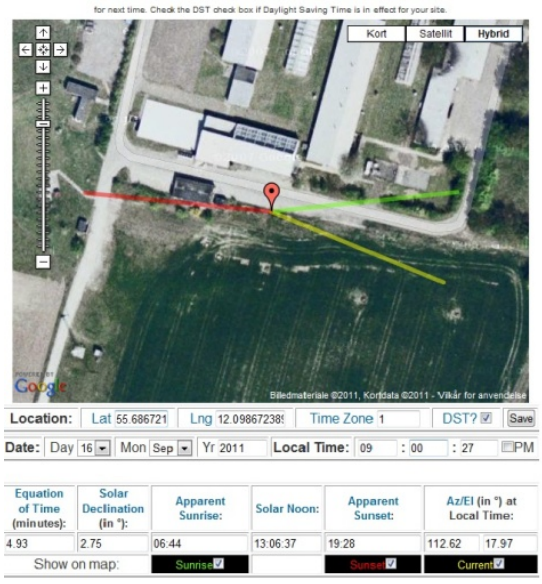

Fig. 2.14. PV panel installation site at SYSLAB facility.

In order to translate the horizontally measured solar irradiance on the actual PV panel, some values and notions have to be reviewed:

Solar hour angle – the geometrical angle between the sun's sky position projected on the ground in each moment of the day and the projection at solar noon; each hour, the sun travels 15° on the sky. It has a negative value before solar noon, zero at solar noon and positive after.

$$SolarHourAngle=15°(SolarNoon-T) \tag{2.27}$$

Equation of time is an astronomical term accounting for changes in the time of solar noon for a given location over the course of a year. Earth's elliptical orbit and Kepler's law of equal areas in equal times are the factors behind this phenomenon. This difference between the astronomical solar noon and twelve o'clock during the calendaristic year are represented, in minutes, in fig. 2.15.

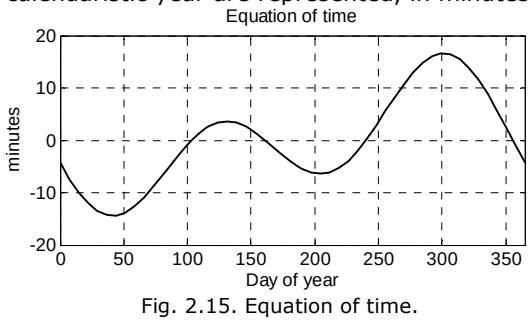

Fig. 2.15. Equation of time.

The maximum deviation of 15 minutes in the equation of time has an equivalent of 4° deviation of the panels from the EW axis, which has an observable effect on the PV output profile.

The equation of time is approximated with a polynomial shown in equation 2.29 that uses the current day (Mday) for defining as input:

$$MM = 2*pi*n/365.25 \quad (2.28)$$

$$EqofTime = (-7.657*\sin(MM)+9.862*\sin(2*MM+3.599))*60 \quad (2.29)$$

The astronomical solar noon, after the correction is:

$$SolarNoon = 12 + EqofTime \quad (2.30)$$

The solar radiation on the surface on the PV panels (G_{cell}), disregarding reflected irradiance, has the time dependent function:

$$G_{cell} = G_{panel}\frac{\cos(SolarHourAngle - Orientation)}{\sin SolarHourAngle} \quad (2.31)$$

where

G_{cell} – solar irradiance considering tilt the angle of the panels

Orientation – orientation of the panels, in degrees, from north (south represents by 180 degrees)

This orientation correction module was implemented in Matlab/Simulink as having the diagram shown in fig. 2.16.

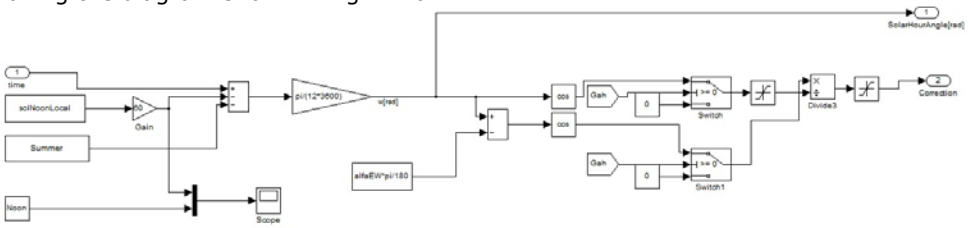

Fig. 2.16. Solar irradiance orientation correction.

2.1.7.3. Comparative results between the measured output power and the model's output power

1. The case when no correction module is considered, and the inputs for the PV module are the weather measurements from the local station

Disregarding the differences of weather conditions between the PV panels surface and the weather station and considering the measured solar irradiance and ambient temperature at the station as the model input, large differences appear in the output power. These differences were explained in detail in Section 2.1.7.

Fig. 2.17 presents the difference in output DC power between the PV inverter's electrical measurements and model's output power, for PV1 from the three PV panel strings from the configuration presented in Fig. 2.1.

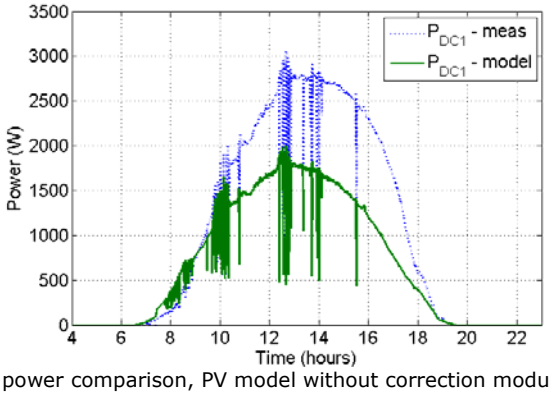

Fig. 2.17. Output power comparison, PV model without correction module, $G_{cell} = G_{meas}$, $T_{cell} = Ta_{meas}$.

2. The case when the correction module with tilt effect is considered as the inputs for the PV module

By considering the tilt angle on the PV panels, and the effect of solar irradiance and wind speed, as discussed in Section 2.1.7, the difference between measured DC output power and model output is shown in Fig. 2.18, and is considerable smaller than the one in Fig. 2.17.

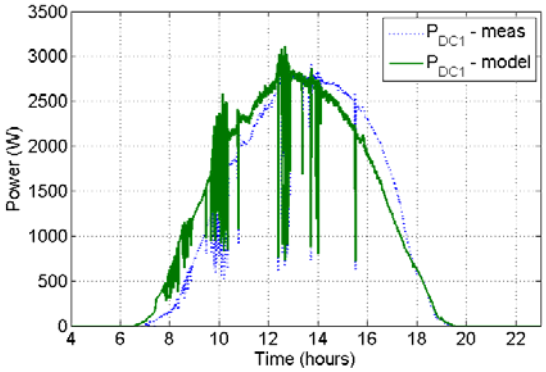

Fig. 2.18. Output power comparison, PV model with additional PV panel tilt angle correction.

3. The case when the correction module with tilt and orientation effect is considered as the inputs for the PV module

The overall output profile from the Fig. 2.18 is very similar for the two plotted values, with a small time shift, the measured power being delayed with around 50 minutes. This delay however, is not caused by any time uncorrelated measurements from the weather station and inverter, which run on different

network nodes, as the disturbances caused by clouds and shadows, are time correlated for the two powers, measured and simulated. This difference is caused by the orientation of the PV panels, as explained in Section 2.1.7.

By including the mathematical relations presented in Section 2.1.7 into the correction module, the model presents very good results; the two outputs present a small difference, as shown in Fig. 2.19.

The difference at around 18:00 hours is due to the vegetation that casts a shadow on the PV panels, as it can be seen from Fig. 2.1, where the PV plant that was used for modelling is presented, with the three PV strings highlighted.

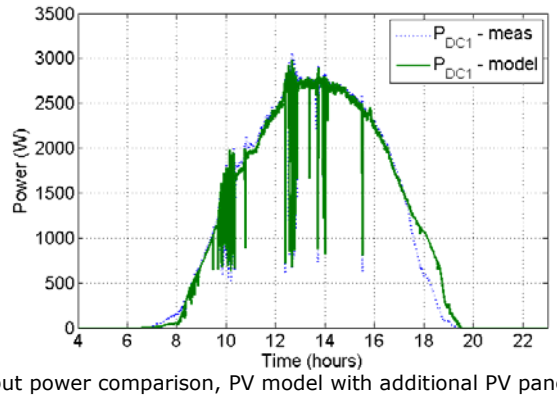

Fig. 2.19. Output power comparison, PV model with additional PV panel orientation angle correction.

2.1.8. PV model interface application

The graphical user interface application considers the PV plant described in chapter PV model and highlighted in Fig. 2.1: three PV strings, where PV1 and PV2 are composed by the same type.

The goal of this graphical tool is to facilitate the usage of the PV model, to clearly present the accuracy and shortcomings of the developed model by comparing the simulation values with the measured data taken from the PV inverter: current, voltage and power, for the entire plant and also on each of the three PV strings.

In the first window of the application it can be selected a day from the dropdown list. By making this selection, the ambient measurements for that day are plotted on the three graphs on the window: solar irradiance, ambient temperature, and wind speed, as shown in Fig. 2.20.

On this window there are three command options:

- Read data – this loads the weather data from the selected day into the memory
- Start simulation – resets the previous results and starts the simulation with the loaded weather data
- Show model – opens the Matlab/Simulink model that is used in the simulation and modifications can be made on it

On all the application's windows there is a text in the upper right corner that gives information about the state of simulation:

- No simulation data – no weather data are loaded into the memory, and no simulation results are available

- Running simulation – the application runs the model with the selected data
- Simulation loaded *date* – the simulation results for the selected *date* are available

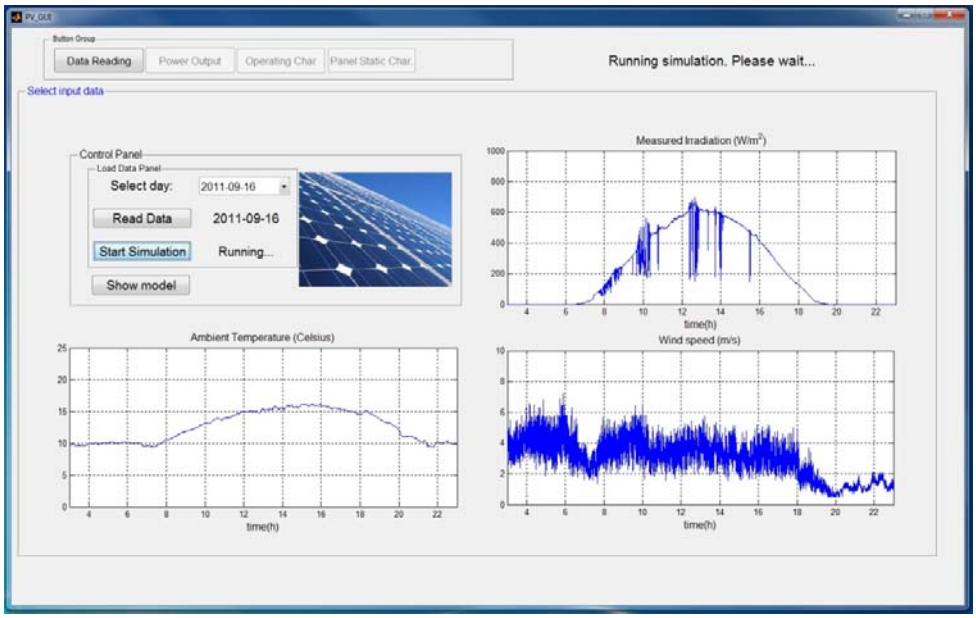

Fig. 2.20. Front window of the PV model interface application.

After running the simulation, the message in the upper right corner indicates that results are available and also enables the other windows for displaying these results:

Power output window

In this window, the selection of each of the three PV strings is possible. As shown in Fig. 2.21, for each PV string, a series of four graphs are represented. The measured data taken from the PV inverter are plotted against the simulation results of the PV model having the selected day's weather data. These four graphs represent:

- The string's DC current
- The string's DC voltage
- The PV string's DC power
- The total DC power over the three PV strings

In Fig. 2.21 the "Power output" window is shown for the day of 16 October 2011, for PV panel 1, made from Schuko panels, and PV panel 3, made from SOLEL 100x panels.

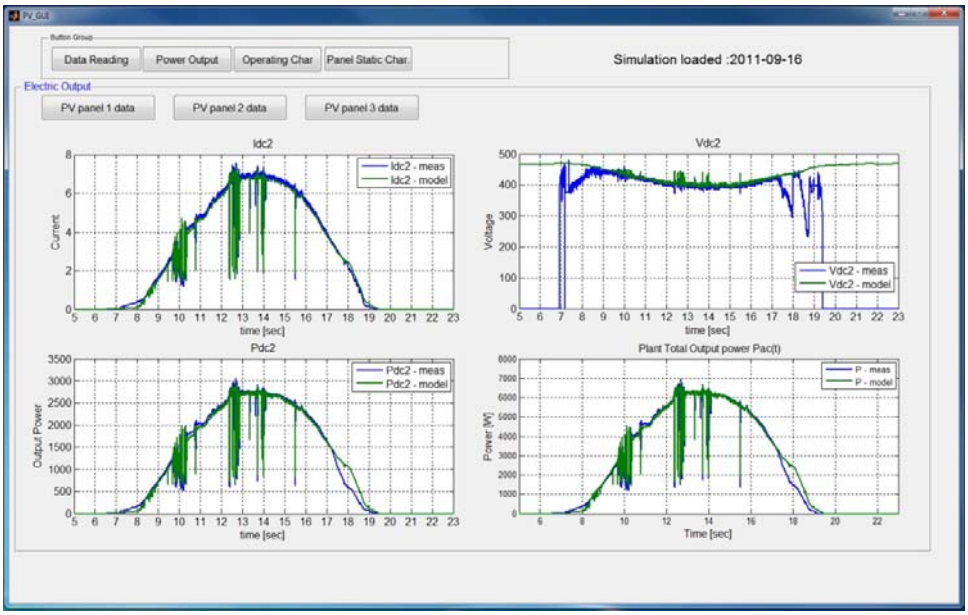

(a) Schuko PV panels outputs

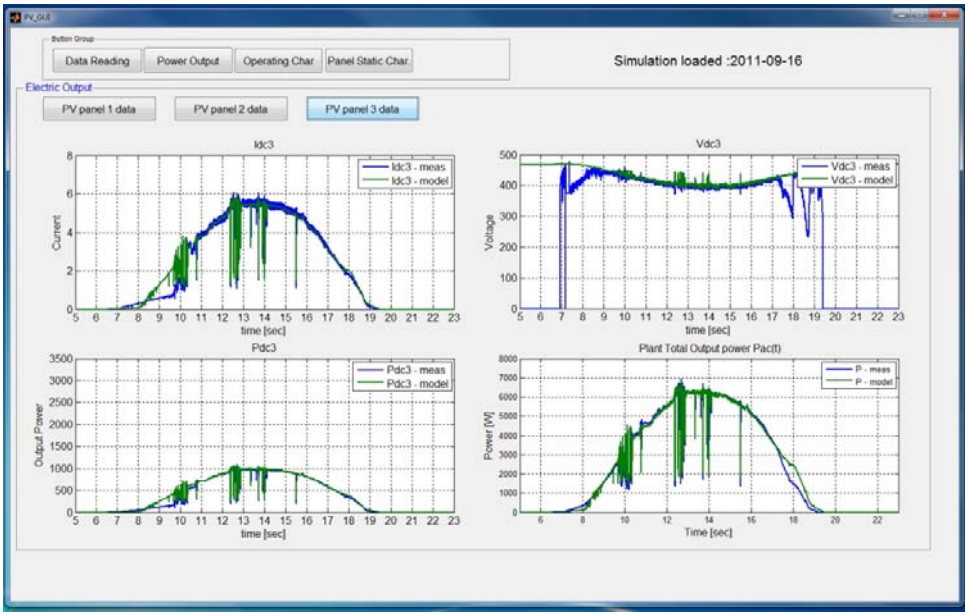

(b) SOLEL PV panels outputs

Fig. 2.21. Results window of the PV model interface application.

Some other important characteristics for ensuring a good model are the current-irradiance, current-voltage, and power-voltage characteristics. In figure 2.22, these simulation values are compared with the measured values.

Operating Characteristics window

In this window three important characteristics are plotted for each of the three PV strings:

- I-G characteristic
- I-V characteristic
- P-v Characteristic

The measured data from the inverter are plotted in blue color and in green are plotted the results from the simulation.

As it can be seen from Fig. 2.20, the measured data is more dispersed than the model's output. This difference comes from the fact that during operation, the inverter has to run a MPPT to follow the maximum power output. That means that, for short intervals, the operation regime differs from the optimal one, represented by the model's output. The model, as discussed in Section 2.1.2, always computes the maximum output power given certain weather data, without electrically tracking the maximum power point. However, these dispersed operation points are rare and the system remains in this operation states for very short periods of time, the electrical time constants being very small, and the MPPT very fast, hence, as it can be seen from Fig. 2.20, the model's output is very close to the measured electrical values.

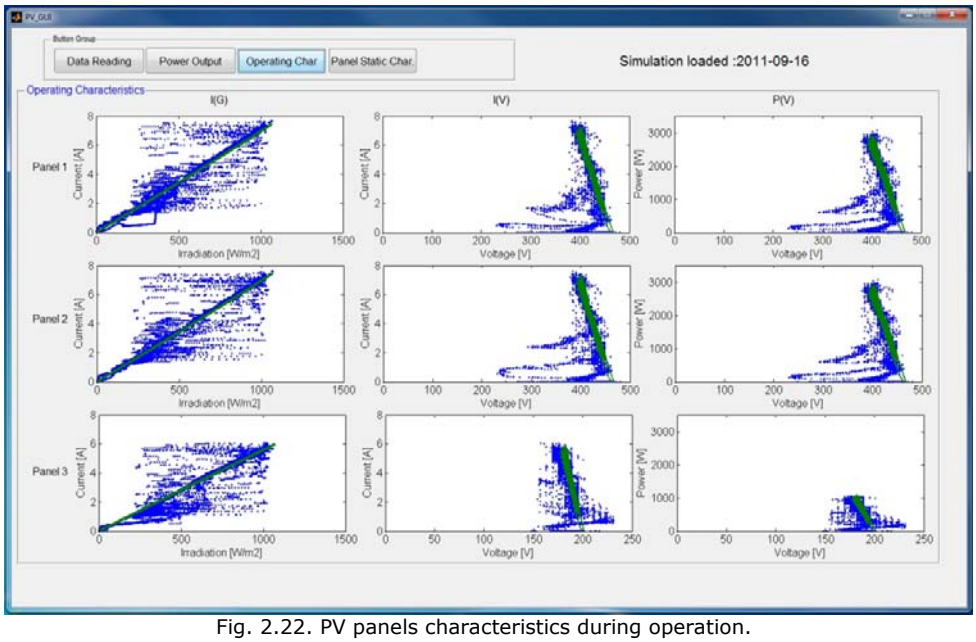

Fig. 2.22. PV panels characteristics during operation.

2.2. Vanadium-redox battery model

2.2.1. Introduction

The energy storage devices are essential in low power distribution grids with RES penetration for acting as an energy buffers between the flexible demand on one hand and flexible production on the other hand.

This subchapter presents the development and validation of a model designed for simulations of different operation regimes of a low voltage microgrid regarding a vanadium-redox flow battery (VRB). The model's parameters are determined through experiments.

A graphical interface application is developed in order to facilitate the use of the model in simulations, by running different sets of measured data, and to show the effect on the battery of changing the electrical parameters of the inverter.

2.2.2. General overview

Energy storage systems are expected to become indispensable for the future electrical grid, considering the large penetration of renewable sources [Yang2011][Koch2011].

With the renewable sources penetration into the grid, the energy generation is becoming more fluctuating [EnStor2003] [Solomon2012][Koch2010], in addition to the load consumption which is variable by nature. This difference between the energy generation and demand produces perturbation in the grid as over and under voltages, and frequency fluctuations as well.

Energy storage devices are being used exactly in the purpose of balancing the energy production and consumption, acting as an energy buffer. Even if load shifting algorithms are extensively developed, as described in [Vandoorn2011] [Ueda07], there are availability constraints regarding the connection of the loads when energy is available, due to consumers' comfort limitations; the energy storage devices are necessary due to the fast response and instant availability. As will be explained in section 2.3, each household load has a comfort penalty cost, which constraints the time shifting usage of the load.

A summary of available and used energy storage batteries are presented in Table 2.4 [Yang2011].

Table 2.4. Technology Comparison of potential batteries for Utility applications.

type	Open circuit voltage (V)	Specific energy (Wk/kg)	Operating temperature (°C)	Discharge time	Self discharge % per month @20°C	Cycle life (deep cycles)	Round trip DC energy efficiency
LAB	2.1	25-40	-40: 60	Up to 8 h	4-50	1000	50-77
NCB	1.35	30-45	-10:45	Up to 4 h	5-20	2000	55-70
VRB	1.4	10-20	10:40	4-12 h	3-9	5000	65-80
LCB	2.1	25-40	-40:60	Up to 4 h		3000	
Na-S	2.1	150-240	300:350	4-8 h	Negligible	4000	75-90
C-LC	3-4	155	-25:40	Up to 4 h	2	1000	94-99
LT-LFP	1.7	50-70	-25:40	Up to 4 h	2	4000	94-99

where

LAB: lead-acid batteries; NCB: nickel-cadmium batteries; VRB: all-vanadium redox flow batteries; LCB: lead-carbon ultrabatteries; Na-S: sodium-sulphur batteries; C-LC: Li-ion batteries of C anode and LiCoO2 cathode; LT-LFP: Li-ion batteries of Li4Ti5O12 anode and LiFePO4 cathode.

There are two directions of energy storage development and deployment [Chowdhury]. The first one is using large storage plants like the example of the 10-MW/40-MWh flooded lead-acid system that was built in 1988 in Chino, CA, which is used at the Chino substation of Southern California Edison Company, or the nickel cadmium system which was commissioned in 2003 in Fairbanks, Alaska, to provide 27 MW ac power for a short period of time (up to 15 min) until back generation comes online [Daughty2010].

The second approach is to include the storage systems into the distribution grids, where the RES penetration is accomplished at the consumer level [Sels2001], with photovoltaic panels mounted on the rooftop or small windturbine being installed in the yard [Barote2010]. A configuration of generators and loads is developing into an entity called microgrid. A survey of experimental microgrid configurations is presented in [Lidula 2010].

The battery technology used and described in this work is the vanadium redox flow battery (VRB).

The word 'redox' is a combination of two words: reduction and oxidation. A redox battery refers to an electrochemical system that generates oxidation and reduction between two active materials, forming a redox system, on the surface of inactive electrodes (the electrodes themselves do not change). A redox flow (RF) battery has the electrolyte including these active materials in external containers, such as tanks, and charges and discharges electricity by supplying the electrolyte to the flow type cell by pumps or other means [Shigematsu2010].

During research and experiments different electrolytes were used, and different technologies evolved. A short history of redox flow battery is presented in Table 2.5[Shigematsu2010]:

Table 2.5. History of RF Battery Development [Shigematsu2010].

year	Event
1949	Kangro (German patent): Cr/Cr
1974	Battelle Cr/Cr, Fe/Cr, V, Mo, Mn
1974	NASA released the principle of the RF battery – U.S. basic patent ('75) Fe/Cr system 1 kW ('78), Final Report ('84) ETL started the research and development of RF Battery
1980	NEDO (Moonlight Project) established the project "Advanced Battery Electric Power Storage System." • RF (ETL./Mitsui Engineering and Shipbuilding [MES]), NaS (Yuasa Battery), Zn/Br (Meidensha), and Zn/Cl2 (Furukawa Electric) • ETL, Fe/Cr system, 1 kW ('82); MES, 60 kW ('84 to'87) NEDO (Sunshine Project) • RF battery for solar power generation (MES and Ebara)
1985	University of New South Wales (UNSW; Australia) released the V system RF battery and applied a basic patent ('86).
1989	ETL. and Kashima Kita Electric Power developed V system RF battery for the use of vanadium from the soot • V system, 1 kW (Ebara, '90); 10 kW (MES, '91); 200 kW (Kashima Kita, '97) KEPCO and Sumitomo Electric

	• Fe/Cr system, 60 kW (’89); V system (450 kW, ’96)
1998	ETL. and Kashima Kita • 10 kW Redox Super Capacitor on-vehicle test
2001	Sumitomo Electric put V system RF battery into practical use (for load leveling, instantaneous voltage sag compensation and emergency use). NEDO verified the RF battery for stabilizing the wind power output fluctuation. Sumitomo Electric: 170 kW (’00), 6 MW (’05)
2011	The development of RF batteries is proceeding worldwide, including in the U.S., Europe and China

Nowadays, more than 20 VRB demonstration systems were installed for a range of energy storage applications around the world. The subsequent demonstration programs include [Skyllas2010]:

- 200kW/800kWh installed by Mitsubishi Chemicals (1996) at Kashima-Kita Electric Power, Japan for load-levelling [Shibata2010]
- 200kW/1.6MWh installed by SEI (2000) at Kansai Electric, Japan for peak shaving
- 250kW/500kWh installed by VRB Power (2001) at Stellenbosch University for ESKOM Power Corporation, South Africa for peak shaving and UPS back-up power
- 42 kW/90kWh installed by SEI in 2001 at CESI, Milan, Italy for R&D into distributed power systems
- a 250 kW/2 MWh VRB installed for Pacific Corp by VRB Power in 2004 in Moab, Utah, USA for voltage support, rural feeder augmentation [Hennessy2006]
- a 4 MW/6 MWh VRB installed by SEI in 2005 for J Power at Subaru Wind Farm, Tomahae, Hokkaido, Japan for wind energy storage and wind power stabilization [McDowell2006]

The major advantages of the vanadium redox battery, as shown in Table 2 and presented in [Bindner2011], are:

- operating at ambient temperatures
- reversible fuel cell – reduction and oxidation of single unique element, vanadium
- electrolyte never wears out
- low self discharge
- battery can charge as fast as it discharges
- battery power scalable by adding/removing cell stacks
- battery energy scalable by increasing/decreasing the electrolyte tanks
- large number of deep cycles

The major disadvantage is the low specific energy, which implies larger volumes of electrolyte in order to cover the energy demand of the site.

2.2.3. Problem statement

The design problem represents the development of a mathematical model that describes the operation of a VRB and the validation with the VRB from the SYSLAB facility. The model is implemented in Matlab and PowerFactory and is used for low voltage distribution grids simulation on power flow and voltage control issues.

The vanadium battery system installed at SYSLAB is connected to the grid via a four quadrant power converter and can deliver 15kW on the ac side and the nominal storage capacity is 180kWh. The battery can operate in two modes: P-Q

mode (where the active and reactive power of the battery is set by the user) and U-f-mode where the power is set according to the grid voltage and frequency and the pre-defined droop-curves. The overview of SYSLAB vanadium-redox battery is presented in fig. 2.23.

Fig. 2.23. Vanadium battery installation seen from above: electrolyte tanks in the back, 3 cell stacks at the front.

The VRB shown in Fig. 2.23 has the following system components:

- Cell stacks 3x42 cells in total
- Electrolyte tanks: 2x6500 liter
- Balance of plant: pipes, pumps
- AC/DC power converter
- Control and communication unit

The VRB power flow during operation is depicted in Fig. 2.24. According to the charge/discharge operation mode, the energy flows from the grid through the AC/DC converter, the cell stack and then changes the form of energy from electrical to chemical, at the electrolyte level; the reduction and oxidation phenomenon appear inside the electrolyte, which is the energy storage medium. The energy flows in the opposite direction during discharge mode.

The auxiliary parts of the battery are supplied with energy from another electric source, not to affect the energy flow and the energy conversion chain efficiency. Each component represented in Fig. 2.24 has its own energy losses, which are influenced by the amount of power circulated through the battery's output, the operation mode charge/discharge and the battery's temperature. All these losses are responsible for the battery efficiency.

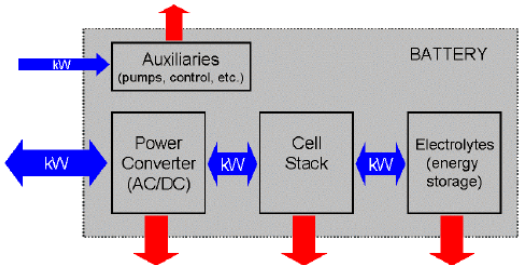

Fig. 2.24. Schematic diagram of the battery system.

2.2.3.1. AC-DC converter efficiency

The power converter efficiency has been estimated from the measured power on both the AC and the DC side. There is a slight difference between the AC to DC efficiency and the DC to AC efficiency: At maximum power in discharge mode is approximately 93% where in charge mode is approximately 91%. In both operation modes the characteristic of the efficiency has a relative large range where it is flat. The absolute efficiency is not very high for a modern power converter. The efficiency curve is presented in section 2.2.5 that describes the simulation model.

2.2.3.2. Cell stacks efficiency

The power delivered to the stack is $P=V_{DC}I$, while the power delivered to the electrolytes is $P = V_{EMF}I$. This means that the stack efficiency is V_{EMF}/ V_{DC} in charge mode (when $I<0$) and V_{DC}/V_{EMF} in discharge mode (when $I>0$). These electrical values are later explained in section 2.2.4.

In [Bindner2011] experiments for determining the battery efficiency which help in the development of the mathematical model are presented. During the testing of the battery it has been has put through a number of different charge and discharge cycles.

Fig. 2.25 presents the efficiency of the cell stacks as function of DC power at different state of charge (SOC) levels, when the battery is running in stable conditions. The figure illustrates how the relative deviation from the EMF grows with the power, leading to a decrease in the cell stack efficiency. There should also be a slight efficiency dependence on temperature, but this is expected to be insignificant in the temperature range that the battery is operated in and it has been disregarded in this study. There is also a dependency of efficiency on SOC since the open circuit voltage is higher when the SOC is higher and thus the current is smaller for the same power resulting in a decrease in the losses and a higher efficiency.

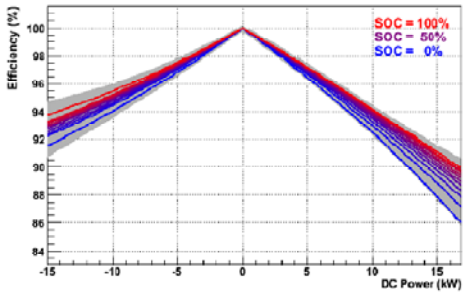

Fig. 2.25. Efficiency of the cell stacks as function of DC power.

2.2.3.3. Other storage losses

As a part of the normal operation of the battery, water will diffuse through the cell membranes when the ionic composition in the two electrolytes differs (due to the osmotic pressure).

This results in a difference in the level of the electrolyte in the two tanks. In order to avoid a too large difference in the level, an equalization process is carried out every 24 hours: a valve between the two tanks is simply opened for about half an hour allowing electrolyte to flow from the tank with the highest electrolyte level to one with the lowest level.

The energy loss during equalization depends on the current SOC and on the difference in electrolyte level. The loss has been measured to be 1.5% SOC (2.7kWh) on average during the measurement period. This corresponds to a constant energy use of about 110 Watts. The losses during equalization are the only observed energy losses in the electrolyte.

2.2.3.4. Auxiliary power consumption

For a vanadium battery, the auxiliary power consumption is significant since the electrolyte has to be circulated for the battery to be operational. The power of the auxiliaries (control system, pumps, etc.) can be derived from the measured AC power of the battery and the total power flow over the bus (when only the battery is connected).

When the battery is off, the power consumption (for the control PC and the displays) is 235W. When the battery is on and the pumps are running the power consumption is between 1.1 and 1.6kW depending on the AC power. This is illustrated on Fig. 2.26.

At low power ($|P_{AC}|<4kW$) a high flow speed of the electrolyte is not required and the pumps speed is reduced, which can be seen in the auxiliary power consumption. At high power ($|P_{AC}|>4kW$), the pumps are running at higher speed and the auxiliary power is about 1.5kW.

The fraction of the auxiliary losses will probably decrease with the size of the battery, e.g. by introducing intermediate stages in the battery's operation that are running only necessary pumps [Bindner2011].

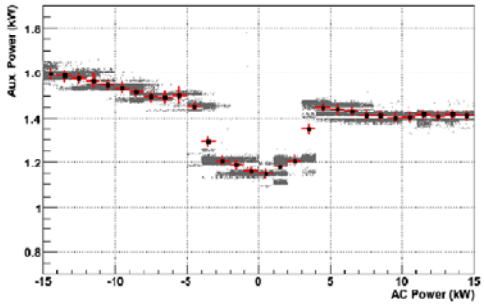

Fig. 2.26 Auxiliary power as function of AC power.

2.2.4. Mathematical model of the VRB

The model for the VRB was implemented in Matlab/Simulink and is based on the power equilibrium between the input and the stored power considering the efficiencies of different components and the power losses. These efficiencies were computed through experiments by measuring different electric values at different locations.

Fig. 2.27 shows the equivalent electrical diagram of the VRB.

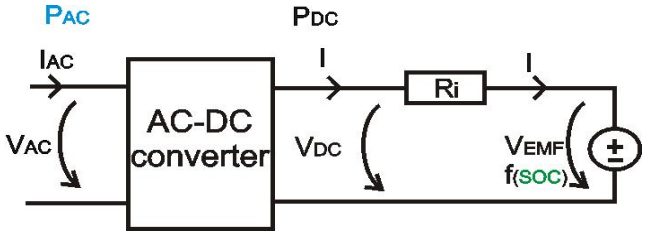

Fig. 2.27. Electrical circuit diagram of the VRB

The developed model has the following variables and parameters:

Input variable (for charge mode): - P_{AC} – AC power at the AC-DC converter

Output variable (for discharge mode): - P_{AC} – AC power at the AC-DC converter

State variable: SOC – state of charge of the battery

Design parameters: R_i – internal resistance
E_{batt} – battery capacity
η_{conv} – AC-DC converter efficiency
SOC_0 – initial state of charge

The amount of energy to be stored in the battery is obtained by integrating the power that enters the electrolyte. This power is the product $I*V_{EMF}$.

From the electric circuit in Fig. 2.27:

$$I = \frac{V_{EMF} - V_{DC}}{R_i} \tag{2.32}$$

Or

$$I = \frac{V_{EMF} - \frac{P_{DC}}{I}}{R_i} \tag{2.33}$$

From which a second order equation in variable I can be written:

$$I^2 R_i - I V_{EMF} + P_{DC} = 0 \tag{2.34}$$

Having the solution:

$$I_{1,2} = \frac{V_{EMF} \pm \sqrt{V_{EMF}^2 - 4R_i P_{DC}}}{2R_i} \tag{2.35}$$

The valid solution, representing the DC current, as a function of the known parameters and measured values is presented in equation (2.36):

$$I = \frac{V_{EMF,SOC} + \sqrt{V_{EMF,SOC}^2 - 4R_i P_{AC} \eta_{conv}}}{2R_i} \tag{2.36}$$

The V_{EMF}(SOC) characteristic was obtained through experiments, by measuring the open circuit voltage at the cell stack end. This measures the voltage across the cells connected in series.

Fig. 2.28 shows the open circuit voltage (V_{EMF}) as function of the SOC.

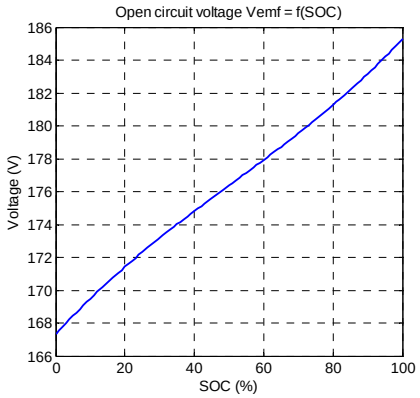

Fig. 2.28. Open circuit voltage (VEMF) as function of the SOC.

The reference power that is given by the system to the battery's converter in order to operate in charge/discharge mode, is the value of Pac_ref. Due to the efficiencies of different components, the actual charge/discharge power that supplies the electrolyte has a different value: in charge mode $P_{AC}>P_{DC}>P_{EMF}$ and in discharge mode $P_{AC}<P_{DC}<P_{EMF}$.

The actual energy stored in the battery has the following equation:

$$E_{Batt} = E_{Batt0} + \int_{t_0}^{t_1} P_{EMF} dt \tag{2.37}$$

Where:
E_{batt0} - initial energy stored in the battery
P_{EMF} - charge/discharge power at the electrolyte side
t_0,t_1 – initial and final time representing the charging interval

The state of charge (SOC) is defined as the amount of energy stored in the battery (in percent)

$$SOC = \frac{E_{Batt}}{E_T} \tag{2.38}$$

where E_T – the total energy capacity of the battery.

2.2.5. Model development

In Fig. 2.29 the VRB block diagram in Matlab/Simulink is presented. The blocks are detailed and explained in the followings.

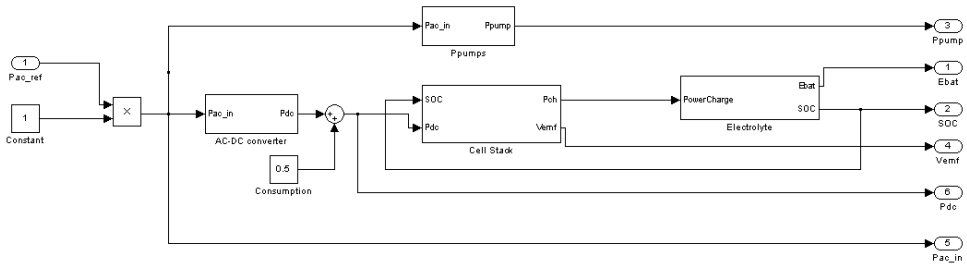

Fig. 2.29 VRB block diagram

Basically, the model reproduces the power flow in the battery, considering the efficiency and losses of each component presented in Section 2.2.3.

Each component has a different behaviour, regarding the mode of operation of the battery: charge/discharge. The model implemented these dynamic behaviours in a modular manner, like shown in Fig. 2.29. The operation mode is considered by each particularly component, rather than having two large blocks, one for charge mode and the other for discharge mode.

2.2.5.1. AC-DC converter efficiency

In Fig. 2.30, the efficiency of the AC-DC converter is shown for both charge and discharge operation modes. From the experimental measurement data obtained during full cycle operation of the VRB, in charge mode the efficiency is 91% where in discharge mode is 93%.

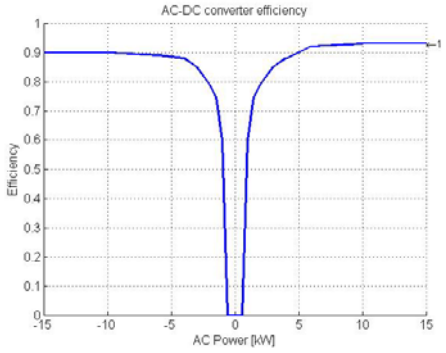

Fig. 2.30 Efficiency of the AC-DC converter

The block diagram for the AC-DC converter implemented in Matlab/Simulink is presented in fig. 2.31. The efficiency of the converter is implemented using a look-up table containing the measured values.

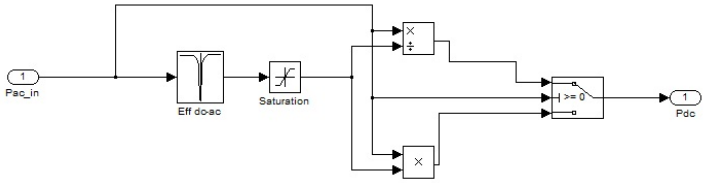

Fig. 2.31 Simulation model for the AC-DC converter

As stated in section 2.2.4, in charge mode $P_{AC}>P_{DC}$ and the converter efficiency is $Eff_{ACDC}=P_{DC}/P_{AC}$; meanwhile, in discharge mode $P_{DC}>P_{AC}$ and the efficiency $Eff_{ACDC}= P_{AC}/P_{DC}$.

2.2.5.2. VRB capacity

The total capacity of the battery can be obtained by multiplying the amount of electrolyte with its energy density. However, the VRB comes with an installed supervisory controller that allows the VRB to function inside more narrow limits; that means the available SOC reported by the controller has different values than the actual SOC of the battery. In other words, the inverter's zero reference SOC represents several percents of the total SOC, and the full state of charge reported by the controller is several percents lower than the full charge of the battery. These safety measurements were taken because the battery represents a new technology and future hands–on experience needs to be gained.

From the operation point of view, the corresponding lower and upper capacity limit were unknown and so was the available capacity of the battery.

The battery total available capacity had to be calculated through experiments and measurements, realized on a time span of 48 hours, as shown in Fig. 2.32. In fig.2.23b, the inverter AC power profile is plotted, having negative values for charging and positive values for discharging. In fig.2.23a, the battery's state of charge is plotted.

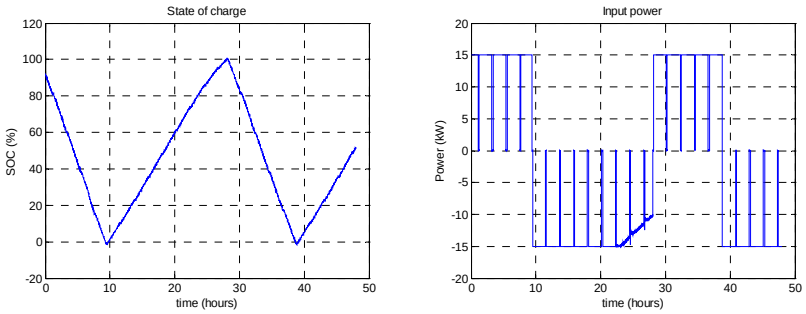

Fig. 2.32. Experimental determination of VRB capacity.

By considering a full charge–discharge cycle and measuring the amount of energy that went in and out of the battery, the available total capacity was calculated. The converters efficiency was considered as stated in section 2.2.5.1.

In a full charge cycle, the amount of stored energy is equal to the input energy after considering losses, or efficiencies, of the electrical components on the conversion line, as shown in fig. 2.24. That is the efficiency of the AC-DC converter (η_{conv}) and the efficiency of the battery itself (η_{batt}), due to the internal resistance losses.

In charge mode, the amount of input energy is:

$$E_{input} = \int_{t_0}^{t_1} P_{ac-charge} dt \tag{2.39}$$

And the amount of energy to be stored is:

$$E_{input} \cdot \eta_{conv} \cdot \eta_{batt} = E_{batt} \tag{2.40}$$

For the experiment shown in fig. 2.23, for a full charge from 0 to 100%, the input energy was:

$$E_{input} = 248.66\ kWh \tag{2.41}$$

In discharge mode, the amount of output energy is given by:

$$E_{output} = \int_{t_0}^{t_1} P_{ac-discharge}\, dt \tag{2.42}$$

Between the stored energy and output energy, considering the electrical components' efficiencies, the following relation is obtained:

$$E_{output} = E_{batt} \cdot \eta_{conv} \cdot \eta_{batt} \tag{2.43}$$

In the case of the experiment, the output power was:

$$E_{output} = 150.23\ kWh \tag{2.44}$$

By considering equations (2.40) and (2.43), a system of two equations with two unknowns is obtained. By solving the system in respect with the battery's capacity, the solution is:

$$E_{batt} = \sqrt{E_{input} \cdot E_{output}} \tag{2.45}$$

For the total capacity of the VRB, using measurements from the experiment, the following result is obtained:

$$E_{batt} = 193\ kWh \tag{2.46}$$

2.2.5.3. VRB internal resistance

Another important parameter in the modelling process is the VRB internal resistance. The internal resistance is the cause of energy losses and lowering the efficiency.

From the equivalent electric circuit from Fig. 2.27 a relation for the internal resistance can be derived:

$$R_i = \frac{V_{EMF} - V_{DC}}{I_{DC}} \tag{2.47}$$

Considering the available measured values the relation can be transformed into:

$$R_i = \frac{f(SOC) - V_{DC}}{\frac{P_{DC}}{V_{DC}}} \tag{2.48}$$

In Fig. 2.33 are presented measurements needed to represent the internal resistance of the battery during the full charge-discharge experiment.

Equation 2.48 is used to calculate the internal resistance value based on the experimental measurements. It can be seen in fig. 2.33a that this value modifies with the change of SOC, ac power and also on the battery temperature. The developed model does not consider the effect of these factors, the average value being used further.

2.2.5.4. Other losses

Other losses refer at operation losses like PC and display supply, and also at the energy loss during equalization, as mentioned in Section 2.2.3.3. They are modelled as a constant 0.5kW loss.

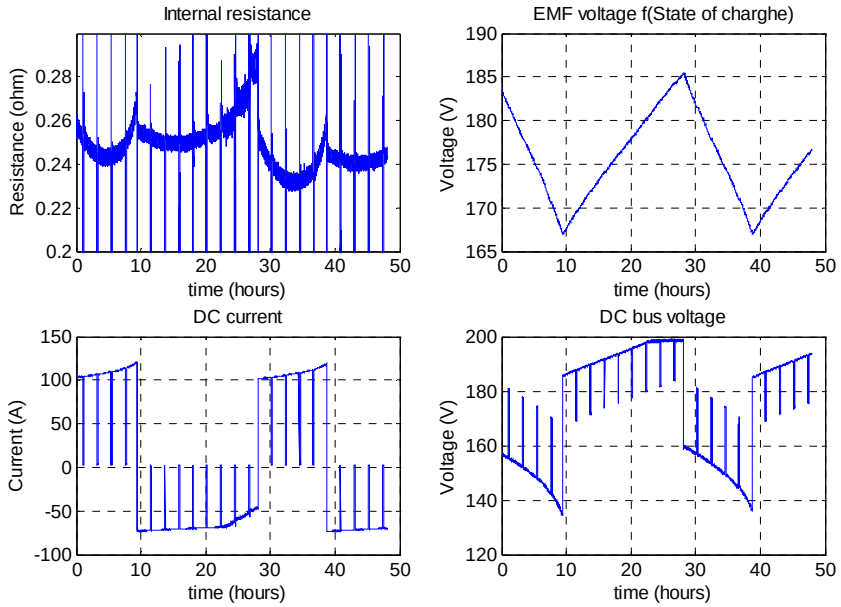

Fig. 2.33. Experimental determination of VRB internal resistance.

2.2.5.5. Pump losses

The power pump (auxiliary power) consumption is modelled with a look up table, considering the experimental data shown in Fig. 2.26. However, it does not influence the power flow from AC side to the battery because it consumes power from a different source, as shown in table 2.6.

Table 2.6. Auxiliary power consumption during VRB operation regimes

Ch. P	(kW)	-15	-13	-10	-7	-5	-4	-3	-2
Pump P	(kW)	1.60	1.55	1.50	1.50	1.40	1.30	1.20	1.20

Ch. P	(kW)	-1	0	1	2	3	4	5	6
Pump P	(kW)	1.18	0	1.15	1.20	1.20	1.30	1.45	1.45

Ch. P	(kW)	7	8	9	10	12	14
Pump P	(kW)	1.43	1.40	1.40	1.40	1.41	1.41

Where:

Ch. P – is the charge/discharge power of the VRB

Pump p – is the power consumed by the pumps to circulate the battery's electrolyte

2.2.5.6. Electrolyte block

In Figure 2.34 is presented the energy storage block that uses equation 2.37 in order to compute the stored energy and the SOC of the battery.

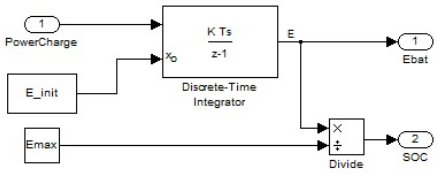

Fig. 2.34. VRB Energy storage model.

2.2.6. Simulation results

In order to validate the model, measurements were taken from the real battery, fed into the model and comparing the output values of the real battery and the values obtained with the model.

The following experiment was considered:

Starting from a SOC=93.5% the battery was discharged with a constant P_{AC}=15kW, until SOC=18%. Then a charge sequence from SOC=14% until SOC=87% at P_{AC}=10kW was considered. This discharge-charge sequence is shown in Fig. 2.35.

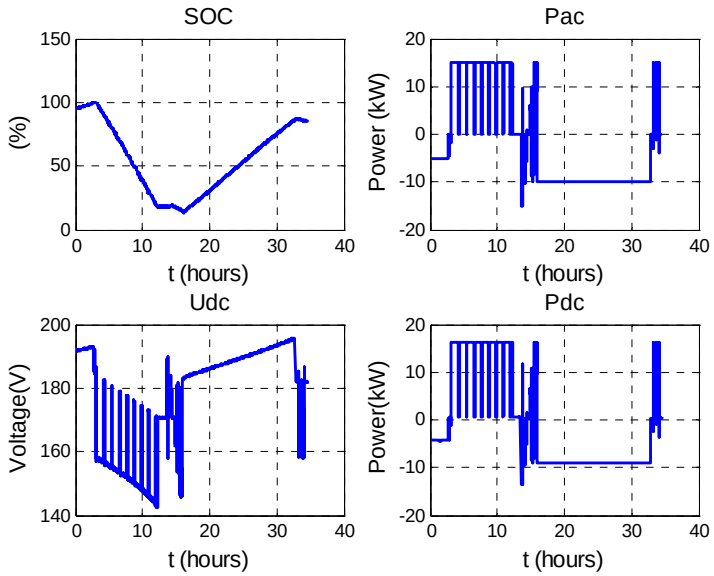

Fig. 2.35. Measured values from the real VRB.

After running the simulation with P_{AC} read from the VRB as input, the result – SOC – was plotted against the measured SOC, as seen in Fig. 2.36.

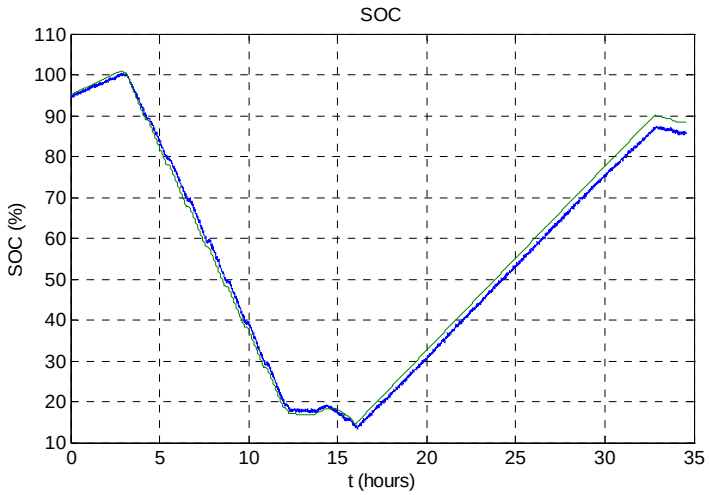

Fig. 2.36. Compared values of SOC: blue – measured; green – simulated.

2.2.7. PowerFactory model

The block diagram of the PowerFactory VRB model is depicted in figure 2.37. It represents the entire VRB, with all the internal components operation and efficiency, modelled after the mathematical equations presented in Section 2.2.4:

- AC-DC converter
- Cell stack
- Operational losses
- Energy storage

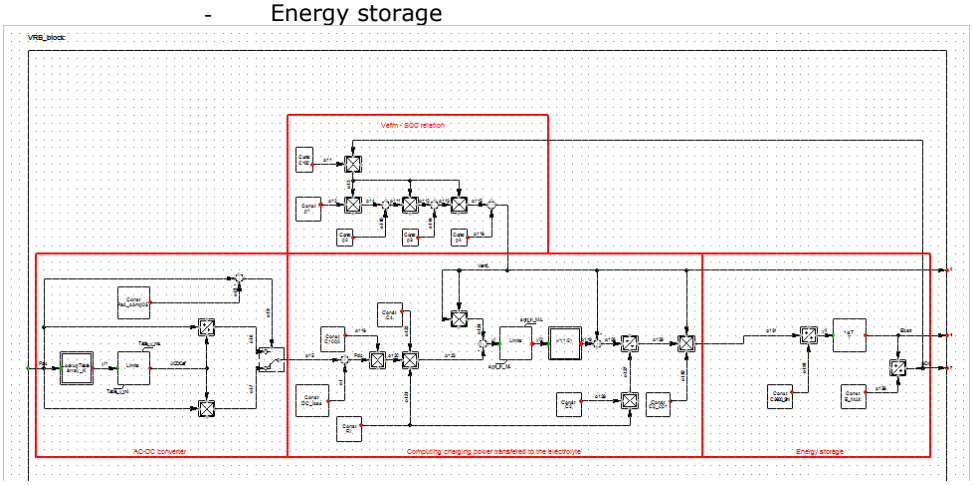

Fig. 2.37. Block diagram of VRB

As for the Matlab model validation, the same input AC power sequence was used for the PowerFactory model as depicted in Fig. 2.35. The compared SOC for the model and for the measurements are plotted in Fig. 2.38.

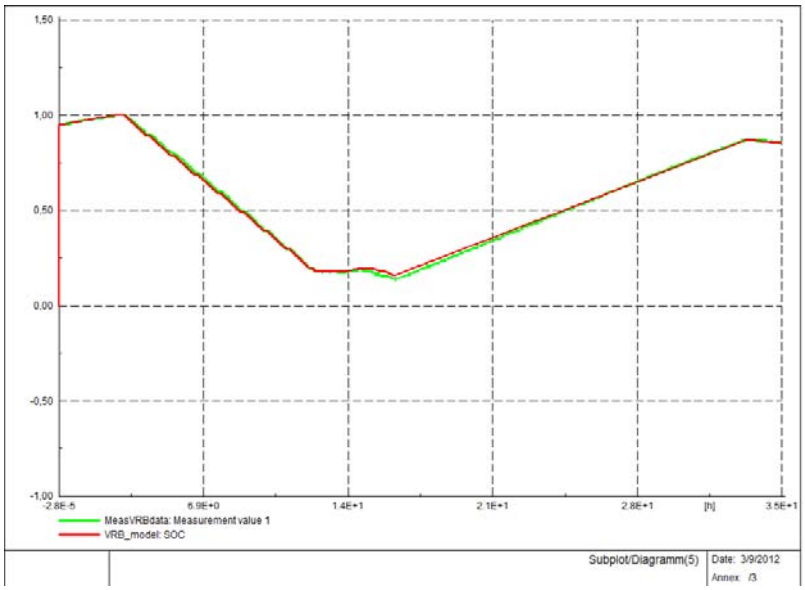

Fig. 2.38. Results comparison between measured and model.

2.2.8. VRB model interface application

A graphical user interface application was developed to serve the developed VRB model. The tool's interface can be seen in Fig. 2.39.

The purpose of this tool was firstly, to validate the model and secondly, to show the effect of VRB parameter changes in the model.

On the application interface there are two editable tables that alow changing model parameters : the first one is for defining the power consumption of the pumps according to the ac input power, and the second one is defining the ac-dc power converter's efficiency. The initial values of these two tables are available to be reloaded by selecting the reload buttons. The values of both tables are graphically represented in two plots, as shown in figure.

The converter's efficiency has an important role in the power conversion line of the battery and this application can emphasis the effect on the overall VRB efficiency by changing the VRB's inverter with one that has a different efficiency characteristic; this is realized by editing the power converter's efficiency table.

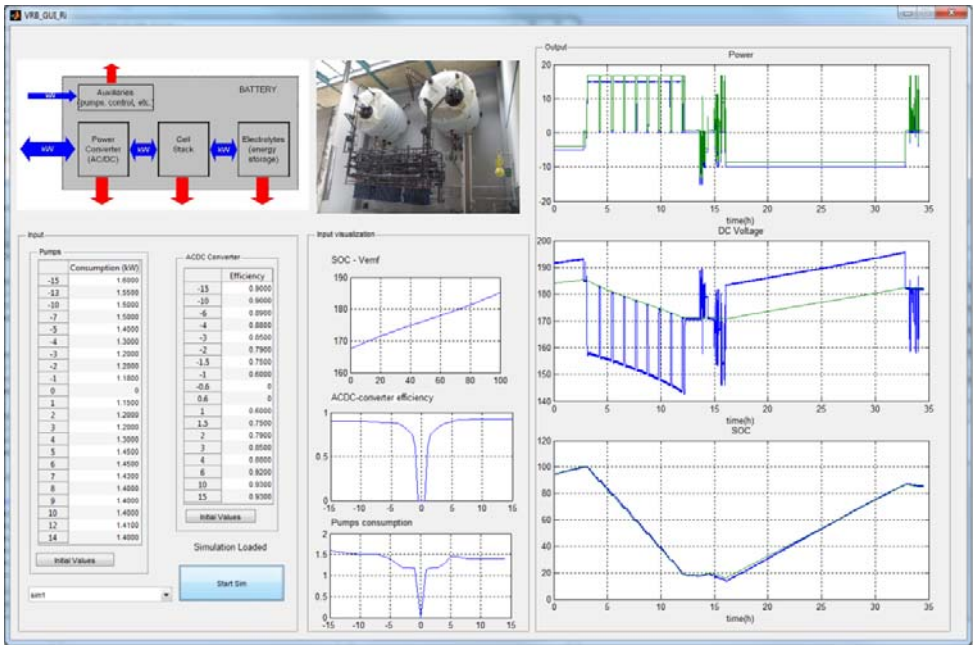

Fig. 2.39. Vanadium redox battery Graphical user interface.

The tool is presented with a dropdown list from which an input file containing an experiment data can be loaded. The input file presents the AC power profile measured from the AC-DC converter and the SOC measured by the VRB's internal controller.

The first plot, located in the right of the interface, is showing the measured ac and dc power at the converter. The second plot presents the measured and simulated dc voltage.

The third plot presents the measured and simulated state of charge of the VRB when using the same power flow as input.

2.3. Building with thermal storage model

2.3.1. Introduction

This subchapter presents the thermal model of a building, as a distributed energy resource (DER) developed for being part of low voltage distribution grid in load management and voltage stability study cases, by using the inside temperature in the comfort zone as (thermal) energy storage.

2.3.2. General Overview

The building sector is the second largest energy consumer in the European union, with an estimated 26.5% of the total global consumption according to

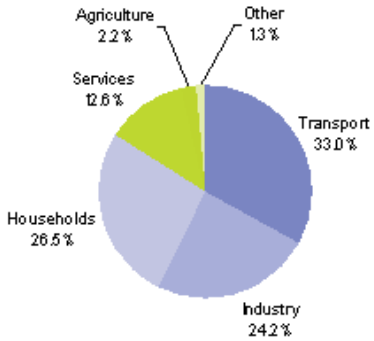

(1) Figures do not sum to 100 % due to rounding.
Source: Eurostat (online data code: tsdpc320)

Fig. 2.40. Energy consumption, EU-27, 2009 (% of total, based on tonnes of oil equivalent).

[eurostat09] in 2009, more than the industry energy consumption, as seen in figure 2.40.

The environment changes, the rising CO2 emissions, the continuing growth of energy demand, put increasing pressure on lowering the energy consumption and emphasis its use more efficient. The large share in energy consumption of households makes them a good candidate for research and implementation of solutions that enable the use the energy more efficient.

The energy consumption in a household can be grouped in loads that serve the building heating, ventilation, and air conditioning (HVAC) systems, the lightning system, the house and kitchen appliances and cooking, and nowadays even electric vehicles. [ENER].

Fig. 2.41 shows the energy consumption at European level for different countries, according to four categories of energy consumers. The data are represented in tons of oil equivalent (Toe) per household.

According on the energy availability or price, different techniques have been developed direct and indirect control of loads and load shifting [Fuller2011] [Lu2011] [Wang 2011].

For each load in the house, disregarding the system that is using it, a certain comfort penalty cost can be attached. That means, from the consumers' perspective, each load has a different time reaction, a different delay between the time the consumer requests that load and the time the load is activated; the comfort penalty cost increases proportional with the delay between the consumers' request and the loads' replay and with a comfort penalty coefficient specific to each load. For example, if the consumer needs to turn on the light in a room, disregarding the energy price, the light will turn on – has a high comfort penalty cost; however, the washing machine can start its program when the energy price is lower, which can happen hours after the consumer has pushed the start button – the washing machine has a small comfort penalty coefficient.

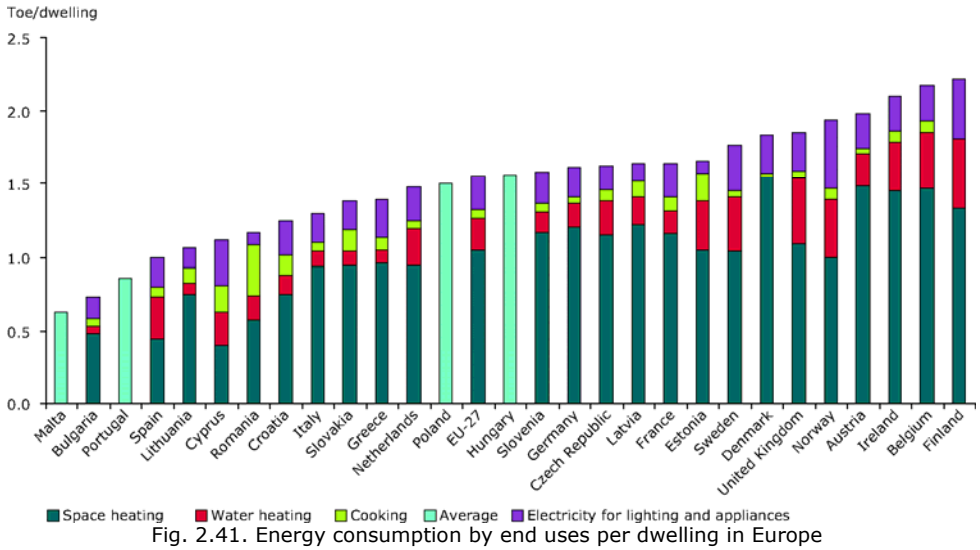

Fig. 2.41. Energy consumption by end uses per dwelling in Europe

The loads with small comfort penalty coefficient can be used according to the 'load shifting' technique, the operation of the loads being moved to the time interval when the operation cost if smaller. An observation has to be made here, that the operation cost considers both the energy cost necessary for the loads but also the comfort penalty cost. In other words, if it is important for the consumer to use a certain load, at a certain time, it will increase the comfort penalty cost outside the selected time interval so the operation cost of the selected time will be the minimized.

A system which presents operation flexibility is the households' heating system. The most common control for the interior temperature is the thermostatic control which considers the lower and upper temperature limit, set by the consumer. When the upper limit is reached, the heaters are turned off, and when the lower limit is reached, the heaters are turned on. Between this two limits that make the comfort zone, the house can be used as a energy storage device, storing thermal energy. This has large implications on the distribution grid with RES penetration, where energy is also produced at the consumer level and energy storage devices are needed to deal with power flow and voltage problems, which make the subject of this thesis.

For studying the power flow and the voltage profile on a low voltage distribution network and design controllers for optimizing consumption according to variable energy production, such a thermal model of a household is necessary.

Such a model was developed for a former office building transformed into a test facility, called FlexHouse, from SYSLAB platform at DTU Elektro RISØ campus. The mathematical modelling and parameter identification was the results of extensive work presented in [Bacher2010] and [Thavlov2008] and was implemented in Matlab and PowerFactory for the work presented in this thesis in Chapters 3 and 4.

2.3.3. Problem statement

FlexHouse is a former office building transformed into a test facility for testing different algorithms that study energy efficient operation, load management, and consumption profiles.

The size of FlexHouse is approximately 125 m^2 divided between eight rooms and a toilet. The rooms have been numbered 0 to 7. A layout can be seen in figure 2.42.

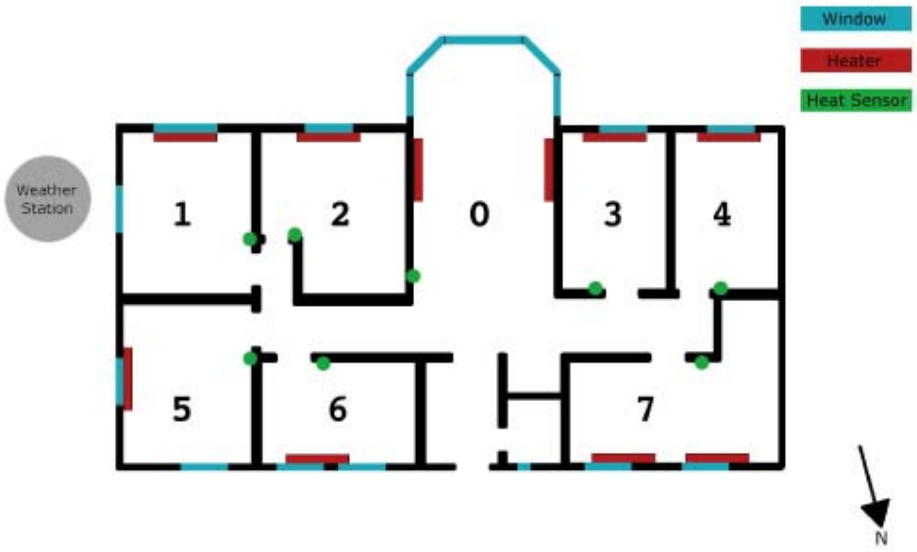

Fig. 2.42. The schema of studied building

Room 1 to 7 have been arranged as small offices, each with a desk, office chair and a computer. The main room, room 0, has been furnished with tables and chairs to accommodate meetings. The southern wall in the main room is dominated by large window facade. Electrical space heaters are mounted in rooms 1 to 7, whereas rooms 0 and 7 have two heaters each.

The temperature dynamics of a given space can be modelled using a resistance-capacitance (RC) circuit analogy, and formulated as a linear state space model.

2.3.4. FlexHouse thermal model

The FlexHouse model approximates the interior of the building to be one room with a uniform inside temperature. The state variable is the inside temperature (Ti), the input is the power to the heaters (PH) and the disturbances are the solar irradiance (G) and the ambient temperature (Ta). A schematic of the FlexHouse model is represented in Fig. 2.43a and the RC-diagram of a linear model is represented in Fig. 2.43b.

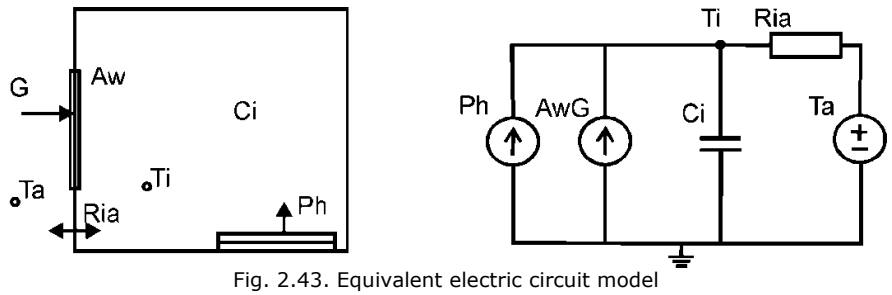

Fig. 2.43. Equivalent electric circuit model

The simplified thermal mass 1 state-space model, the M1 model, is represented by the following differential equation:

$$C_i \frac{dT_i}{dt} = \frac{1}{R_{ia}}(T_a - T_i) + A_w G + \mathrm{P}_h \tag{2.49}$$

where

C_i - is the heat capacity of the house. This includes the indoor air and the interior objects

R_{ia} - is the thermal resistance from the indoor to the ambient environment

A_w - is the effective window area of the house with heating influence. For the model, only 50% of the windows on the southern side are considered to play a role in the thermal dynamics of the house interior

For testing algorithms that deal with non-perfect models of the system a three state-space model was used for the building's thermal dynamics; this three states-model is presented in the work of Bacher and Tavlov (Bacher, 2010) as well as the parameters identification presented in Table 2.7 for both M1and M3.

This extended three states model, the M3 model, is represented by the following equations, representing the equivalent RC electric circuit represented in Figure 2.44:

$$\begin{cases} C_i \frac{dT_i}{dt} = \frac{1}{R_{ia}}(T_a - T_i) + \frac{1}{R_{im}}(T_m - T_i) + \frac{1}{R_{ih}}(T_h - T_i) + A_w G \\ C_m \frac{dT_m}{dt} = \frac{1}{R_{im}}(T_i - T_m) \\ C_h \frac{dT_h}{dt} = \frac{1}{R_{ih}}(T_i - T_h) + P_h \end{cases} \tag{2.50}$$

Where the state space variables are

Ti – inside temperature

Tm – a second inside temperature which defines a internal medium

Th – temperature in the electrical heaters

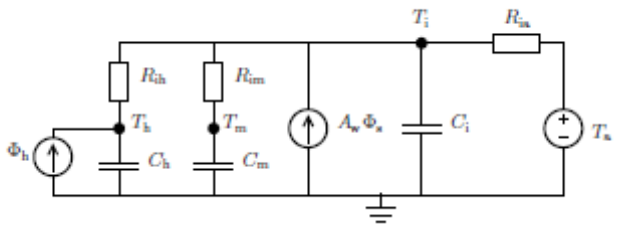

Fig. 2.44. Extended three states thermal model.

Table 2.7. Extended three states thermal model parameters

Parameter	C_i	C_m	C_h	R_{ia}	R_{im}	R_{ih}	A_w
Units	kWh/°C	kWh/°C	kWh/°C	°C/kW	°C/kW	°C/kW	m^2
M1	3.42			4.87			5.53
M3	2.66	3.08	0.00384	4.82	3.45	33.3	5.53

For the three influence factors on the model: ambient temperature, solar irradiance, and heaters output power, step input simulations are conducted and results are presented in figure 2.45.

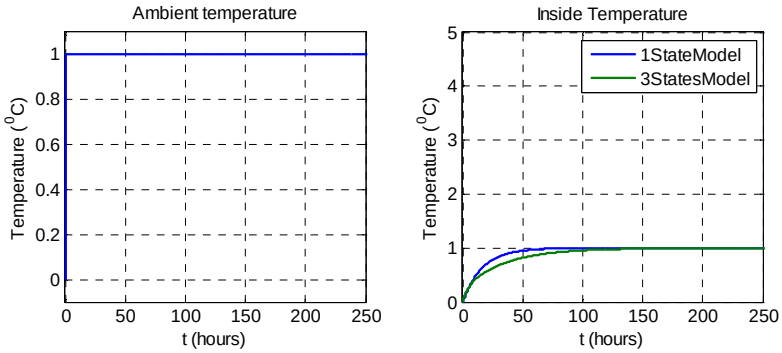

(a) Ambient temperature influence

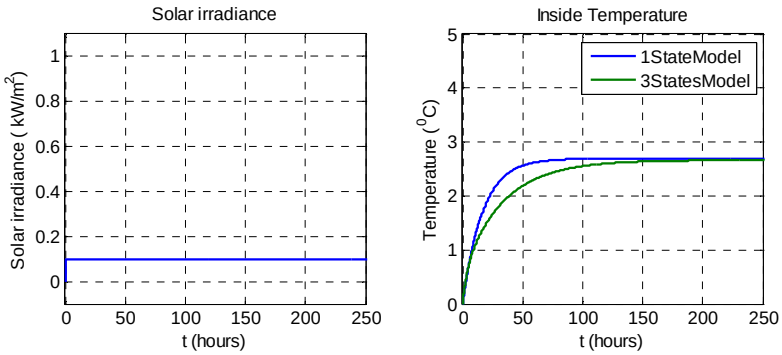

(b) Solar irradiance influence

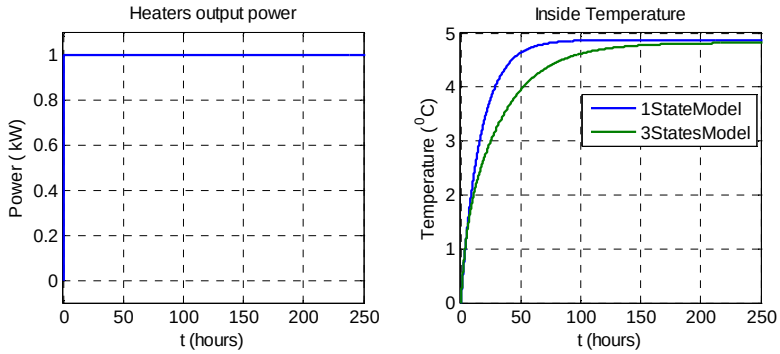

(c) Heaters output power influence

Fig. 2.45. Step response of the FlexHouse Matlab model.

The three factors that influence the inside temperature represented as step changing input signals in figure 2.45 are:

a) The ambient temperature

The step is considered one degree change in the ambient temperature which acts on heating the house walls and windows, and in 70 hours the system reaches a steady state temperature, equal to the ambient

b) The solar irradiance

The step considered for the solar irradiance is 100 W/m^2 change, having in mind that at the studied location the maximum amount of radiation is around 1100 W/m^2. It is seen from figure 2.45 that this change in solar irradiance gives an increase of 2.8 degrees Celsius inside the FlexHouse. This radiation acts in two ways: 1) heats the exterior walls of the house and more important, having a larger effect, 2) through the glass windows it heats the interior walls and furniture. This second effect is modelled in equation 2.49 with parameter Aw.

c) The heaters output power

The Flexhouse is equipped with 10 heaters, each considered to have 1kW of output power and the same effect on the interior temperature. In the real life the situation is slightly different, the heaters have from 0.8 to 1.4 kW output power, and by using a one room model of the house, additional errors appear, as discussed in Chapter 4, during experimental results.

For now, it can be seen that one heater increases the temperature with about 5 degrees Celsius the inside temperature, having the largest influence between the three factors.

The heaters output power is, in the same time, the only controlled input to the model, the ambient temperature and solar irradiance being the disturbances that the controller has to consider in order to maintain the inside temperature in comfort operation limits.

2.4. Conclusions

The first part of this chapter presented the development of mathematical models for specific photovoltaic panels installed at SYSLAB facility and their implementation in specialized software for later investigated microgrid simulation

study cases. Two types of models were implemented: the one diode equivalent circuit and a power model, which were than validated through comparison with real measurements during experiments.

Using the one diode equivalent circuit of the studied PV panels, the static characteristics under standard temperature conditions (STC) present the same evolution of the electrical performance, temperature dependence, and irradiance dependence as presented in the technical data sheet of the panels. From the comparison between the model's outputs and the measured values on the PV panels during one day operation it is concluded that this one diode model is achieving good results; as stated in the literature, the single diode model is sufficient for studies of power system simulations, the use of other extended models, like the two diodes model, is adding little value with large computation cost.

The simulations and comparisons presented in this chapter conclude that for simulating the PV output power, the power model is very accurate. This model can be used if the manufacturer provides the necessary coefficients describing the linearized dependences between the current and the voltage on one hand and the weather conditions of solar irradiance, outside temperature, and wind speed on the other hand. This model also has the major advantage of being extremely easy to implement on any software since it consists only in simple arithmetic operations.

The weather correction module proposed and developed in this chapter was needed to estimate the weather conditions on the PV panels surface (PV solar irradiance, PV temperature) based on the weather data collected from the local weather station: horizontal solar irradiance, outside ambient temperature, and horizontal wind speed. The data from the local weather station were measured on a horizontal plane and at a height of 12 meters.

As the facility had many PV panels mounted at different locations, different tilt angles and orientations, and no measurement devices installed on their surface, the proposed correction module was very efficient in estimating the necessary weather data.

Both solar irradiance on the PV surface and the PV cells temperature influence the PV panels' current and voltage and hence the output power.

The correction module emphasizes the effect of the PV tilt angle and orientation on the dc current and voltage. It also highlights the less obvious effect of solar irradiance and wind speed on the PV temperature, which is influencing the dc voltage: the solar irradiance increases the panels' temperature meanwhile the wind speed has a cooling effect. In places where the wind speed average is below 2 m/s its effect on the cells temperature is neglected; however, in places like Denmark, where strong winds are present, the wind's cooling effect has to be accounted.

The introduction of the correction module increases the number of variables needed to run the simulations as the module uses the calendar number of the current day, the latitude and longitude of the PV's geographic location, and the local time for calculating the angle difference that the sun makes with the horizontal plane where the solar irradiance is measured and the PV panel's surface orientation.

The correction module is a software solution of estimating the weather conditions on different PV panels when only one measurement device exists.

The hardware solution is to connect a solar irradiance and temperature sensor on PV panels having the same orientation as the studied panels; these panels can be the PV strings used to produce energy or just PV cells having the same orientation conditions as the installed PVs.

The second part of the chapter presents the development of a mathematical model for a vanadium redox battery based on experimental measurements.

This type of battery represents a new technology that has not yet reached the mature state but has some important characteristics that makes it a good candidate for operating as an energy storage device on the grid to regulate the energy flow.

The major advantages are

- the operating temperature, between 10 and 40 degrees Celsius – that is easy maintained and has no dangerous potential
- deep cycle life of over 5000 – that makes it a robust and reliable energy storage device
- the modularity of the design:
  - to increase the power one can add extra cells and
  - to increase the energy capacity one adds a larger electrolyte tank
- one can fully charge the battery by simply changing the electrolyte in the battery's tanks with a charged electrolyte, similar to a clinical blood transfusion

The major shortcoming of this battery is the low specific energy, of just 10-20 Wh/kg, which makes the battery extremely large for usage. The modelled battery had 1300 litters of electrolyte and a usable capacity of 180 kWh.

By developing graphical user interface applications, the two developed models can be tested and validated through comparisons with measured data considering specific operation scenarios.

The two implemented thermal models for the building will be used in power flow simulations and experiments and in designing and validating different control algorithms presented in future chapters.

3. Voltage Control

The energy produced by various power plants is transported over great distances at high voltages through transition power lines to the point of consumption like settlements or a light to medium industry consumers. Here the bulk power is transferred to distribution substations which by using transformers lower the voltage to values of 400 V line to line. A typical distribution grid will serve one to as many of ten feeder circuits [Grigsby2007].

As part of the power system, the low voltage distribution grid has the objective to provide energy to the end consumer.

The loading over the distribution feeder is unbalanced due to large number of different and unequal single-phase loads that must be served.

The connecting points of the components will be referred to as nodes.

A properly designed and operated power system should meet the following fundamental requirements [Kundur94]:

- The system should be able to meet the continually changing load demand for active and reactive power
- The system should supply energy at minimum cost and with minimum ecological impact
- The 'quality' of power supply must meet certain minimum standards with regard to the following factors:
    - Constancy of frequency
    - Constancy of voltage and
    - Level of reliability

The power system is a highly nonlinear system as it consists of many components both on the production part and the consumption which operate in different regimes and have different response characteristics.

An important characteristic of the power system is the line impedance. At distribution level this can be estimated by using different techniques which take into account the grid configuration and cables properties, along side other assumptions. Depending on the accuracy required, one can use simpler models which call for a wide variety of assumptions or the Carson equations for a more reliable result [Kundur94].

This impedance also is responsible for the grid 'stiffness', as the power flow affects the voltage profile.

Another important aspect of designing the distribution grid are the cable used for the grid deployment: overhead or underground they have to be properly prepared and coated in order to cope with the necessary power flow and also with the natural environment, that is humidity, temperature, magnetic fields interference, and others.

The flows of active and reactive power in a transmission network are fairly independent of each other. Active power control is closely related to frequency control, and reactive power control is related to voltage control. As constancy of frequency and voltage are fundamental requirements for power system performance.

The frequency should be kept nearly constant during grid operation. The constancy of frequency ensures constant speed of the synchronous motors used both in industry and in household appliances. Also the transformers were designed

for a nominal frequency and a change of it could mean high magnetization currents. In some applications the frequency is used for timing purposes as electric clocks are used. As a consequence, it is necessary to regulate not only the frequency itself, but also its integral [Kundur94].

The frequency is affected by the overall active power production-consumption balance at the grid level; it has the same value over the entire grid, which is limited by transformers representing large geographical areas, and its change in value manifests instantaneous.

By comparison the voltage profile is highly flexible as voltage drops occur on every feeder and consumer. Along the power system substations have to be used to control the voltage profile in order to respect the quality requirements and voltage limit constraints [Koch2011].

The problem of maintaining voltages within the required limits is complicated by the fact that the power system supplies power to a vast number of loads and is supplied from many generation units. As loads vary, the reactive power requirements of the transmission system vary. Since reactive power cannot be transmitted over long distances, voltage control has to be assured by using special devices dispersed throughout the system [Kundur94].

In the distribution grids the R/X ratio of the feeder is high compared to the one in the transmission lines. This implies that in distribution grids the active power affects the voltage more that the reactive power, as typical for the transmissions line.

This is the case of the facility that was the subject of this study, presented briefly in Appendix A. In this case, the R/X ratio is around 2.

Figure 3.1 presents the consumer's configuration along a feeder in a low voltage distribution grid. A transformer is used to connect the high voltage grid to the consumers via a feeder. The consumers are connected to this feeder at certain distance between one another as the feeder can reach several hundred meters in length. The configuration and connection points can be seen in fig. 3.1a). As the power is consumed by the users, the voltage drops from the first user, the closest to the transformer, to the last one. The distribution grid is designed that all the consumers to have the voltage at the connection point between acceptable limits (plotted in fig. 3.1b).

Because all the connection points have to have the voltage between the desired values at all times, tap changers are used in the transformer substation to change the voltage at the transformer output [Jiavi2008]. These changes in the high voltage end of the feeder are made because in different moments of the day, the voltage profile drops with different slopes along the feeder: in the morning and afternoon when the consumption is at its peak for all the houses the slope is more abrupt and the initial voltage has to be larger in order that the last consumer to remain in desired voltage limits.

However, this distribution grid configuration was design for the users to consume energy; nowadays more and more consumers are installing renewable energy sources and the voltage profile is changing from a down slope to any possible form. As the energy is produced at a household level, the power is injected into the grid by raising the voltage at the coupling point. If many neighbour households are equipped with renewable power generation units, the voltage profile can became a raising slope and the voltage upper limit can be breached, especially at the end of the feeder, for the last consumers. For the consumer, this over voltage translates in the fact that the inverters and appliances equipped with safety modules

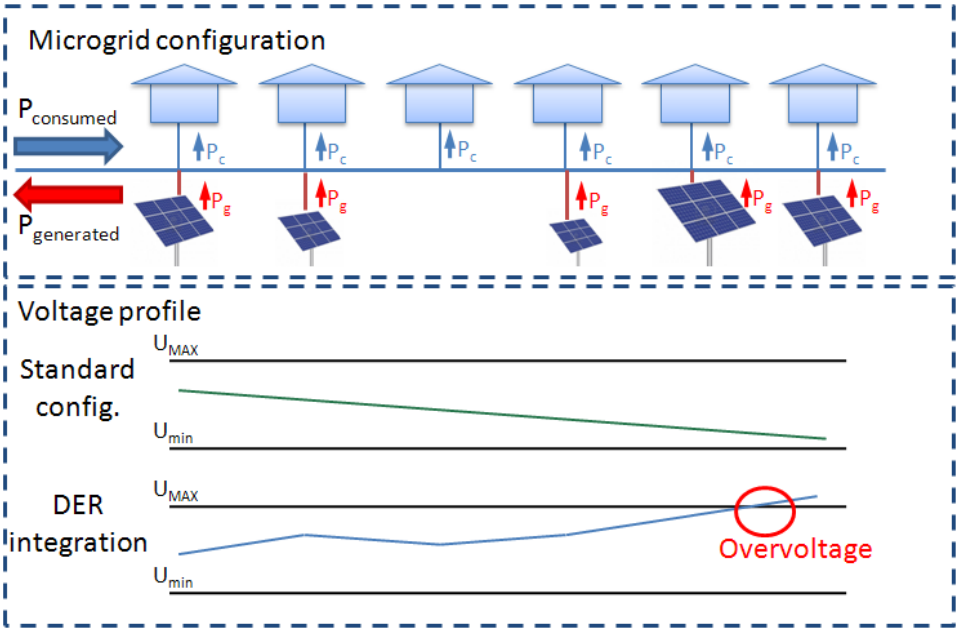

Fig. 3.1. Voltage profile in a low voltage distribution grid.

will disconnect and others they will just break down or burn their circuitry [IEA2009].

The main issue, as stated in [Vandoorn2011] and [Prodanovic2006] is that the electrical distribution grid was not designed with bi-directional power flow in mind, i.e. that not only would power flow to the lower voltage levels where most consumer are connected, but that it could also flow "up" to the higher voltage levels away from the consumers.

The increased amount of PV plants in the distribution grid introduces some complications, such as the fluctuating nature of PV production which has limited predictability. There are fast fluctuations, due to cloud transients, which cause problems with voltage regulation. There are also slower fluctuations due to the movement of the sun and changes in cloud cover, so if the PV plant generation is not coordinated with the local consumption it might be necessary to invest in more grid capacity as presented in [Ueda2007].

The distribution grid does not only see an increase in renewable energy production, there is also a foreseeable increase in new types of loads, such as heat pumps and electric vehicles, both loads that can to some degree act as flexible loads as shown in [Madureira2009] [Koch2011].

If loads that are flexible can be intelligently managed, it could be possible to help the distribution grids to cope with both increased renewable production and increased loads. Furthermore, this intelligent control could also reduce the need for expensive grid extensions if loads and production are coordinated locally.

3.1. Problem statement

The present work is not focusing on power system design or overall control of the grid on large scale; it proposes a number of control strategies on the consumer level of load control with respect of local measurements and voltage limitations. The controllers do not poses knowledge on the electric grid parameters as impedance or reactance and they operate on voltage measurements taken from the consumer's bus bar, where the household is coupled to the distribution grid as shown in figure 3.2.

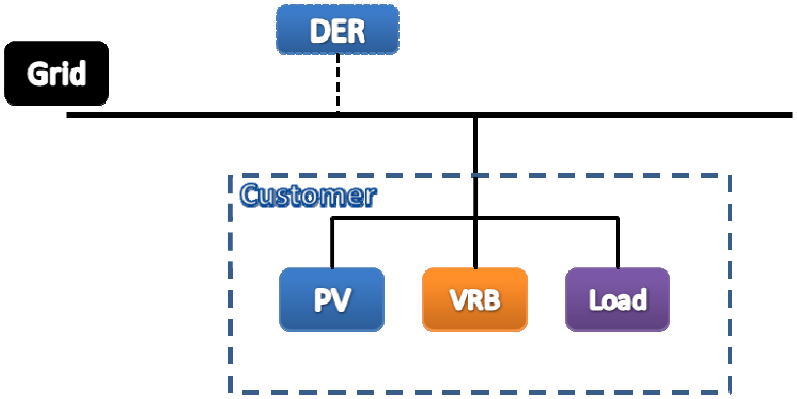

Fig. 3.2. Consumer grid connection diagram.

The power system which is the subject of the study in this work is represented in figure 3.2. The customer is represented as having loads, a renewable energy source, most common a PV system installed on the roof top, and a storage device, usually a lead-acid battery, but others can be also considered as the following methods and studies propose.

A consumer, in this case a household, is connected to the low voltage distribution grid at a certain point along the feeder. Along side the feeder other consumers are using power and distributed energy resources are injecting power into the grid altering the voltage profile at the common coupling point of the customer. This fluctuation is unpredictable due to different consumers' behaviour and to the varying weather conditions as solar irradiance and wind speeds.

In this thesis the approach taken is to develop control strategies at local consumers' level that have no information about the status of the larger power system as configuration or different parameters, at matter of fact no information about the feeder configuration on which the consumer is coupled. The available information is the voltage at the point of common couple.

3.2. Voltage profile control

In this section a study on the voltage profile of a local configuration in a distribution grid configuration is conducted. For the study, the simulations were conducted in the specialized Power Factory software from DigSILENT Company. The simulations are using the distributed energy resources (DER) models that were developed and presented in Chapter 2.

The setup consists on three buses connected through two long feeders. At one bus the local grid is connected to the distribution grid. In the second bus, in the middle, a storage device is simulated. The storage device is the vanadium redox battery (VRB) described in chapter 2, section 2.2. At the last bus both a load and the PV plant modelled in section 2.1 are placed.

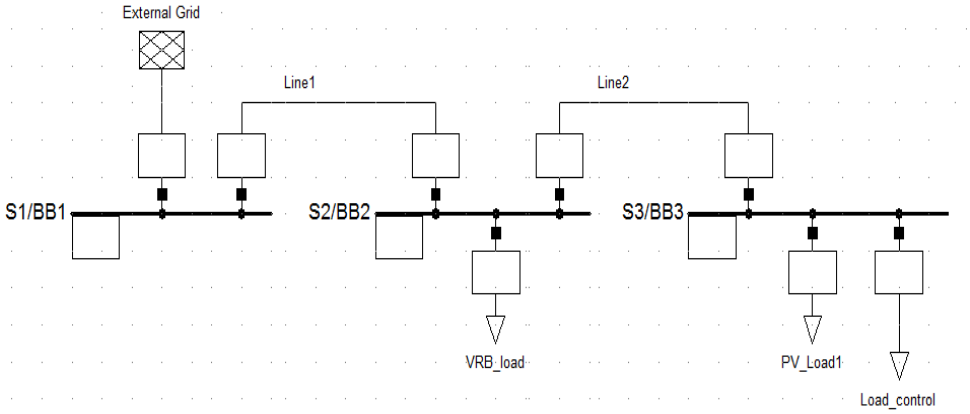

Fig. 3.3. Low voltage grid configuration.

This study reproduces an experiment where the VRB controller is set to maintain a constant output power from the local system to the grid during operation.

The grid is assumed to be stiff and without variations, so the voltage at bus1, the connection point between the local grid and the distribution grid is constant.

Further, two cases are considered for busbar 3:

a) a constant load of 1kW and a PV modelled as in section 2.1

b) a PV installation modelled as described in section 2.1 and a variable load that is used to maintain constant voltage at bus3.

For the two cases, the voltage profiles of the three busses of the local system are shown in figure 3.4.

At the first bus bar (BB1), the voltage will measure the voltage of the grid; in this case, as the grid is considered stiff, the voltage will remain constant.

At the second bus bar (BB2), where the VRB is connected, the injected power to the grid will remain at a constant value, as the VRB controller is set to do, and consequently, the voltage difference between BB1 and BB2 will be kept constant, and so, the voltage will remain constant at BB2.

This is valid for both cases, as the battery is used to absorb any excess power from the local grid and inject a constant power to the distribution grid. The difference between the two cases comes from the voltage evolution of the third bus bar (BB3): in the first case the voltage fluctuates according to the PV output power variation as it rises with the increase of PV production.

In the second case, the produced PV power is locally consumed by a shiftable load. The load is equipped with a PI controller that regulates the power consumption in order to achieve the desired voltage at the busbar. This load is a unspecified type of loads as, at this moment, the purpose of the simulation is to see

a) VRB voltage control b)local consumption of PV power

Fig. 3.4. Voltage profile at the three buses during operation.

a qualitative effect of power flow over voltages at different locations of the power grid.

Figure 3.5 represents the evolution over the operation interval of the simulation considering the first study case.

The first plot represents powers:

- the constant 1 kW load connected to the BB3
- the power injected into the distribution grid at a constant value at BB1
- the PV output power produced under weather conditions measured at 15 September 2011, presented also in chapter 2
- the VRB output power used to balance the output power to the grid

The second plot represents the state of charge (SOC) of the VRB during operation.

The third plot presents the bus voltages for the three busbars during 24 hours simulation, under weather conditions taken from measurements for the day of 15 September 2011.

During the simulation, 3kW are constantly injected into the grid at BB1 and a 1kW load is consuming power at BB3. At the start of the simulation, the only source of energy in the local grid is the VRB which supplies power for both BB1 and BB3. The VRB is discharging as it can be seen in the SOC plot. At this moment BB2, where the VRB is connected, has the highest voltage level as the power flows from this bus to the grid and to the load. This voltage profile is shown in the third plot of figure 3.5.

As the PV plant starts to produce power, due to solar irradiance, and to inject it into the grid, the voltage at BB3 will increase. As the VRB controller is set to maintain the BB2 voltage at a constant value, it starts to accumulate the excessive energy, as seen in the state of charge plot. The voltage profile fluctuates at BB3 as presented in figure 3.4.a.

In the evening, when the PV production drops under 1kw, the needed power for the 1kW load is again taken from the VRB. As the sun sets, the VRB becomes again the sole energy producer and has to supply both the grid and the load.

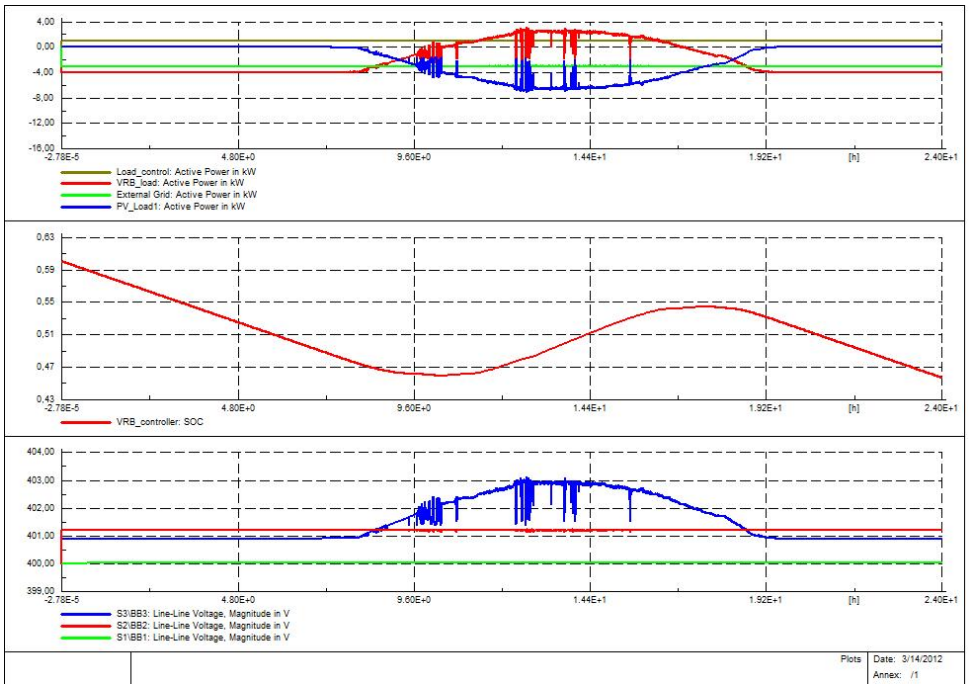

Fig. 3.5. Electric measurement during VRB voltage control operation

Figure 3.6 graphically represents the second case when a load control is implemented in order to consume the produced power in order to maintain the bus voltage at a certain prescribed value. The load control is implemented as a PI controller that reduces the difference between the reference and the measured voltage.

As in the first case, the plots are representing the powers, the state of charge of the vanadium redox battery and the voltages at the three busbars.

One can see that the voltage profile is rather constant during operation, as in figure 3.4.b. Also little energy is transported from bus3 to bus 2 as one can see from the small variation in the VRB's state of charge. This, almost residual, power from the bus3 is due to the fact that weather measurements that affect the PV output power are taken at a one second interval and they can present large differences from one reading to the next as shadows are cast on the PV panels which affect the controller's efficiency. In this case the measurements are slower that the process changes and the controller is unable to react with better performance, that is to follow the quick variations of the PV output.

As power flows from high voltage to low voltage, by imposing the voltage profile from figure 3.4.b on the system, the load controller will also produce power in intervals that the PV installation is not injecting enough power. This load can be considered, in this case, as being a mixture of loads and power generators, as diesel generators, in order to achieve an energy independence of the local grid as well as having the possibility to sell the surplus energy to the distribution grid.

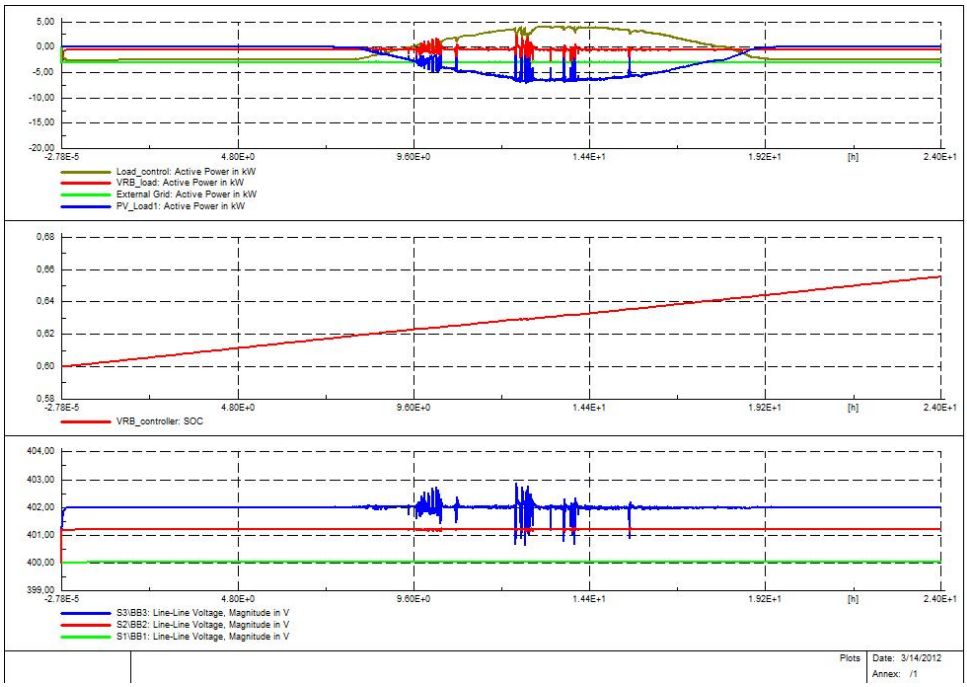

Fig. 3.6. Electric measurement during VRB voltage control and load control operation

3.3. Voltage control by load shifting

As seen from the study in the last section, an efficient way of controlling the voltage is to control the power consumption at the current bus.

In this section simulations are presented that consider the model of the SYSLAB microgrid, presented in Appendix A. From the SYSLAB infrastructure, accurately modelled as a PowerFactory line diagram as shown in figure 3.7, a microgrid is formed with two buses and feeder. At one bus, the distribution grid is connected and at the other bus both a PV system, as described in section 2.1, and a house model as presented in section 2.3. For representing the house as a grid consumer the thermal model is used and the loads are represented by the ten 1kW electric heaters.

The feeder is considered as having 1.4 km, as it runs through all the feeders and the buses of the modelled facility. This distance over the resistive feeder allows the voltage at the second bus to fluctuate and both the effect of power injection disturbance and the voltage controller response are easier to be seen. At the grid bus, the voltage is kept by the grid and a shorter feeder to bus2 would mean that the influence of the grid would be greater at the second bus.

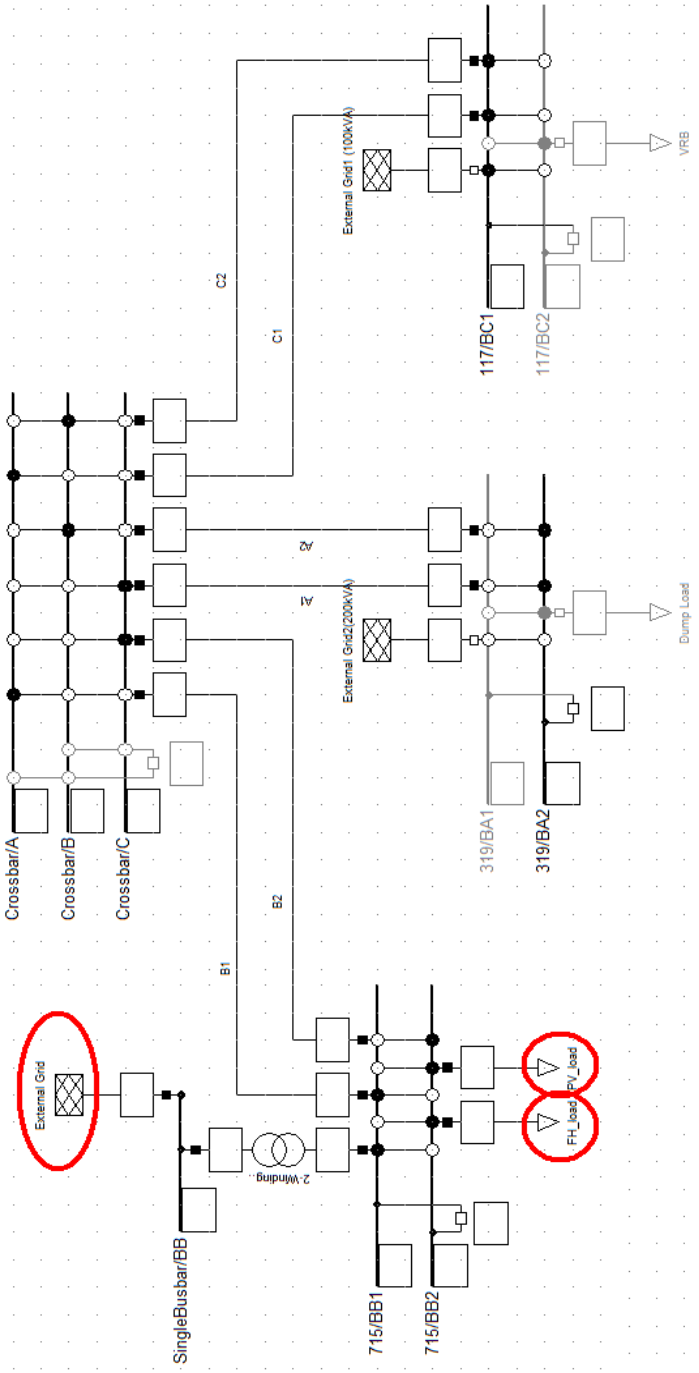

Fig. 3.7. One line diagram of the studied microgrid based on SYSLAB infrastructure

The PV plant at the bus bar BB2, that is named PV_load in the system diagram presented in figure 3.7, is the same as discussed in chapter 2. It produces output power according to the weather conditions. In the simulations the weather measurements were taken from the local station, having a one second measurement interval.

The house is represented in Figure 3.7 as FH_load. The house represents the load of the microgrid and it consists in the heating system loads, the electric heaters. For the house was used the model described in section 2.3, which is a thermal model of FlexHouse, the testing building from the SYSLAB facility.

The overall Flexhouse controller is presented in the block diagram from figure 3.8; these blocs represent:

- FH_ThermalSlot – contains the mathematical equations of the thermal model of FlexHouse; the inside temperature in the building is influenced by the solar irradiance and outside ambient temperature as well as by the electric heaters
- FH_InputMeasurementsSlot – reads the weather conditions, the solar irradiance and ambient temperature, stored by the local weather station
- FH_MeasSlot – is a voltage probe that measures the voltage at the bus bar where the house and PV are connected
- FH_load – is the controlled load seen in the one line diagram which represents the power consumption of the electric heaters inside the FlexHouse
- FH_Controller – is the developed controller slot; the controller's diagram is presented in figure 3.9.

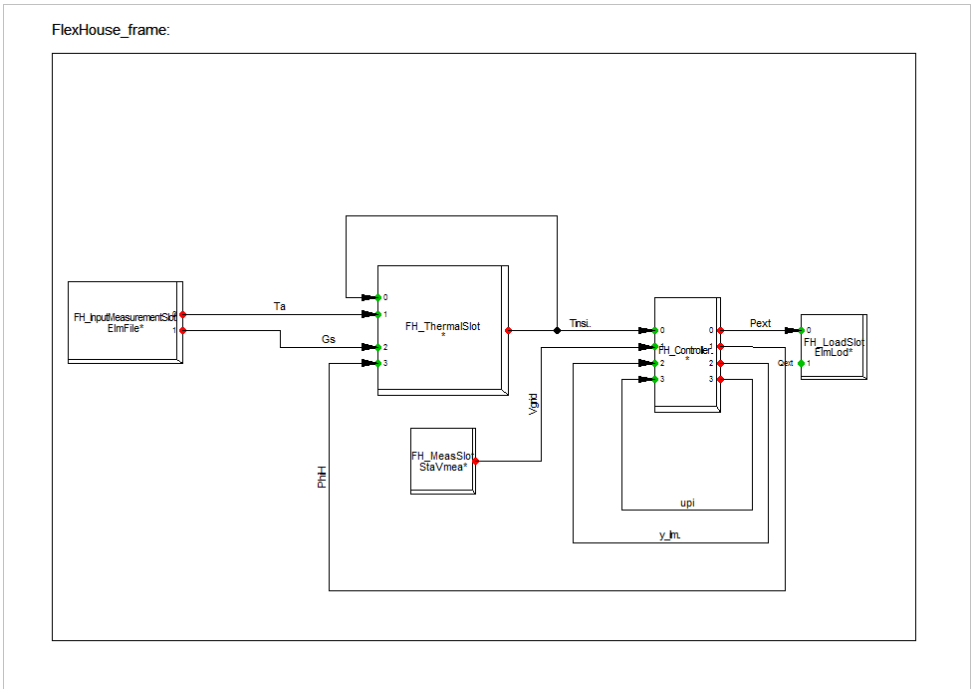

Fig. 3.8. Controlled load circuit diagram

The diagram presented in figure 3.8 represents the frame needed in PowerFactory in order to define a 'composite' model and connect all the components. The composite model will contain a table of cross reference between the slots defined in the frame and the 'common models'.

The common models are objects of a certain defined type which have the inputs and outputs used in the frame's definition. These common models will have numerically defined parameters for the specific simulation.

The only slot that is visible in the simulation, and is connected in the one line diagram is the FH_Load which represent the electrical heaters.

Two simulation scenarios were studied:

- a temperature control that maintains the inside temperature at a certain reference (Tmp_ref))
- a thermostatic control that maintains the inside temperature inside a given range with regard to the bus voltage.

Both cases are intended to study and develop local voltage control techniques at the consumer level.

The FlexHouse controller used in these simulations are presented in figure 3.9. It was develop to include both types of controllers and the possibility to switch between then.

For the first study case a PI controller was used to maintain the temperature at a constant value, as presented in the graphical representation of the simulation results from figure 3.10.

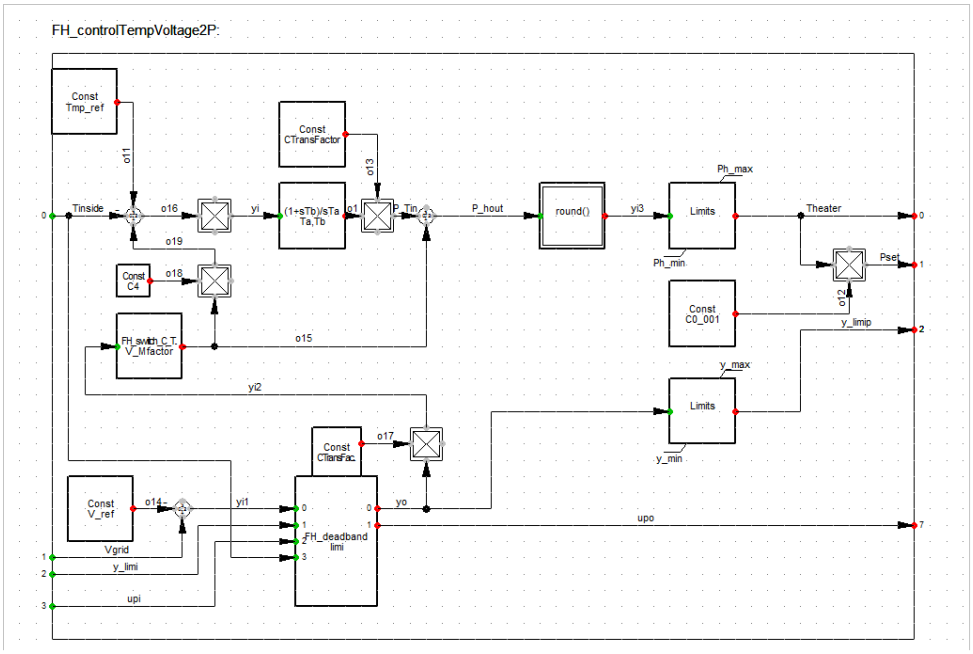

Fig. 3.9. FlexHouse heaters controller diagram

A round function is used to transform the controller's command to the heaters into integer numbers, for operating the ten 1kW electric heaters. Further

on, the command is limited to the available output power between 0 and 10kW. A coefficient is used to scale the command to the load's active power set in the one line diagram.

The second controller is a modified thermostatic controller whose operation is overwritten when an over voltage is measured at the bus bar, by connecting additional loads (heaters) to the local grid.

The controller sequence is written in DSL (DigSILENT Simulation Language) using some specific functions:

$$select(bool, X, Y) = \begin{cases} X, & bool = true \\ Y, & bool = false \end{cases}$$

$$\lim(X, min, \max) = \begin{cases} min, & X < min \\ max, & X > max \\ X, & min \le X \le max \end{cases}$$

$$flipflop(boolset, boolreset) = \begin{cases} 0 \to 1, & boolset = 1 \; and \; boolreset = 0 \\ 1 \to 0, & boolset = 0 \; and \; boolreset = 1 \end{cases}$$

The controller code is presented in the following:

T_{max}=21
T_{min}=19
X=flipflop(T_{inside}<T_{min},T_{inside}>T_{max})
H_{out}=select(X=1, yi2+0.01, yi2-0.01)
Y_o=select(yi1>limi, yi2+0.01, select(yi1<limi-0.004.and.upi=1, yi2-0.001, H_{out}))
U_{po} = select(yi1>limi, 1, select(yi1<limi-0.004.and.upi=1, 0, upi))

This controller was also implemented in Matlab and a state flow diagram is presented in figure 3.12.

Basically, what the controller does is to maintain the output power of the heaters until a temperature limit is reached. If the upper limit is reached, the controller disconnects one heater and waits for the effect; the algorithm is repeated until the inside temperature remains under the upper limit, in the comfort zone, or all the heaters are turned off.

The same algorithm is used in the case that the lower temperature limit is reached: the heaters are turned on one at a time until the temperature remains inside the comfort zone or all the heaters are turned on.

If an over voltage is measured at the bus, the controller overwrites the above described states and increments the output power in 1kW steps until the voltage is at a convenient value or all the heaters are turned on.

The simulation results for using the two controllers are shown in figures 3.9 and 3.9. The plots have the following signification:

- the first plot presents the solar irradiance values (in kW/m^2) for a simulation time interval of six days
- the second plot presents the outside ambient temperature for the considered days

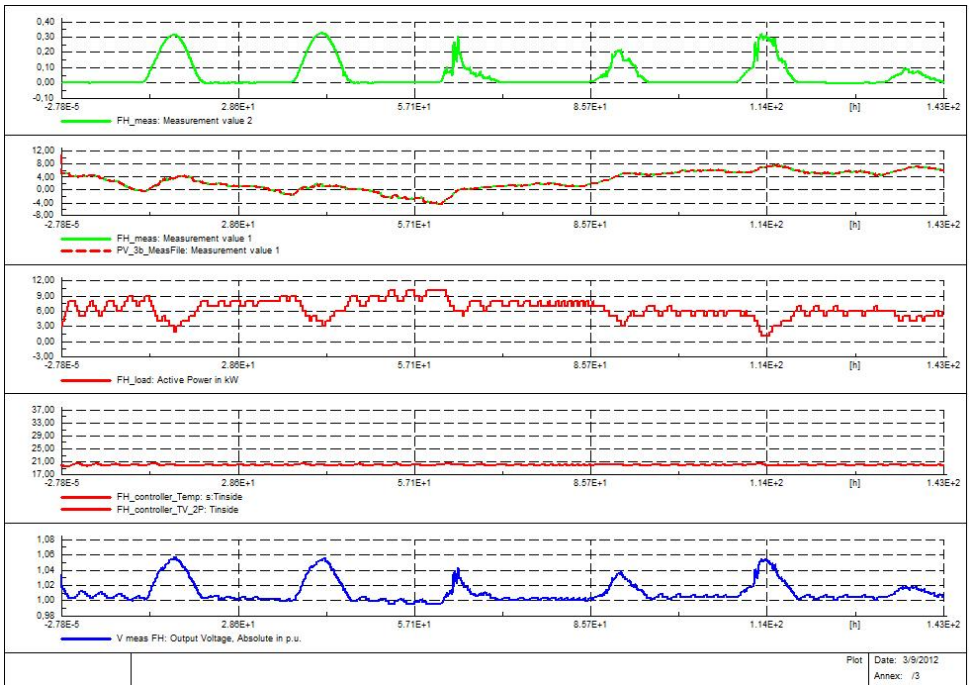

Fig. 3.10. Simulation results when using a constant temperature controller

- the third plot represents the electric heaters output power as they are commanded by the controller
- the fourth plot presents the inside temperature in the FlexHouse
- the fifth on shows the voltage at the consumers bus, in per unit values

Figure 3.10 shows the results from the first simulation, which maintains a constant temperature inside the FlexHouse for the entire simulation interval, as seen in the fourth plot.

The electric heaters' power consumption is seen in the third plot. One can see that during mid day, when the solar irradiance is heating the house walls and windows and implicitly the inside of the house, the heaters' consumption diminishes. Also during this moment of day the PV panels are injecting power into the local grid at the point of common coupling. The injection of power form one hand and the decrease in consumption on another hand has the effect of raising the voltage at the connection point, as illustrated in the fifth plot.

This increase in voltage over an admissible value will generate the protection mechanisms to trigger and to disconnect different electric equipment from the bus bar.

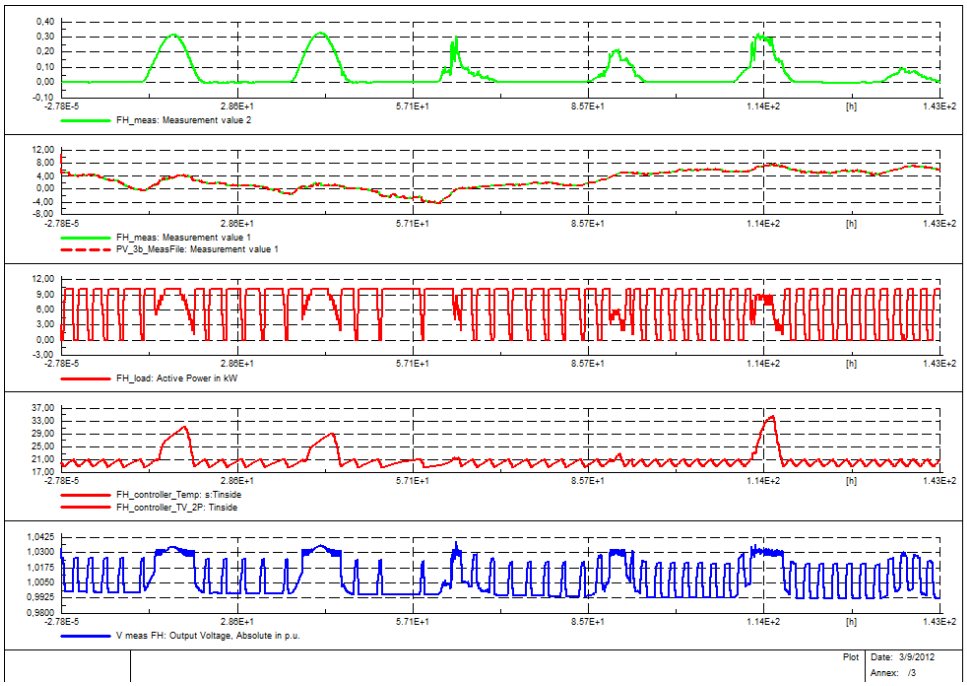

Fig. 3.11. Simulation results when using a modified thermostatic controller with over voltage protection

Figure 3.11 presents the simulation results when using a modified thermostatic controller with overwrite for voltage protection. In this case one can see that the inside temperature, fourth plot, is maintained at the preset temperature [19…21] during most of the time interval. However, when the injected power from the PV installation increases at mid day, the heaters are turned and maintained on, despite the fact that, as highlighted in the first case, at this moment the sun also has a heating effect on the house and the consumption would normally be lower.

The fifth plot shows that the voltage is kept below 103% of the nominal voltage also during PV production, keeping the heaters on but increasing the inside temperature high above the thermal comfort zone.

In the next chapter this problem will be again tackled and an advanced control algorithm will be implemented and used to shift the load, the electric heater consumption, to intervals with PV production also keeping the inside temperature between comfort limits.

3.4. Voltage control by using a finite states machine

The thermostatic controller presented in the last section was further developed in Matlab/Simulink by using the StateFlow toolbox. The controller was designed as a finite state machine having the schematic presented in figure 3.12.

The control algorithm consists in three main states:

- *Tcontrol* – the thermostatic control state; it is responsible for maintaining the inside temperature between certain comfort limits. This state contains three substates:

- *same* state – in this state the current output of the controller (PH) is equal to the last output (Pi); in other words, the controller's output remains the same as before

- *on* state – this state is responsible for turning on an additional electric heater at each state entry; the state is activated by two transitions: firstly, when the inside temperature is below the comfort lower limit (Tmin) and the second one is basically a loop that is made each 100 time-samples; if after this 100 time samples interval the transition condition from state 'on' to state 'same' is not validated, the 'on' state is re-entered and an additional heater is connected. The condition that the inside temperature is higher than the minimum temperature implies that the heaters output power should be kept constant as the system operation translates to state 'same'

- *off* state – is the state responsible for turning off one electric heater at a time. The operation and transition at the 'same' state is identical to the one presented for the 'on' state with the sole difference that this state refers to the upper comfort limit and so, the referred limits are Tmax

- *VOver_control* – is the state activated when the measured voltage at the bus is over the maximum set voltage. The objective of this state is to decrease the voltage by increasing the consumed power – for this case, this translates by connecting additional heaters. At each state entry, an additional heater is turned on. The state is entered when the voltage is higher that the maximum bus voltage and repeatedly entered after 35 time samples, due to the loop, until the voltage is lowered below VmaxLow, which is defined below, and a state transition occur to the 'Tcontrol' state.

- *VUnder_control* – is the state activated when the measured bus voltage is bellow the minimum set voltage. It operates similar to the state 'VOver_control' with the difference the transitions are related to the minimum voltage value and the heaters are turned off at the entry in this state in order to reduce the consumption and increase the voltage.

The state machine has internal parameters as the prescribed limits of the temperature and voltage:

- *Tmax* – the maximum limit of the thermal comfort interval
- *Tmin* - the minimum limit of the thermal comfort interval

Intended to eliminate the oscillations in the control process of the electric switches, deadband intervals were defined as below and a graphical representation is shown in figure 3.14 representing the conducted experiment's results:

- *VmaxHigh* – is the upper limit of the bus voltage at which the controller is designed to increase the power consumption that is to connect more heaters
- *VmaxLow* – a dead band is define as the voltage level at which the controller switches from the over-voltage control state to the thermal control state
- *VminHigh* - a dead band is define as the voltage level at which the controller switches from the underr-voltage control state to the thermal control state
- *VminLow* - is the lower limit of the bus voltage at which the controller is designed to reduce the power consumption; that is to disconnect more heaters

as well as input measurement signals:

- *Tinside* – the measured inside temperature of the FlexHouse
- *Vbus* – the measured voltage at the FlexHouse's bus bar
- *Pi* – the output power of the electric heaters at the last sample time

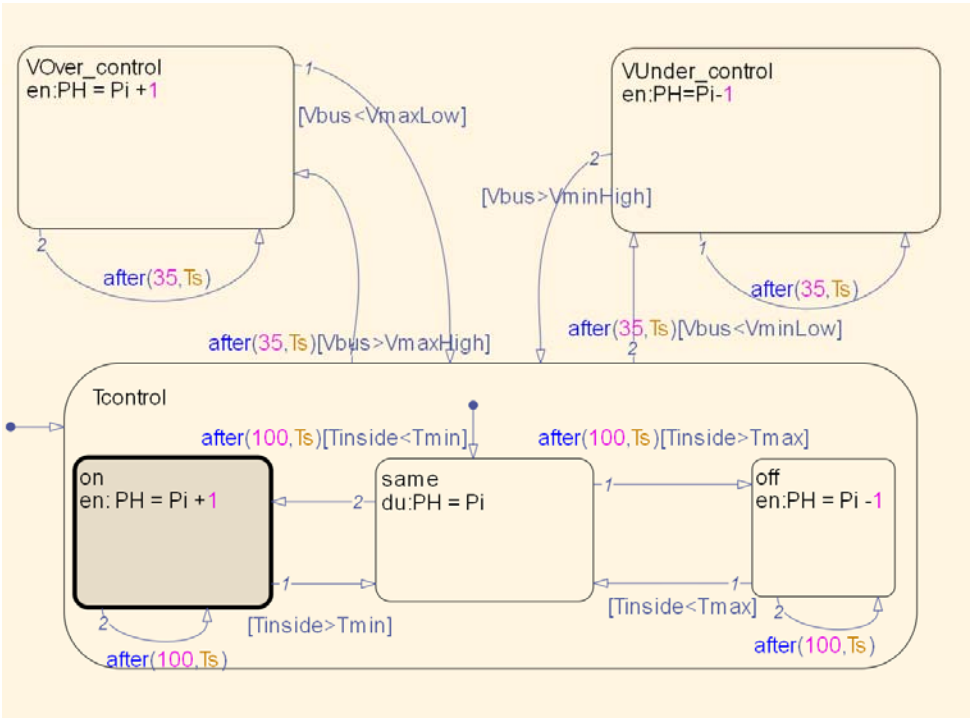

Fig. 3.12. Finite states machine diagram

and an output signal

- *PH* – represents the electric heaters output power commanded by the controller

For the controller, the time sample (Ts) is considered to be 1 second.

Due to large time constants of the thermal process the electrical heaters' effect on the inside temperature can be measured, with the available devices, after a few seconds.

Figure 3.13 shows the Matlab/Simulink line diagram of the finite state machine used with the thermal model of the FlexHouse presented previously in section 2.3. Here one can see the inputs and outputs of the overall system. This configuration was used both for simulation and for experiments.

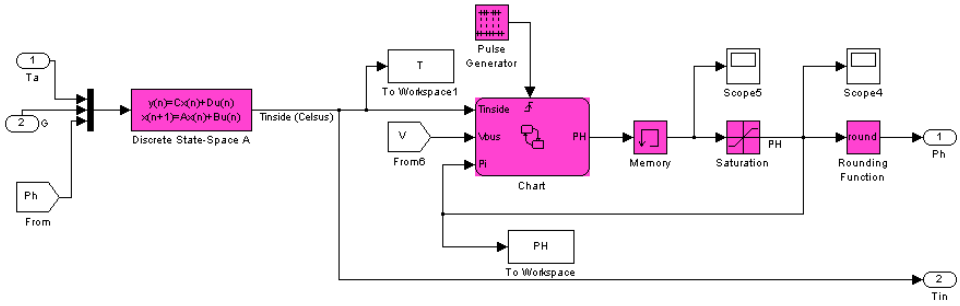

Fig. 3.13. FlexHouse state machine control diagram

An experiment was conducted to test the algorithm at the SYSLAB facility. The SYSLAB configuration used in the experiment is accurately represented in the one line diagram of figure 3.6, and presented for the simulation study described in section 3.3.

For altering the voltage at the FlexHouse bus bar in the experiment the vanadium battery was connected at bus bar BC2, as seen in the facility's diagram, figure 3.7. The VRB was used both to inject power into the grid along the feeder and thus raise the voltage, and also to consume power; thus disturbing the voltage profile along the feeder, the control algorithm was tested for both over and under voltage conditions.

Figure 3.14 represents the experimental results. The first plot shows the electric heater's consumed power, the second plot represents the inside temperature and the third one, the voltage at the FlexHouse bus bar.

One can see in the third plot all four voltage limits: the maximum and minimum set voltage for the current bus bar as well as the two limits defining the dead band responsible for stabilizing the system and avoiding oscillations as defined above.

The events that trigger state transitions in the plots are marked with coloured circles. The marks in the first plot correspond to the controller's reactions and are the effect of the voltage limit intersection with the voltage at the house's bus bar, seen in the third plot:

- red circles represent events when the bus bar voltage is reaching the upper limit; as a consequence, the controller connects electrical heaters until the voltage reaches a safe limit, VmaxLow
- blue circles represent events when safe voltage limits are reached and the controller turns back to the 'Tcontrol' state; these events correspond with the voltage exceeding the dead band imposed in order to prevent oscillations at the limits;
- green circles represent events when the lower voltage boundary is reached; in this case the controller turns off heaters to lower the power consumption; when enough heaters were turned on and the voltage is in safety limits, the controller changes the state to 'Tcontrol'

The results prove the concept of controlling the voltage profile by using the heating system as using the electric heaters' power consumption when the voltage at the bus bar is due to power injection from other sources.

One shortfall of this method is the fact that the inside temperature can exceed the comfort limit and could not be used any more; other types of loads can be used or in the case that the injected power along the feeder, that produces the increase in voltage, comes from a local installed renewable energy source as PV or wind turbine, the inverter that connects the RES to the grid can be set to inject reactive power into the low voltage grid instead of active power. In low voltage grids, where the R/X ration is higher than one, this will lead to smaller increases in the local voltage.

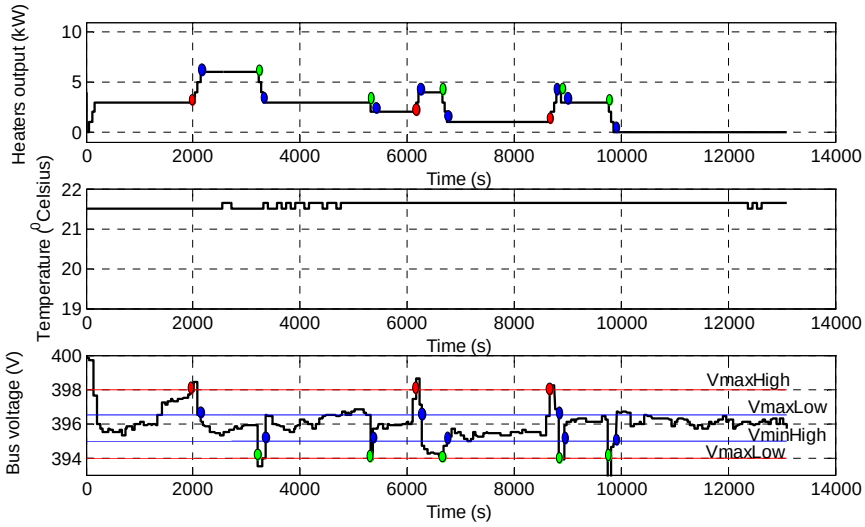

Fig. 3.14. Experimental results of using load shifting for voltage control

3.5. Voltage control methods applicable in low voltage grids

This section presents an overview on three proposed control algorithms for controlling the bus bar voltage at the connecting point of a household at the local low voltage grid.

The simulations consider the following assumptions:

- The system configuration is depicted in figure 3.2: the consumer is connected to the grid along a feeder; at the consumer level there are renewable energy sources, in the form of PV system, loads, represented by the electric heaters, and an energy storage device, represented by the modelled VRB.
- The loads at the consumer level are represented only by the 1kW output power electric heaters
- 1kW modifies the voltage with +/- 0.5%
- The voltage is in per unit (p.u.)
- For all the simulations, a thermostatic control like the one from figure 3.15 is used the control the inside temperature of the FlexHouse; this controller runs independently of the PV or VRB
- The simulation time step is one second equal to the time sample of the weather measurements; for the controller, Ts is chosen to be equal to 10 simulation steps – this can be changed, and should be enlarged during an experiment

- The VRB is discharging during the night
- For the VRB capacity, instead of 190kWh which was the real battery subject to modelling in section 2.2, this section considers a 20 and 10 kWh capacity battery that would be used for an individual consumer.

The proposed thermostatic controller was developed by using a finite state space machine as shown in figure 3.15. Unlike the classical thermostatic controller that has two states: all heaters on – when the lower temperature limit is reached and all heaters off – when the upper limit is reached, the proposed controller has three states, as explained in section 3.4.

By including an additional '*same*' state, the controller is able to achieve a more constant consumption over time, without having the large variations between zero and full power as in the case of a classical thermostatic control, as it is seen in the simulations presented in the following.

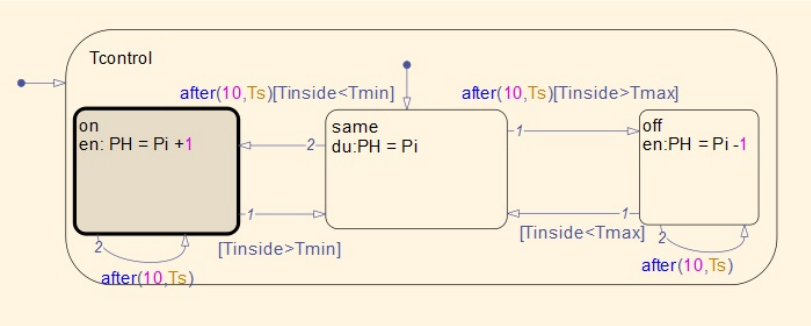

Fig. 3.15. Thermostatic control.

The circuit diagram used in simulations is presented in figure 3.16. It uses the models developed for the PV plant, FlexHouse and vanadium redox battery that were presented in Chapter 2.

The output powers were connected to the same bus with an additional disturbance on the grid voltage and considering the above mentioned assumptions.

Four simulation cases were investigated:

1. *Normal operation*

- Due to the PV output, the voltage increases over the limit and the PV inverter shuts down.

2. *Voltage control by load shifting*

- the thermostatic control from figure 3.15 is overwritten by states that maintain the voltage between limits as a priority, disregarding the inside temperature
- when the voltage is reduced, the thermal controller is again activated.

3. *VRB control: voltage control mode*

- will charge the battery only when the PCS's output terminal voltage exceeds the set point. If the voltage is always lower than the set point, the battery will never be charged.

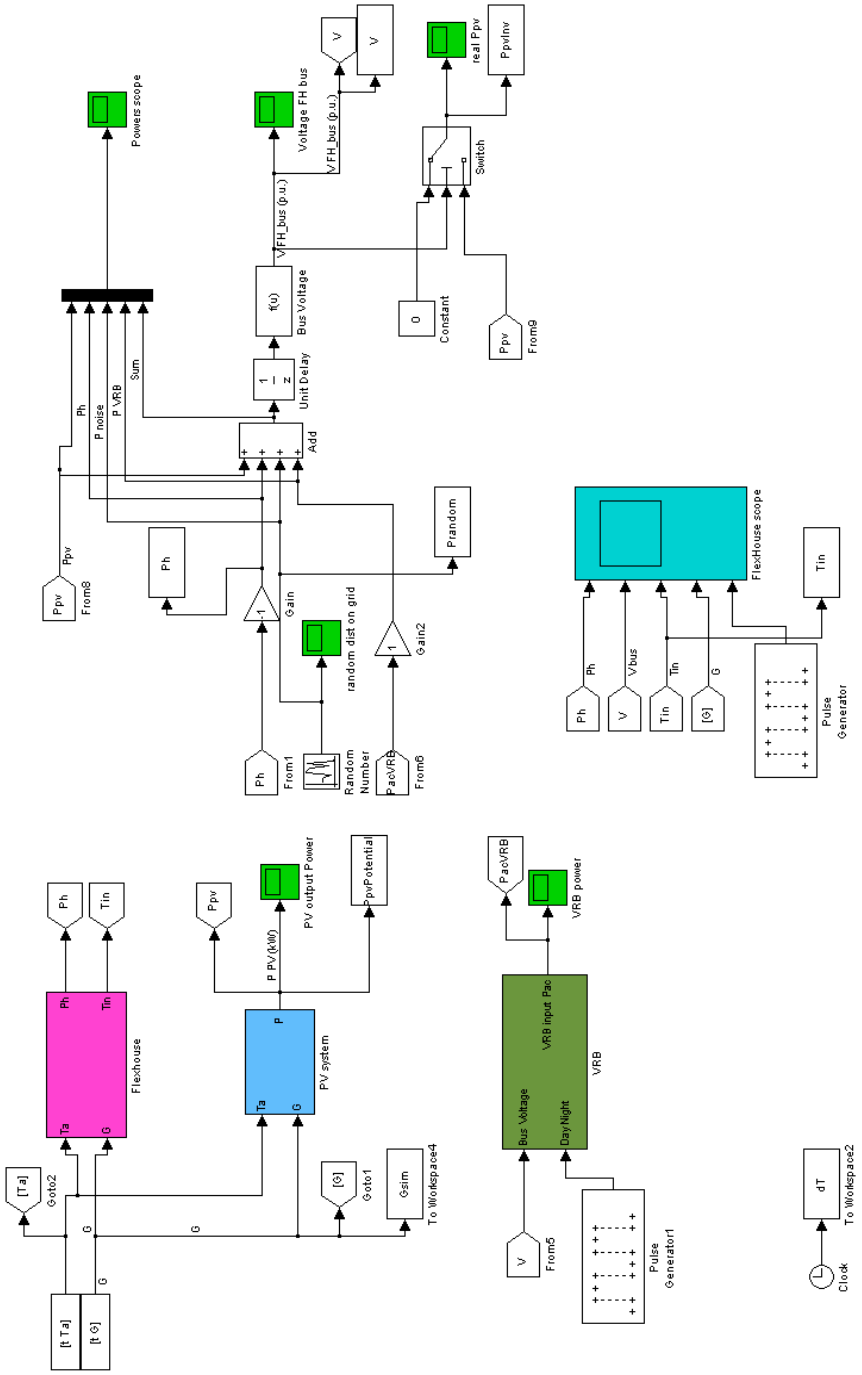

Fig. 3.16. Low voltage grid simulation diagram

4. VRB control: schedule mode

- will charge the battery based on the schedule. For example, battery will be charged from 10:00 to 18:00 everyday regardless the voltage. Since most of the over voltage occurred in between 10:00 to 18:00, this mode can avoid most of the output energy loss. The charge sequence is [-1 -4 -4 -1] kW, changed at two hours time interval.

3.5.1. Normal operation

In figure 3.17 the simulation results are shown of a six day period interval when only the thermostatic control is used and no voltage control is implemented.

In the first plot are displayed the measured bus voltage at the coupling point, in the blue line, and the maximum voltage limit with a green line. The voltage at the coupling point is influenced by the power consumption, which lowers it, and the power injection due to the PV system production.

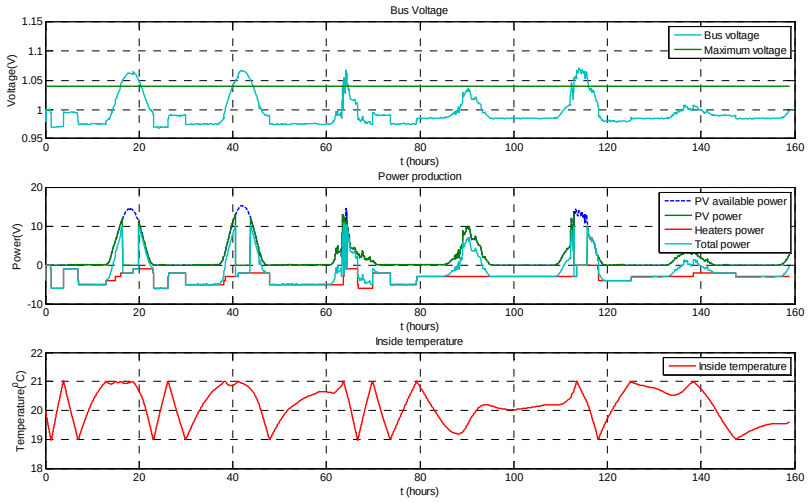

Fig. 3.17. Normal operation scenario

The second plot represents powers:

- The available PV power – the power that the PV installation is able to produce given the current weather conditions
- The PV output power – the actual power produced by the PV system; when the bus voltage reaches the maximum value, the PV inverters disconnect and thus the PV system stops producing power
- Heaters power – the power consumed by the heaters using the thermostatic controller
- Total power – is the power that is moved at the coupling point between the grid and the local consumer; if this power is positive on the graphic, the power is injected in the grid, due to PV production, and if the power is negative, the power is consumed

The third plot presents the inside temperature evolution during the simulation interval while is kept inside the comfort zone of 19-21 degrees Celsius.

One can see the controller's actions of smoothing the power consumption of the heaters in the second plot which has the effect of a 'loose' inside temperature evolution inside the preset boundaries: for example, in the interval starting from the 80^{th} our to the 110^{th}, the heaters' consumption is constant and the inside temperature changes inside the limits as a result of weather conditions as the solar irradiance and outside air temperature.

The most important effect seen in this figure is the bus over voltage due to the PV power injection. As the injected power from the PV increases due to the solar irradiance during mid day, the voltage increases as well; when the maximum voltage is reached, the inverters are disconnecting the PV and the PV power production is stopped exactly when, otherwise, the largest amount of green power is available.

3.5.2. Voltage control by load shifting

Figure 3.18 presents the case discussed before in section 3.4 of using the electric heaters in order to increase consumption during high PV production intervals and lower the bus voltage to safe values.

As the voltage increases over the limit, the controller, presented in figure 3.12, is switching to the *VOver_control* state and connects additional heaters as seen in the second plot of figure 3.18; the increase in consumption lower the power injected into the grid (light blue line) and the voltage is kept under the maximum limit. This control, however, increases the inside temperature over the desired limits and is not practical.

In practice this control would not allow the temperature limits to be breached and the temperature control to be overwritten by voltage control because the thermal comfort is of great importance to the consumer and thus, other types of controls have to be developed.

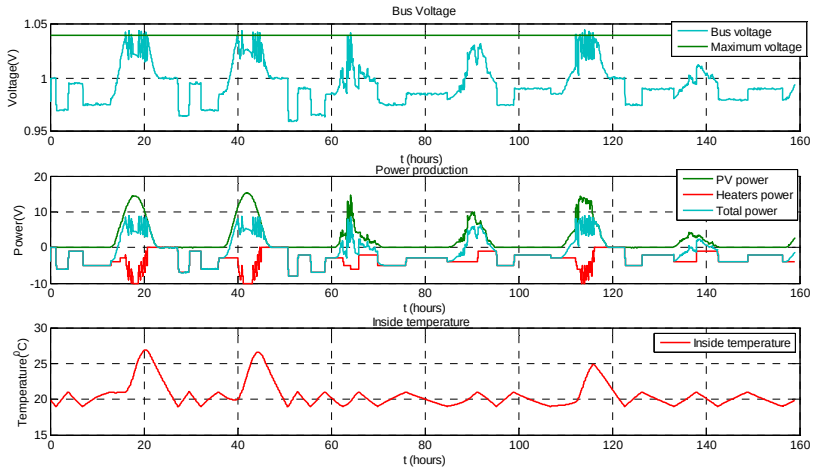

Fig. 3.18. Voltage control by load shifting scenario

3.5.3. VRB control – Voltage control mode

The problem with the electric energy is that it cannot be stored; it must be transformed in another kind of energy, two of which are used in this work: the thermal energy stored inside the building's capacity and chemical energy inside a battery, a vanadium battery.

For this study, the VRB model developed and presented in section 2.2 is used. The difference is in the capacity which is considered lower, 20kWh, as this case is for a single house usage.

The VRB's operation is defined as using the voltage control mode during day time, when the PV is able to inject power into the grid, and a constant discharge of 1kW during the night.

The voltage control mode is defined as the VRB operation mode when the battery is charging only when an overvoltage is detected.

In figure 3.19 an additional plot is introduced that shows the VRB's state of charge during the simulation interval.

One can see the same evolution of the heaters' consumption as in the first scenario, as the thermostatic controller is running in parallel with the VRB.

The difference is introducing the 'VRB power', seen in the second plot. The VRB is connected when an over voltage occurs and it consumes the excess power until the power injected into the grid is not affecting the bus voltage to exceed the voltage limit.

One can see form the state of charge plot that during cloudy days, when the PV production is low and no over voltage is manifesting, the VRB is unused.

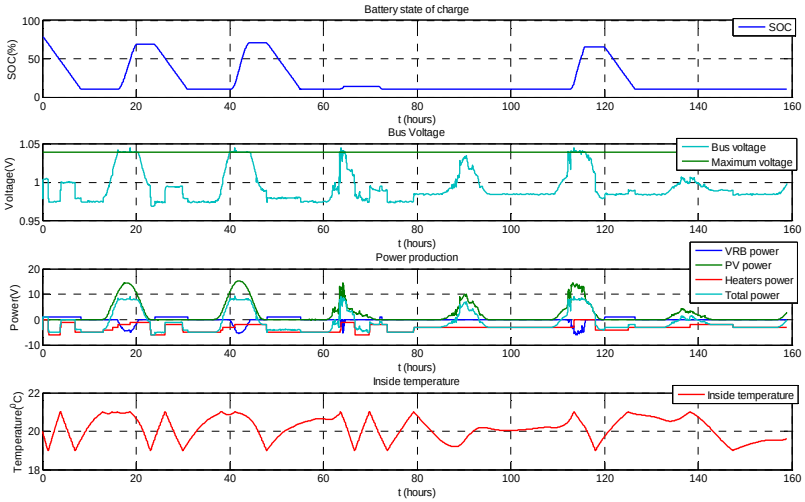

Fig. 3.19. VRB control – Voltage control mode scenario

If the VRB is not well defined, its capacity being smaller than a full day PV energy production, the battery will charge to its limit and fail to provide voltage control over the entire time interval.

This case is seen in figure 3.20: as the VRB is controlling the voltage by charging itself with the extra power from the PVs, it reaches maximum capacity; at this moment the over voltage occurs and the PV inverter is disconnecting as seen in the fourth plot, the green line representing the PV output power dropping to zero.

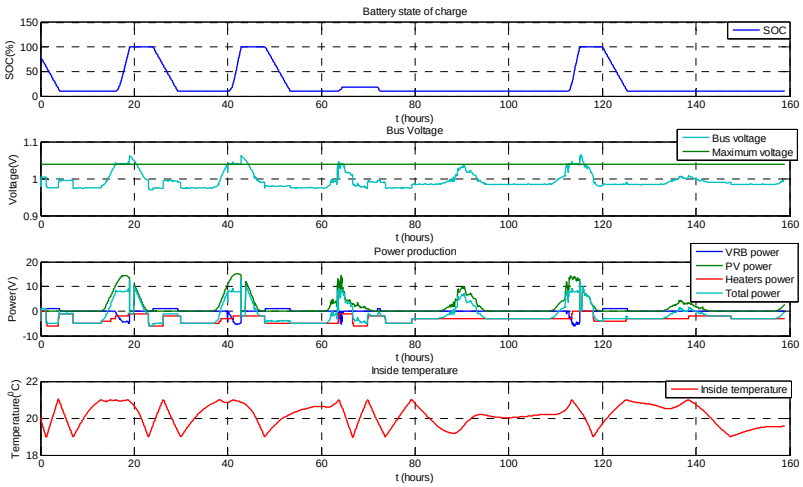

Fig. 3.20. VRB control – Voltage control mode with low capacity scenario

3.5.4. VRB control – Schedule mode

Another method of controlling the voltage with the help of the storage device is to set the VRB to run in schedule mode. Than means the battery is scheduled to operate regarding the weather conditions or voltage measurements: at predefined moments of the day, between 10:00 and 18:00, the battery is charging with a sequence of [-1 -4 -4 -1] kW, changed at two hours time interval and during the night it is discharging.

The simulation results of using a 20kWh VRB in schedule mode can be seen in figure 3.21.

This method is not requiring any voltage measurements on the bus bar; however, in order to operate in an efficient way, the VRB has to be appropriately scheduled of charging itself with the right amount of energy at mid day.

One can see that the state of charge has the same profile along for each day in the studied interval, as it runs independently on the over voltage manifestation on the bus bar.

Figure 3.22 shows the same schedule mode operation of the VRB in the case when the battery capacity is 10kWh, which is smaller than necessary for eliminating the over voltage.

In this case, the battery is charging at the preset intervals, but doe to the small capacity it is not able to operate during the entire mid day power production of the PV. As the VRB is reaching its full charge mode, the PV power is injected into the grid and thus the bus voltage rises over the limit; at this moment the PV inverter is disconnecting and no more power is produced.

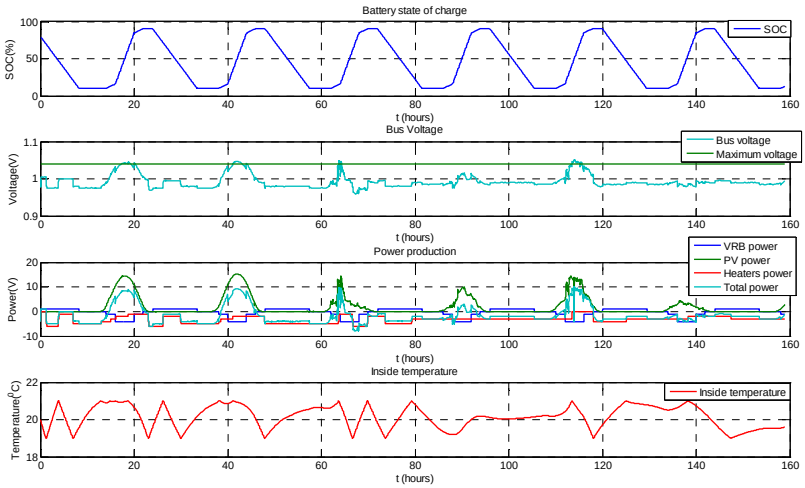

Fig. 3.21. VRB control – Schedule mode scenario.

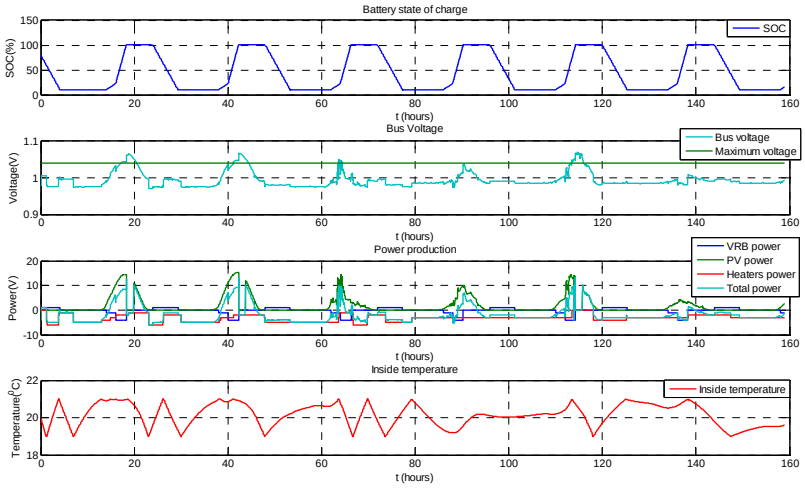

Fig. 3.22. VRB control – Schedule mode with low capacity scenario

3.6. Conclusions:

In the first part of the chapter is presented a study of the voltage profile along a feeder in a microgrid in the presence of a PV installation. From this study it is concluded that the voltage profile can be controlled by using energy storage

devices and shiftable loads that are able to store or consume the power injected by the renewable energy resources.

Further on, the chapter presents the development, implementation, and simulations of a proposed thermostatic controller designed as a state machine that operates with more constant power consumption that the classic thermostatic controller which turns all the heaters on/off at the same time. The proposed controller is affecting the voltage in a smaller way due to the 'smoother' consumption.

An extension of the state space machine controller with additional under- and over- voltage states, tested both in simulations and experimental scenarios, proved the possibility of using this type of controller approach in order to shift the loads, the electric heaters, to consume the excess energy at time when the bus voltage is reaching high values, especially during mid day, when the PVs are injecting power.

This controller has the shortcomings of having two sets of constraints that are hard to respect at the same time during the entire operation: the internal temperature constraints and the bus voltage limit constraints. The shortcoming comes from the fact that while the solar irradiance acts both on heating the inside of the house and on the increase of voltage due to the injected PV power, the controller uses the heaters to lower the voltage which also increase the inside temperature. From this perspective, some observations can be made for future development and improvement on the controller:

- The controller can be designed to use other electric loads that do not affect the inside temperature, like different household appliances, to control the bus voltage
- The controller can have states to set the PV's inverters to operate in different regimes: injecting reactive power into the grid instead of active power, which in low voltage grids has a smaller influence on the voltage, or to limit the amount of harvested PV power by moving the panel's operating power point away from the maximum, to a value that does not exceeds the voltage constraints – however, this is achieved with economic losses since the PV is operating far from the maximum available sun power;

Further study cases at the end of the chapter presented additional control algorithms when using energy storage devices as batteries. These batteries can be set to operate in various modes, as the chapter presents the voltage control mode and the schedule mode. One can conclude that the easiest way of storing energy is by using batteries and, if they are large enough, they will prevent all over voltages; however, this is the most expensive solution and more 'intelligent' solutions have to be developed in order to control the distribution grid voltage and to support the increase of RES penetration.

Load shifting is the right solution by which the loads are turned on when the local RES are producing energy. As a consequence, the consumer becomes more independent of the national grid which in return becomes more likely to avoid power grid congestions.

Implementing complex energetic solutions on customer level will enhance the power system stability starting from the distribution grid and will boost the profitability of the power system both on local and general level.

4. Model Predictive Control for an Energy Efficient Building

4.1. Introduction

The MPC algorithm is difficult to be attributed to a single individual since it appeared in different forms and contexts; however, among the first implementations of MPC in industrial applications was the work of Cutler [Cutler1980] developing the so called Dynamic matrix control (DMC) and of Richalet [Richalet1978]. All the model predictive control algorithms formulations are based on an explicit model of the process. The initial conditions for the MPC used to project the state values over the prediction horizon depend on the explicit model used to describe the plant. These early MPC formulations used finite-impulse and step-response models in order to predict future system states.

Generalized predictive control introduced by Clarke [Clarke1987] used autoregressive models as ARMAX and ARIMAX. In addition to the first generation of MPC, this approach allowed to specify the disturbance as a polynomial rather than a step change. The autoregressive models are still used due to the fact that simpler system identification algorithms are applied for model development. Such models are used in the work of [Huusom2010][Huusom2011].

State-space formulations of MPC were proposed later by Marquis [Marquis1988] Kwon [Kwon1988] and Rawlings and Muske [Rawlings1993]. In these formulations, disturbance rejection and offset free control is achieved by augmenting the state-space with integrating characteristics. This is the most common representation of a process, as in [Beccuti2009] [Begovich2007] [Joosten2008] [Mariethoz2008] [Prasath2010] [Zarkogianni2011] and almost exclusively in building control as in [Balan2010] [Bemporad2002] [Chen1996] [Chen2002] [Halvgaard2012] [Henze2004] [Hazyuk2012ab] [Kumert2001] [Ma2009, 2010, 2011, 2012] [Nagai2002] [Oldewurtel2010, 2012] [Pannochia2003] [Privara 2011] [Wu2008] [Koch2012a] [Koch2012b] [Xie2009] [Zong2011] [Zong2012] [Braun1990] [Kolokosta2009] [Winn1985].

From the application type perspective, at the beginning, model predictive control was used for systems with large time constants like, for example, the processes in the petrochemical industry as in [Cutler1979], irrigation canal control as in [Begovich2007], and cement mill plants [Prasath2010].

As the computational power of digital devices increased both in speed and memory size, additional research areas were opened to MPC: for power electronics in DC-DC converter applications [Mariethoz2007] [Geyer2008] [Xie2009] or electric generators as in [Nanayakkara1997] [Bououden2012].

Another domain for using MPC is the power systems control and operation on individual power system tasks as voltage control problem in Beccuti [Beccuti2007], a dispatch MPC in Xie and Ilic [Xie 2009] or on cascaded different time scales approach as in Ulbig [Ulbig 2011] or for large power system as in [Puglia2011] [Patrinos2011].

MPC solutions are studied in the field of diabetes treatment, in developing controls for artificial pancreases which maintain the glucose concentration inside a min/max envelope by controlling the injected dose of insulin [Markakis2008] [Amjad2010] [Zarkogianni2011].

The automotive industry is adopting MPC solutions for developing power management control of hybrid electrical vehicles as presented in [Ripaccioli2010] and [Bernardini2009].

The MPC is implemented also in the aerospace industry as it is a well suited candidate for providing trajectories and control commands adapted to the new flight conditions as presented in [Alexis2011] [Song2010] [Bemporad2011] [Joosten2008] as the fault tolerant flight control is an important topic in the flight industry which enables the controller to operate the aircraft subject to physical damage.

In [Wu2008] is presented a model predictive control that improves the ventilation and the associated indoor environment in livestock barns.

An extended survey on the industrial applications and developed software for solving MPC problems is presented by Qin [Qin2003] and the latest developments and diversifications of MPC algorithms are reviewed in [Lee2011].

Different augmented models were developed and presented in the literature for the system to present offset free operation in the presence of unknown and unmeasured disturbances. In the modelling process it is generally accepted the assumption that the disturbance is constant in time, from one step to the next, that is $\eta_{k+1}= \eta_k$. This disturbance can be considered to affect the state of the system [Muske2002] [Huusom2010], case in which the augmented state-space system is called the input disturbance model or, the output disturbance model when the disturbance is affecting only the output of the system [Levine2011]. Other works like [Morari91] represent the output disturbance as a ramp signal, in order to improve the rejection of input disturbance. Regarding the unmeasured disturbances, the best achievable closed-loop performance can be obtained by making the most realistic model of the real disturbance which is an identification problem based on experimental results. In addition to the deterministic term of a disturbance, stochastic evolution can be considered, as in [Huusom2010] represented by white noise [Koch2012a] [Koch2012b], integrating white noise or a combination of the two [Huusom2011].

One potential problem of using the augmented models is the lack of detectability which means that is there cannot be more disturbances states, which have an integrating effect, than the number of system outputs for detectability to hold. Hence, in the design step, the engineer would have to choose between the input or output disturbance augmented model as well as for the system presented in this work, where there are two disturbances affecting the system, the solar irradiance and the ambient temperature.

A method of obtaining offset-free control is to use a variation approach [Muske1993][Muske2002][Koch2012], where the variation of the process states are used as the state variable; in the present work the variation of the inside temperature is chosen to be the state variable, and not just the inside temperature, as it will be explained in later sections.

The main advantage of this method is that there is no need to compute steady state targets since the state variation (Δx) and command variation (Δu) approach zero at steady state [Muske2002], as in the present system the steady state is achieved when there is no change in the inside temperature ($\Delta x=0$) and no variation in the output power of the heaters ($\Delta u=0$).

The downside of this augmented state approach is especially manifested in large systems with many states and disturbances, where the computational time increases rapidly. In these cases, special attention has to be paid in the development stages to the systems' coefficients order of magnitude, which can have large differences; when the controller projects the states over the prediction

horizon, some coefficients can tend to very large numbers and others can get close to zero; these large differences will introduce errors in solving the optimization algorithm.

The MPC became very attractive due to its ability to handle process constraints on different variables. The ability of handling the constraints, represented by hard physical limitation of actuators eliminates the use of anti-windup as for the case of PID controllers improving the operation near the optimal performance.

Another advantage is the ability to control large multi variable processes with respect to constraints and assure stability as described in [Sahin2009] for two applications: hot blast stoves and water level regulation in a cascade of river power plants.

Another important use of constraints is the presence, in many applications, like in the case of energy efficient buildings thermal control, of buffer tanks. These buffer tanks can be storage places for materials, storage elements for electrical energy [Borhan2010], or the thermal capacity of a building for storing thermal energy [Balan2010] [Bemporad2002] [Chen1996] [Chen2002] [Halvgaard2012] [Henze2004] [Hazyuk2012ab] [Kumert2001] [Ma2009, 2010, 2011, 2012] [Nagai2002] [Oldewurtel2010, 2012] [Pannochia2003] [Privara2011] [Wu2008] [Koch2012a] [Xie2009] [Zong2011] [Zong2012]. The buffer can be used to store any percentage of its capacity providing the MPC the ability to absorb the effect of disturbances and to optimize the use of different resources, as for the case of buildings, the thermal capacity is used to store energy at a low price (by reaching the upper limit) and consume it when the price is high (no electric heat is produced, and the inside temperature drops until the low limit is reached).

However, the MPC cannot operate to close to the limits due to the unknown disturbances present in any processes. When information about these disturbances are available, deterministic and stochastic models can be made and the performance is considerably improved.

Since the length of the prediction horizon of an MPC algorithm remains constant as it slides from one sample time to the next, repeating the optimization problem for the new interval, this algorithm is also called the receding horizon strategy.

For heating, ventilation, and air conditioning (HVAC) systems for both private houses and office buildings, bang-bang and PID control has been widely used for decades. Shortcoming of these methods is the large thermal lags of the systems and varying set points (as different temperature and humidity conditions for specific hours) which in addition to disturbances due to outside weather conditions and occupancy are having difficulties in adapting to large changes in system dynamics.

A comparison between an on-off controller, a PI and a generalized model predictive control is shown in [Chen2002] regarding a floor heating system with large thermal lag simulation. The controller uses an ARIMAX model of the system and the objective is to track the reference inside temperature.

While the building thermal capacity is considered a passive method of thermal energy storage, the active methods are using an additional fluid to charge and discharge a storage tank like in the case of water heaters and floor heating system. In literature both approaches are studied, independently or in combination: passive methods are presented in works like [Braun1990] [Koch2012] and active methods are resented in the work of [Chen2001] [Halvgaard2011] [Hazyuk2012] [Henze2004] [Houwing2008].

The opportunities of MPC, as being able to use the occupancy schedule and weather forecasts for optimal inside temperature control are the subject of research in [Hazyuk2012a]. The equivalent electric circuit analogy is used to model the thermal capacity of a building in the state-space form, considering three states: the wall temperature, the zone temperature and the floor temperature. The heating system uses water radiators which request special modelling attention due to nonlinearities in transmitting the command from the controller. The paper identifies the nonlinearities in the building's thermal behaviour and represents the building by separating linear and nonlinear blocks. This paper focuses on building parameter identification as it uses pseudo-random binary signal (PRBS) for identification of building thermal model parameters.

Next is presented a short overview of the existing literature on model predictive control usage in energy efficient buildings.

Early work in this field is done by Winn [Winn1985] which presents a simulated optimal control of minimizing the energy cost and keeping the inside temperature in comfort limits based on simple models for the building and for the HVAC system.

The work of Henze [Henze2004] presents a simulated MPC that combines the passive and active thermal energy storage approach for an office building using a quadratic program. It considers perfect predicted disturbances: occupancy for the office building, the solar irradiance and the outside temperature as well as a perfect model of the system. Comparisons between the usage of active, passive, and combined thermal energy storage MPC methods are made; the paper does not consider any disturbance rejection or estimation.

Houwing [Houwing2008] focuses on the usage of a micro-combined heat and power (micro-CHP) system for illustrating the potential of operational cost savings. It considers predictions on heat and electricity demand and energy prices. The optimization function is linear, as well as the equality and inequality constraints. As the system variables are both continuous and binary, this is a mixed-integer linear programming problem. The paper presents simulations to validate the controller algorithm.

Kolokotsa [Kolokotsa2009] experiments with 10 minutes time interval, a quadratic program. For energy efficient building inside temperature control advanced control techniques can be implemented based on artificial intelligence like neural networks, fuzzy controllers, and genetic algorithms. The benefits are the low computational time of deployed algorithms and the low effort in modelling the system; the downside is the need of large sets of measured data to train the controller, and the lack of adaptability in the case which the process operates outside the data set available during training.

Kummert [Kummert2001] uses a state estimator for the zone temperature radiator supply and return water temperature; these values are fed into the optimization problem which is a trade-off between the thermal comfort and energy cost. The algorithm uses a 15 minutes prediction starting from the estimated variables. The optimization problem output is the water supply temperature for the water heating system, which is tracked with a PID controller. The cost function is a quadratic-linear function. It is shown that during sunny days, the upper comfort limit can be exceeded due to the large effect of solar radiation on the internal temperature, the errors in thermal model and in the prediction and the fact that the controller can only increase the temperature and not to cool down the temperature. Additional errors are due to water dynamics in the boiler and pipes. Simulations on the entire season show important savings 15-20% for an improved thermal comfort.

The paper concludes that energy savings in the range of 10% can be achieved to the "reference controller", with a similar thermal comfort. If the occupants of an office building or a household that uses MPC desire to change the inside temperature, they just have to change the reference and the controller will adapt to the new desires.

Liu and Henze in [Liu2004] evaluate the impact of modelling accuracy on the MPC of both active and passive thermal energy storage. Model errors due to simplification of factors like building's geometry, zoning, construction materials, internal heat gains (light, equipment and, occupancy), and characteristics of the plan, including the base chillers and thermal energy storage system were studied. There is a trade-off between model simplification and computational effort which have to be studied for each application through experiments.

Oldewurtel [Oldewurtel2012] presents a study conducted with data available from four different locations where MPC was used on a set of data spanning over one year. Conducts a comparison study between using different control algorithms: rule based control, deterministic MPC, and stochastic MPC. Stochastic MPC is a newly developed algorithm for the purpose of building inside temperature control and is able to deal with uncertainties by using weather and occupancy forecast. The difference between the deterministic and the stochastic MPC relies on the constraints formulation. By using stochastic MPC, in the optimization problem for the future states in the prediction horizon a stochastic term is added (chance constrain), which considers the forecast covariance error; during the time horizon, this term accumulates, proportionally with the dimension of the horizon, and influences the solution, by tightening the constraints, and forcing the algorithm to operate further away from the limits. To deal with this problem, a new term is presented in order to deal with the variations during the prediction horizon, which is the affine disturbance feedback.

A large part of literature presents model predictive control for inside temperature or water heating systems only in the state of simulations [Winn1985] [Hazyuk2012a,b] [Henze2004] [Houwing2008] [Hovgaard2011] [Koch2012S]; however, in some places projects were started and experiment facilities were constructed with the purpose of developing and testing a usable large scale applicable technology involving MPC for energy efficient building and integration of distributed energy resources into the low voltage distribution grid.

Research facilities were developed in order to study the impact of implementing intelligent solutions, especially the MPC, for energy efficient buildings. Such a project is OptiControl [OptiControlRep] from ETH Zurich which "aims at reducing their energy consumption at modest investment and operating costs, while at the same time improving occupant comfort and reducing peak power demand" [OptiControl] described in the work of [Oldewurtel2012]. Or at UC Merced Campus [Berkley] which transformed the campus in a "living laboratory" described in the papers of Ma [Ma2009] and []. At the Czech Technical University MPC were also deployed as shown in the work of Prívara and Siroky [Privara2011].

Another test building is "FlexHouse" from SYSLAB facility at Elektro department DTU at RISØ campus. This building is presented in [Backer] and in chapter 2. The MPC implementation with cost optimization are presented in [Zong2012,2011] and with local PV produced output power in [KochCiobotaru2012].

4.2. Objectives

Model predictive control has its roots in the dynamic optimization which starts with a discrete dynamic model represented by the equation

$$x(k + 1) = g(x(k), u(k)), \qquad x(0) = x0$$

that describes the evolution of the state x(k) with time, starting from the initial condition x(0), as it is affected by the manipulated input u(k).

The goal of the dynamic optimization procedure is to find the vector of manipulated inputs U_N = [u(0)', ..., u(N −1)']' such that the objective function is optimized over some time horizon N, typically:

$$\min_{u} \Phi = \sum_{k=0}^{N-1} q\big(x(k), u(k)\big) + p\big(x(N)\big)$$

The terms q(x, u) and p(x) are referred to as the stage cost and terminal cost, respectively [Borreli2011]. The terminal cost is introduced to insure stability of the system as explained in [Mayne2003].

From this optimization law sequence U_N, only the first term is applied to the process. This is due to the unknown disturbances that can appear during the operation and can alter the system's trajectory far from the optimal solution computed by the algorithm. Instead, the optimization problem is recalculated at the next step, considering the new measurements and system state. This feedback of the measurement information to the optimization endows the whole procedure with a robustness typical of closed-loop systems [Borreli2011].

If in the finite time optimal control problem solved by MPC at each time step, system model and constraints are linear and the performance index is expressed as weighted sum of 2-norm, 1-norm or∞-norm vectors, then the resulting optimization problem can be cast as a quadratic program (QP) or linear program (LP), respectively, for which a rich variety of efficient active-set and interior-point solvers are available [Borreli2011].

The optimization function is a quadratic problem and so it is a convex program, meaning a global optimal solution within a specified tolerance can be assured [Levine2011].

The conventional approach for solving QP is the so called active set method. The method consists of assuming a starting set of active constraints and solving the resulting least-squares problem through Lagrange multipliers, where the active constraints are treated as equality constraints. In general, this starting set is not the correct set which satisfies the inequality constraints of the problem. Through the use of Karush-Kuhn-Tucker (KKT) conditions the set is iteratively modified until the correction is found [Levine2011].

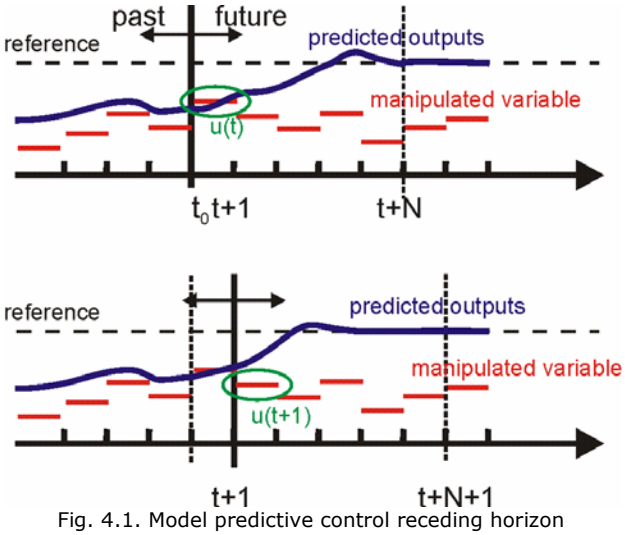

Fig. 4.1. Model predictive control receding horizon

More recently, a promising new approach called the interior point (IP) method has been developed for solving the QP. The idea of the IP method is to "trap" the solution within the feasible region by including a so-called "barrier" function in the objective function. Within the modified objective function, the Newton iteration is applied to find the solution. Though originally developed for LPs, the IP method can be readily generalized to QPs and other more general constrained optimization problems. [Levine2011]

In the case of large systems, with multiple controlled and manipulated variables, considering constraints on every variable can be very demanding on the time needed for the control algorithm to solve the quadratic problem. A common approach is to consider constraints for the system's variables only at selected time steps in the predicted horizon instead of all future steps. It is generally accepted that unless dealing with a highly oscillatory system, a few output constraints at the beginning and one at the end of the predicted horizon should keep the output more or less inside the constraints throughout the horizon. Even when constraints violations occur in the prediction, this does not imply constraints violations in the actual implementation because of the moving horizon. [Levine2011]

While unconstrained MPC is a form of linear feedback control, constrained MPC is a nonlinear control algorithm. Thus, the behaviour for small deviations can be drastically different from that for large deviations [Levine2011].

The objective of this chapter is to present the development of MPC algorithm that controls the inside temperature of a household by commanding the electrical heaters installed in the heating system. Having a controller that maintains the inside temperature at specified values, the energy consumption of the heating system can be minimized by applying an efficient temperature reference profile during the day.

The MPC has to be formulated to achieve offset free control by augmenting the state space with additional states and using an observer to estimate the additional states, in order to eliminate the effect of modelling errors and unknown disturbances coming from weather data prediction errors.

Both the MPC algorithms are tested and validated through simulations and experiment and a comparison of the considered study cases is presented at the end

of the chapter which emphasizes the high performance of using the offset free MPC in tracking the reference in the presence of unknown errors and disturbances.

4.3. Model of the system

The objective of the optimization function is to control the inside temperature of a building, according to different model predictive control algorithms, by tracking a prescribed reference or to minimize the cost of energy used to heat the house by using the electric energy from the grid or with the local produced PV power.

For simulations and experiments carried out in this work, the MPC algorithm uses the building thermal model presented in chapter 2, a state-space model with one state variable:

$$\frac{dT_i}{dt} = -\frac{1}{C_i R_{ia}} T_i + \frac{1}{Ci} \mathrm{P}_h + \frac{1}{C_i R_{ia}} T_a + \frac{A_w}{C_i} G \tag{4.1}$$

Where C_i is the heat capacity of the house. This includes the indoor air and the interior objects (=3.42 [kW/°C])

R_{ia} is the thermal resistance from the indoor to the ambient environment (=4.87 [°C/kW])

A_w is the effective window area of the house with heating influence. (=5.53 [m^2])

The discrete state-space representation of this model, having a time step of 10 minutes is:

$$x_{k+1} = Ax_k + Bu_k + Ed_k \tag{4.2a}$$
$$z_k = Cx_k \tag{4.2b}$$

Where:

A=[0.99] B=[0.0487] E=[0.01 0.2695] C =[1]

Simulations were carried out for the two cases: when the thermal model is a perfect match of the system and when a different model is used.

For testing algorithms that deal with modelling errors, a three state-space model was used for the building's thermal dynamics; this three states-model is presented in the work of Bacher and Tavlov (Bacher2010) as well as the parameters identification presented in Table 2.7.

This extended three states model is represented by the following equations, representing the equivalent RC electric circuit represented in figure 2.44:

$$\begin{cases} C_i \dfrac{dT_i}{dt} = \dfrac{1}{R_{ia}}(T_a - T_i) + \dfrac{1}{R_{im}}(T_m - T_i) + \dfrac{1}{R_{ih}}(T_h - T_i) + A_w G \\ C_m \dfrac{dT_m}{dt} = \dfrac{1}{R_{im}}(T_i - T_m) \\ C_h \dfrac{dT_h}{dt} = \dfrac{1}{R_{ih}}(T_i - T_h) + P_h \end{cases} \tag{4.3}$$

Where the state space variables are

Ti – inside temperature

Tm – a second inside temperature which defines a internal medium
Th – temperature in the electrical heaters

The extended thermal model is represented in a discrete state-space form, having a time step of 10 minutes:

$$x_{k+1} = Ax_k + Bu_k + Ed_k \quad (4.4a)$$
$$z_k = Cx_k \quad (4.4b)$$

Where

$$A = \begin{bmatrix} 0.967 & 0.0182 & 0.0019 \\ 0.0157 & 0.9843 & 0 \\ 1.3034 & 0 & -0.3034 \end{bmatrix} B = \begin{bmatrix} 0 \\ 0 \\ 43.4028 \end{bmatrix}$$

$$E = \begin{bmatrix} 0.013 & 0.3465 \\ 0 & 0 \\ 0 & 0 \end{bmatrix} C = [1 \quad 0 \quad 0] \; D = 0$$

x_k – state variable $[T_i;T_h;T_m]$
u_k – heaters output power
d_k – disturbances vector,

4.4. Tracking MPC algorithm

4.4.1. Algorithm development

The objective of this particular MPC is to control the inside temperature (z_k) to track the a priori described reference (r_k) with constraints on the output power rate of the heaters, by using the one state model described in section 4.3, subject to model uncertainties, unknown disturbances and process and measurement noise, as presented in the study cases.

The MPC output is chosen to be the solution of a constrained finite horizon quadratic optimization problem presented by the objective function (OF) in equation 4.5 that is computed at each time step k using measured and predicted values. The solution represents the future N values for the command from witch only the first one is implemented on the process and the computation is repeated at the next simulation step with the new measured and predicted values.

The diagram of the model predicitve control algorithm is presented in figure 4.2. The variables with 'p' index are a priori known by the controller, as the case for the reference r and the weather forcast (Ta_p and G_p). In square brackets are represented vectors of length equal to the predicted horizon, data which are used by the controller to solve the optimization function over the predicted horizon.

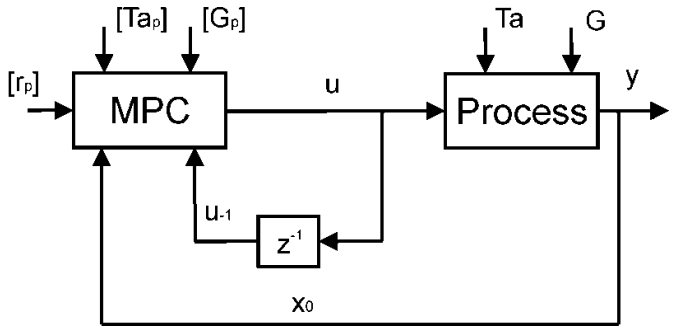

Fig. 4.2. MPC algorithm diagram considering a perfect model and perfect weather (disturbance) forecast

The model predictive control is formulated by the following mathematical equations:

The objective function:

$$\min_{u\in R^n} \mathrm{f(u)} = \frac{1}{2}\sum_{k=0}^{N} \|z_k - r_k\|_Q^2 + \frac{1}{2}\sum_{k=0}^{N-1} \|\Delta u_k\|_S^2 \quad (4.5a)$$

Subject to:

the discrete state-space model of the system:

$$x_{k+1} = Ax_k + Bu_k + Ed_k \quad (4.5b)$$

$$z_k = Cx_k \quad (4.5c)$$

and constraints:

$$u_{min} \le u_k \le u_{max} \quad (4.5d)$$

$$\Delta u_{k,min} \le \Delta u_k \le \Delta u_{k,max} \quad (4.5e)$$

$$z_{min} \le z_k \le z_{max} \quad (4.5f)$$

The first optimization term from equation 4.5a forces the output of the process to follow the given trajectory, that is the inside temperature to track the prescribed trajectory.

The second term considers minimizing the variation of the command signal u, representing the electric heaters output power.

Another important aspect of this control is the ability to modify the importance of the optimization terms in the optimization function by using weight coefficients, in this case Q for minimizing the trajectory difference and S for minimizing the variations of the manipulated variables.

The MPC algorithm was implemented in the Matlab software environment and the *quadprog* solver from the optimization toolbox was used for the optimization problem. In order to use the Matlab predefined function, the optimization problem formulated in the form of equation 4.5. has to be rewritten in the specific form of the solver as in equation 4.6:

$$\min_U \mathrm{f} = \frac{1}{2}U'HU + g'U \quad (4.6)$$

Subject to

$$A_q U \leq b_q \tag{4.7}$$

The model predictive control is an optimization problem that considers the projected states of the system over a prediction horizon in order to minimize an objective function. From equation 4.2, the next z_{k+i} , (i=1...N) values over the prediction horizon can be computed considering:

- x_0 as the initial value for the state variable at each time step interval,
- D - the predicted disturbance vector over the predicted horizon
- U - the system input, the command variable, in this case the output power of the heaters:

$$\underbrace{\begin{bmatrix} z_1 \\ z_2 \\ z_3 \\ \vdots \\ z_N \end{bmatrix}}_{=Z} = \underbrace{\begin{bmatrix} CA \\ CA^2 \\ CA^3 \\ \vdots \\ CA^N \end{bmatrix}}_{=\Phi} x_0 + \underbrace{\begin{bmatrix} H_1 & 0 & 0 & \cdots & 0 \\ H_2 & H_1 & 0 & \cdots & 0 \\ H_3 & H_2 & H_1 & \cdots & 0 \\ \vdots & \vdots & \vdots & \ddots & \vdots \\ H_N & H_{N-1} & H_{N-2} & \cdots & H_1 \end{bmatrix}}_{=\Gamma} \begin{bmatrix} u_0 \\ u_1 \\ u_2 \\ \vdots \\ u_{N-1} \end{bmatrix} + \underbrace{\begin{bmatrix} H_{1,d} & 0 & 0 & \cdots & 0 \\ H_{2,d} & H_{1,d} & 0 & \cdots & 0 \\ H_{3,d} & H_{2,d} & H_{1,d} & \cdots & 0 \\ \vdots & \vdots & \vdots & \ddots & \vdots \\ H_{N,d} & H_{N-1,d} & H_{N-2,d} & \cdots & H_{1,d} \end{bmatrix}}_{=\Gamma_d} \begin{bmatrix} d_0 \\ d_1 \\ d_2 \\ \vdots \\ d_{N-1} \end{bmatrix} \tag{4.8}$$

$H_k = CA^{k-1}B$
$H_{k,d} = CA^{k-1}E$

Which can be written in a short form:

$$Z = \Phi x_0 + \Gamma U + \Gamma_d D \tag{4.9}$$

The objective function defined in equation 4.5 has to be reformulated as a function of U, representing the manipulated variable, in this case the electrical heaters' output power.

By developing the first term of the OF from equation 4.5, and using equation 4.9, the next form is obtained:

$$\mathrm{f}_z = \frac{1}{2}\sum_{k=0}^{N} \|z_k - r_k\|_Q^2 = \frac{1}{2}\|Z - R\|_Q^2 = \frac{1}{2}\|\Gamma U - b\|_Q^2 \tag{4.10}$$

With the additional notation:

$$b = R - \Phi x_0 - \Gamma_d D \tag{4.11}$$

The transformation into the required form of equation 4.6 is represented by the following equation:

$$\mathrm{f}_z = \frac{1}{2}\|\Gamma U - b\|_Q^2 = \frac{1}{2}(\Gamma U - b)'Q(\Gamma U - b) = \frac{1}{2}U'\Gamma'Q\Gamma U - \left(\Gamma'Qb\right)'U + \frac{1}{2}b'Qb \tag{4.12}$$

For the second term of the objective function, the command variation penalty, the reformulation evolves as:

$$\mathrm{f}_{\Delta} = \frac{1}{2}\sum_{k=0}^{N-1}\|\Delta u_k\|_S^2 = \frac{1}{2}\| \begin{bmatrix} u_0 \\ u_1 \\ \vdots \\ u_{N-1} \end{bmatrix} - \begin{bmatrix} u_{-1} \\ u_0 \\ \vdots \\ u_{N-2} \end{bmatrix} \|_S^2 \tag{4.13}$$

And in the extended form:

$$\mathrm{f}_{\Delta} = \frac{1}{2}\begin{bmatrix} u_0 \\ u_1 \\ u_2 \\ \vdots \\ u_{N-1} \end{bmatrix}' \underbrace{\begin{bmatrix} 2S & -S & 0 & \cdots & 0 \\ -S & 2S & -S & \cdots & 0 \\ 0 & -S & 2S & \cdots & 0 \\ \vdots & \vdots & \vdots & \ddots & -S \\ 0 & 0 & 0 & -S & S \end{bmatrix}}_{=H_S} \cdot \begin{bmatrix} u_0 \\ u_1 \\ u_2 \\ \vdots \\ u_{N-1} \end{bmatrix} + \underbrace{\left(- \begin{bmatrix} S \\ 0 \\ 0 \\ \vdots \\ 0 \end{bmatrix} \right)'}_{=H'_{u_{-1}}} u_{-1} \begin{bmatrix} u_0 \\ u_1 \\ u_2 \\ \vdots \\ u_{N-1} \end{bmatrix} \tag{4.14}$$

And in a more compact, matrix form, the second term becomes:

$$\mathrm{f}_{\Delta} = \frac{1}{2}U'H_S U + M_{u_{-1}}u_{-1}U \tag{4.15}$$

From equation 4.12 and 4.15, the initial optimization function from equation 4.5 can be rewritten in the form of equation 4.6, with an additional term p which is independent of u, having the following coefficients:

$$H = \Gamma' Q \Gamma + \mathrm{H_S} \tag{4.16}$$

$$g = -\Gamma' Q(R - \Phi x_0 - \Gamma_d D) + M_{u_{-1}}u_{-1} \tag{4.17}$$

$$p = \frac{1}{2}b'Qb \tag{4.18}$$

The developed MPC algorithm implements hard constraints on:

- the manipulated variable

$$U_{min} \le U \le U_{max}, k = 0 \dots N-1 \tag{4.19}$$

- the controlled variable:

$$Z_{min} \le Z \le Z_{max}, k = 1 \dots N \tag{4.20}$$

As all the constraints have to be define according to U, by replacing equation 4.8 in equation 4.20 the following relations are obtained:

$$\begin{matrix} Z_{min} - \Phi x_0 - \Gamma_d D \le \Gamma U \\ \Gamma U \le Z_{max} - \Phi x_0 - \Gamma_d D \ , k = 1 \dots N \end{matrix} \tag{4.21}$$

$$A_q = \begin{bmatrix} I_N \\ -I_N \\ -\Gamma \\ \Gamma \end{bmatrix} \quad b_q = \begin{bmatrix} U_{max} \\ -U_{min} \\ -Z_{min} + \Phi x_0 + \Gamma_d D \\ -\mathrm{Z_{max}} + \Phi x_0 - \Gamma_d D \end{bmatrix} \tag{4.22}$$

The obtained equations 4.16, 4.17, and 4.22 are used as the parameters for the Matlab solver – equations 4.6 and 4.7, which returns the solution for the optimization problem as a N dimensions vector, representing the next N values of the heaters output power:

$$U = \text{quadprog}(H, g, A_q, b_q) \tag{4.23}$$

The Matlab functions used to implement the MPC algorithm described in this section are presented in Apendix B.

4.4.2. Offset Free Control

In section 4.4.1 was presented the methodology of implementing the model predictive control starting from the explicit model of the thermodynamic process of the building, equation 4.2 and having the optimization function stated in equation 4.3. However, so far, the model is considered to be a perfect representation of the plant dynamics, and the disturbances, the ambient data of solar irradiance and ambient temperature, were considered to be accurate predicted.

These assumptions are forced away from the reality, where both the real system and the disturbances will present errors compared with the model and the predictions available to the control developer. Not considered, the errors will produce offsets of the systems output, the system will reach undesired states, will disregard the optimization objectives and constraints will be violated.

The errors have to be introduced in the MPC, as an integrator element, in order to minimize the errors and achieve offset free operation. These errors can be experimentally observed and statistical data can be used in control algorithms in order to achieve better results.

The solution is to use augmented state-space models of the system, by introducing additional states as in [Muske93] [Huusom10][Koch12]. If these additional states are not directly measurable, observers must be used; if the system is deterministic, a Luenberger observer can be successfully used; if the plant's states and output are assumed to be subject to white noise with a known covariance, a Kalman filter must be used such that the mean square state estimation error is minimized.

4.4.2.1. Augmented state-space system

For this application, as in the general case, the predicted disturbances values (d_k), represented here by the solar irradiance and ambient temperature, present an error (η_k) compared to the real measured values ($d_{real,k}$), as in equation 4.24. In order to eliminate the offset caused by these differences, the system's model has to be augmented with additional states, one for each of the disturbances [Maciejovski2002].

$$d_{real,k} = d_k + \eta_k \tag{4.24}$$

For the unknown errors in the disturbances, the assumption is made that they are constant and persistent, that is:

$$\eta_{k+1} = \eta_k \tag{4.25}$$

The resulting process model used by the MPC, including the unknown disturbance, has the form:

$$x_{k+1} = Ax_k + Bu_k + E(d_k + \eta_k) \tag{4.26a}$$
$$\eta_{k+1} = \eta_k \tag{4.26b}$$
$$z_k = Cx_k \tag{4.26c}$$

Using the augmented model, two consecutive states at moments k and k+1 are calculated as:

$$x_k = Ax_{k-1} + Bu_{k-1} + E(d_{k-1} + \eta_{k-1}) \tag{4.27}$$

$$x_{k+1} = Ax_k + Bu_k + E(d_k + \eta_k) \tag{4.28}$$

The difference between the two consecutive states, or the evolution of the state after one step is:

$$x_{k+1} - x_k = A(x_k - x_{k-1}) + B(u_k u_{k-1}) + E(d_k + \eta_k - d_{k-1} - \eta_{k-1}) \tag{4.29}$$

Using the assumption of persistent disturbance (4.24), a variation based model is obtained:

$$\Delta x_{k+1} = A\Delta x_k + B\Delta u_k + E\Delta d_k \tag{4.30a}$$
$$\eta_{k+1} = \eta_k \tag{4.30b}$$
$$\Delta z_k = C\Delta x_k \tag{4.30c}$$

The augmented state space variation based model has the form:

$$\underbrace{\begin{bmatrix}\Delta x_{k+1}\\ \eta_{k+1}\end{bmatrix}}_{=x_{a,k+1}} = \underbrace{\begin{bmatrix}A & E\\ 0 & A_d\end{bmatrix}}_{=\tilde{A}} \underbrace{\begin{bmatrix}\Delta x_k\\ \eta_k\end{bmatrix}}_{=x_{a,k}} + \underbrace{\begin{bmatrix}B\\ 0\end{bmatrix}}_{=\tilde{B}} \Delta u_k + \underbrace{\begin{bmatrix}E\\ 0\end{bmatrix}}_{=\tilde{E}} \Delta d_k \tag{4.31a}$$

$$\Delta z_k = \underbrace{[C\ 0]}_{=\tilde{C}} \underbrace{\begin{bmatrix}\Delta x_k\\ \eta_k\end{bmatrix}}_{=x_{a,k}} \tag{4.31b}$$

The augmented state-space system described in equation 4.31 has the state variable represented by:

$$x_{ak} = \begin{bmatrix}\Delta x_k\\ \eta_{Ta,k}\\ \eta_{G,k}\end{bmatrix} \tag{4.32}$$

Where:

- Δx_k – the evolution of the inside temperature, how much it changed from the last step, as the effect of the variations in heaters' output power (Δu_k) and the variation of the predicted disturbances ($\Delta d_{k)}$ as well as of model error compared to the real system

- $\eta_{Ta,k}$ – the unknown disturbance error on predicted ambient temperature
- $\eta_{G,k}$ – the unknown disturbance error on predicted solar irradiance

As the controller is not provided with actual measurements but only predictions, these errors and the ones produced by the differences between the model and the real system, an observer has to be used for estimating the state variable x_k.

This augmented variation based model, equation 4.30 can be used as the explicit model for the MPC algorithm described in section 4.3.

The diagram of the developed MPC algorithm, used in future simulations and experiment is presented in Figure 4.3.

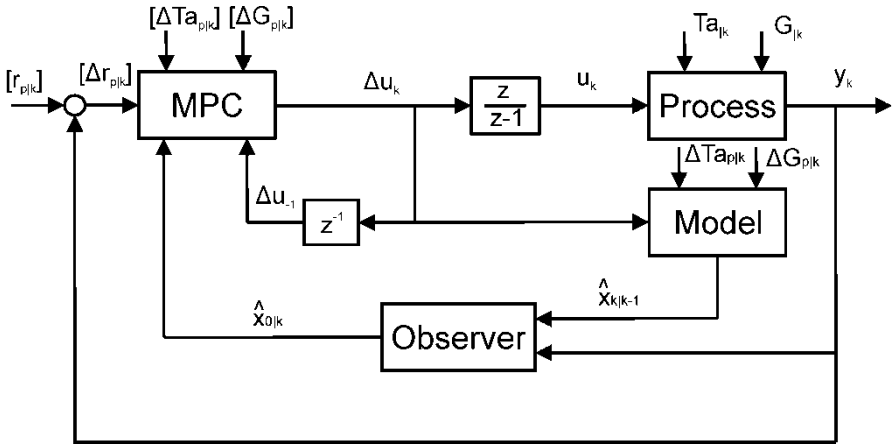

Fig. 4.3. MPC algorithm diagram considering an identified model and non-perfect weather (disturbance) forecast

For the MPC algorithm described in figure 4.3, the optimization function remains the one from equation 4.3, that is the inside temperature (the system's output) to track the prescribed reference, with minimized variation on the heaters output power (the manipulated variable) in order to achieve a smooth energy consumption for reducing power peaks that can affect the voltage profile on a distribution grid.

The modifications on the MPC are as follow:

- in this case, the result of the MPC optimization problem is the difference Δu_k and the command to the system is $u_k = u_{k-1} + \Delta u_k$.
- the input reference for this MPC is not the prescribed reference over the prediction horizon N at the moment k - $[r_{p|k}]$ as for the case when using the system from equation 4.6, but the difference $[\Delta r_{p|k}]$ between these N references and the current inside temperature y_k.

$$[\Delta r_{p,k}] = [r_{p,k} - y_k \quad r_{p,k+1} - y_k \quad \cdots \quad r_{p,N} - y_k] \tag{4.33}$$

- the input predicted disturbances are represented by their variation at each step k, for the next N length prediction horizon, that is:

$$[\Delta Ta_{p,k}] = [Ta_{p,k} - Ta_{p,k-1} \quad Ta_{p,k+1} - Ta_{p,k} \quad \cdots \quad Ta_{p,N} - Ta_{p,N-1}] \tag{4.34}$$

$$[\Delta G_{p,k}] = [G_{p,k} - G_{p,k-1} \quad G_{p,k+1} - G_{p,k} \quad \cdots \quad G_{p,N} - G_{p,N-1}] \tag{4.35}$$

- the previous step command (Δu_{-1}) has to be considered in order to include in the optimization function the variation of the manipulated variable, as it appears in equation 4.14. This term is responsible for smoothing the power peaks

- as the state variables cannot be measured, an observer must be used to estimate the initial state Xa_0 for each time step k. This is used to project the state-space model through the next N steps and the solution of the optimization problem is directly affected by this initial state of the model used in calculating equation 4.8.

- the model used to estimate the state vector is presented in equation 4.30.

The equations of the observer are:

$$\hat{x_a}(k+1|k) = \tilde{A}\hat{x_a}(k|k) + \tilde{B}\Delta u(k) + \tilde{E}\Delta d(k) \tag{4.36}$$

$$\widehat{\Delta y}(k|k-1) = \tilde{C}\hat{x_a}(k|k-1) \tag{4.37}$$

$$\hat{x_a}(k|k) = \hat{x_a}(k|k-1) + L\left[\underbrace{r(k) - y(k)}_{=\Delta\hat{y}(k)} - \tilde{C}\hat{x_a}(k|k-1)\right] \tag{4.38}$$

If we define the state estimation error as

$$e(k) = x_a(k) - \hat{x_a}(k|k-1) \tag{4.39}$$

And using equations (4.32) and (4.34), the recurrent relation of the state estimation error becomes:

$$e(k+1) = \left(\tilde{A} - L\tilde{C}\right)e(k) \tag{4.40}$$

Equation 4.40 shows that the state estimation error converges to zero if the observer is stable, at a rate determined by the eigenvalues of A-LC.

The values of L can be computed using a Luenberger observer, if the disturbance is deterministic or, if stochastic disturbances are supposed to affect the plant, which is more often the case, a Kalman filter is used.

4.4.2.2. Kalman filter observer

The Kalman filter is used to estimate values when a stochastic disturbance is affecting the states of a system or the measurements. Such a process is described by the state-space formulation of equation 4.41:

$$x_{k+1} = Ax_k + Bu_k + Ed_k + w_k \tag{4.41a}$$

$$z_k = Cx_k + v_k \tag{4.41b}$$

where:

w_k represents the input white noise, considered to have the covariance

$$E\{w(k)w^T(k)\} = Q \tag{4.42}$$

v_k represents the output white noise having the covariance:

$$E\{v(k)v^T(k)\} = R \tag{4.43}$$

The usage of a Kalman filter in the algorithm consists of two stages that run cyclically:

Time update – responsible for projecting the state ahead, based on the available state space model

$$x_{e,k+1} = A_e x_{p,k} + B_e u_k + E_e d_k \tag{4.44}$$

Measurement update – which has the role to 'correct' the estimated values by considering the last measurements taken from the system; at the end of this state, the observer is providing the best estimation, given the available measured data:

$$x_{p,k} = x_{e,k} + K_f\left(z_k - Cx_{e,k}\right) \tag{4.45}$$

As extensively presented in Appendix A, the Kalman filter minimizes the trace of the covariance error. The solution of the observer meaning the covariance of the innovations R_e and the predictive Kalman gain K_f are computed using equations 4.46 and 4.47:

$$R_e = CPC^{'} + R \tag{4.46}$$

$$K_f = PC'R_e^{-1} \tag{4.47}$$

The covariance of the error from equation 4.47 is defined as:

$$P(k) = E\{e(k)e^T(k)\} \tag{4.48}$$

The covariance P is a symmetric positive semidefinite matrix, the solution of the discrete Ricatti equation:

$$P = APA^{'} + Q - APC^{'}\left(CPC^{'} + R\right)^{-1}CPA' \tag{4.49}$$

4.4.3. Simulations

For testing and validating the model predictive controllers formulated in the previous sections, the controllers were implemented in Matlab. Simulations under different considerations were carried out as well as real-time experiments on the real FlexHouse building.

Simulations are run for the two MPC controllers, the one that uses no observers and the one that defines additional states for the disturbances and uses a Kalman filter to eliminate the modelling errors and the unknown disturbances. The two are compared and the benefits of using the MPC based on the augmented state-space model is emphasised.

Both the MPC formulations are based on the thermodynamic mathematical model of FlexHouse presented in equation 4.6 for the specific case of controlling the inside temperature of the building, subject to restrictions.

The second implemented MPC is using the augmented state-space variation based model, presented in equation 4.31 which, for the present system, is written as:

$$\begin{bmatrix} \Delta x_{k+1} \\ \eta_{Ta,k+1} \\ \eta_{G,k+1} \end{bmatrix} = \begin{bmatrix} 0.99 & 0.01 & 0.2695 \\ 0 & 1 & 0 \\ 0 & 0 & 1 \end{bmatrix} \begin{bmatrix} \Delta x_k \\ \eta_{Ta,k} \\ \eta_{G,k} \end{bmatrix} + \begin{bmatrix} 0.0487 \\ 0 \\ 0 \end{bmatrix} \Delta u_k + \begin{bmatrix} 0.01 & 0.2695 \\ 0 & 0 \\ 0 & 0 \end{bmatrix} \begin{bmatrix} \Delta \mathrm{d_{Ta,k}} \\ \Delta \mathrm{d_{G,k}} \end{bmatrix} \quad (4.50a)$$

$$z_k = \begin{bmatrix} 1 & 0 & 0 \end{bmatrix} \begin{bmatrix} x_k \\ \eta_{Ta,k} \\ \eta_{G,k} \end{bmatrix} \quad (4.50b)$$

The optimization function refers to penalizing the difference between the prescribed reference and the actual inside temperature

$$\min_{u \in R^n} \mathrm{f(u)} = \frac{1}{2} \sum_{k=0}^{N} \|z_k - r_k\|_Q^2 + \frac{1}{2} \sum_{k=0}^{N-1} \|\Delta u_k\|_S^2 \quad (4.50c)$$

Subject to constraints:

$$0 \le u_k \le 10 \quad (4.50d)$$

$$u_{k-1} \le \Delta u_k \le 10 - u_{k-1} \quad (4.50e)$$

$$18 \le z_k \le 22 \quad (4.50f)$$

Where:

z_k – is the controlled variable, the system's output and the inside temperature in FlexHouse at step k

u_k – is the manipulated variable, the heaters' output power in kW

Figure 4.4 presents the decision flow of the developed MPC algorithm used both for the simulations and experimental validation.

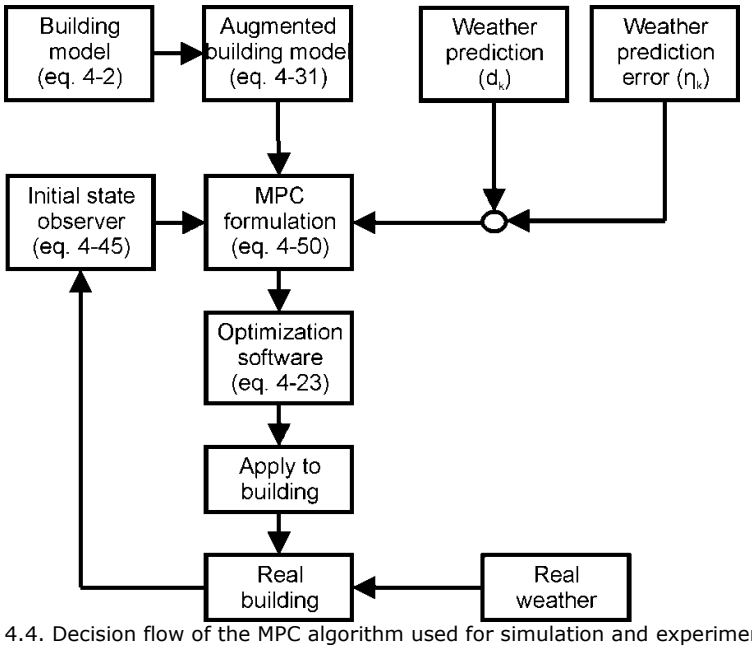

Fig. 4.4. Decision flow of the MPC algorithm used for simulation and experiments

The weight parameters from equation 4.5 are chosen to be Q = 1 and S=0.1. The term that penalizing the error between the reference and the measured inside temperature has a weight coefficient that is one order of magnitude larger than the one penalizing the variation in command. This last weight has to be considered to prevent the case of high frequency variations in the command (most likely at every time sample) due to the system trying to eliminate the smallest unmeasured disturbances with the sole objective to accurately track the prescribed reference. By not considering a factor S, the controller's command is likely to oscillate

The noise was considered as having the following covariance:
Q=0.5 – for the disturbances noise
R=0.001 – for the output noise

4.4.4. Simulation results

In this section, a number of simulated case studies representing combinations of different assumptions, available data or actuator type, are presented:

- For the **system model** were used the one state variable model from equation 4.4, the model *M1*, as well as the model with three states, *M3*, presented in equation 4.6.
- Three cases of **weather forecast** were considered:
  - perfect forecast – *W1*
  - the 24 hours ahead forecast taken from a weather service – *W2*

  - no weather forecast available, when an average temperature was used and an half of the maximum solar irradiance available for that day – *W3*

- As for the **stochastic noise**, the cases *S0* – no noise and *S1* – with white noise were studied.
- The **electrical heaters** can be regarded as having a continuous output power, represented by a real number between zero and the maximum power, the case *H0*, and the realistic case *H1*, where the heaters output represent an integer number between zero and ten, the sum of all the electrical heaters' output power
- The **initial state** X0 for the MPC calculation of future states, can be used from the last step state, by operating in open loop, *O0*, or by using an observer to estimate the current state *O1*;

In each study case, both the results of using and not using a state observer are plotted in order to give a representation of the necessity and utility of such a component.

The performances of the MPC algorithms will be defined by a cost function that reflects the operation of the system over the simulation horizon:

$$\bar{\Phi} = \frac{1}{2(T_f - T_0)} \sum_{t=T_0}^{T_f} [(z_k - r_k)^2] \tag{4.51}$$

Where

T_f – the final time step considered by the MPC, equal to the difference between the simulated horizon and the predicted horizon of the controller

T_0 – initial time step moment

z_k – the measured inside temperature at each time step

r_k – the prescribed reference

A large number of simulations scenarios can result from different combinations of assumptions, available data or actuator type as presented above. However, only ten of the most significant results are presented and discussed here.

The simulation results presented in the figures are numbered by the simulation number from the first column of table 4.1 and coded in the same table by their weather prediction availability, stochastic perturbation, type of models used for the controller and for the plant, and the type of heaters.

Each simulation result is presented in a four plots figure, representing, from top to bottom: in the first plot the prescribed reference of the inside temperature, the simulated current temperature when using the Kalman filter as a state observer for the augmented state variation based MPC described by equation 4.31 and the MPC described in equation 4.5, with no state observer and no offset free control; the second plot shows the manipulated heaters' output power for the two PMC algorithms developed in this chapter; the third and fourth plot present the predicted and measured weather data as the solar irradiance and outside temperature.

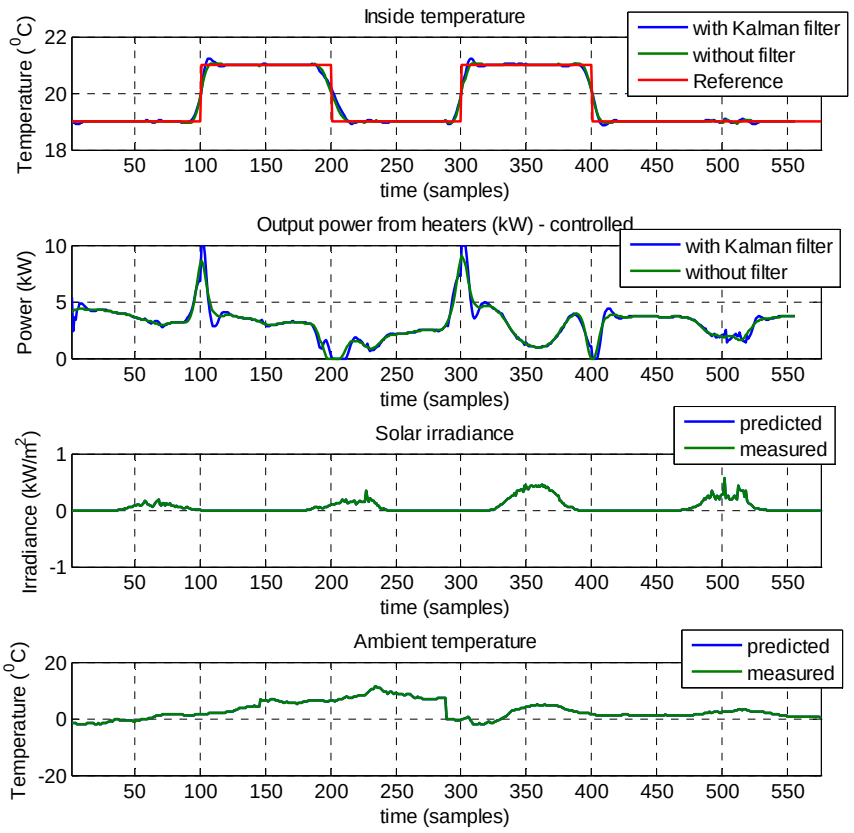

Fig. 4.5. Simulation Sim1 results Φ_{O0}= 0.0148 Φ_{O1}= 0.0163

Figure 4.5 shows the evolution of the inside temperature in the case of **Sim2** by using the two MPC strategies under the ideal conditions: the process is accurately modelled, the disturbances are perfectly predicted, there is no noise present in the system, and the heaters can be continuously controlled. This study case is far from reality, but it can be used as a bench mark.

Under these conditions, the overall performance cost is Φ_{O0}= 0.0148 for the normal MPC, and Φ_{O1}= 0.0163 for the augmented state-space MPC.

In figure 4.5 one can see very clearly a specific feature of the MPC strategy: prior to and after the step change in the reference, the system's output (the inside temperature in this case) presents and overshoot before stabilizing. This is due to the fact that the MPC has prior knowledge of the step change of the reference and performs actions so that the overall difference between the system's output and the prescribed reference to be minimal over the entire simulation horizon, as define in the optimization function of the MPC formulation.

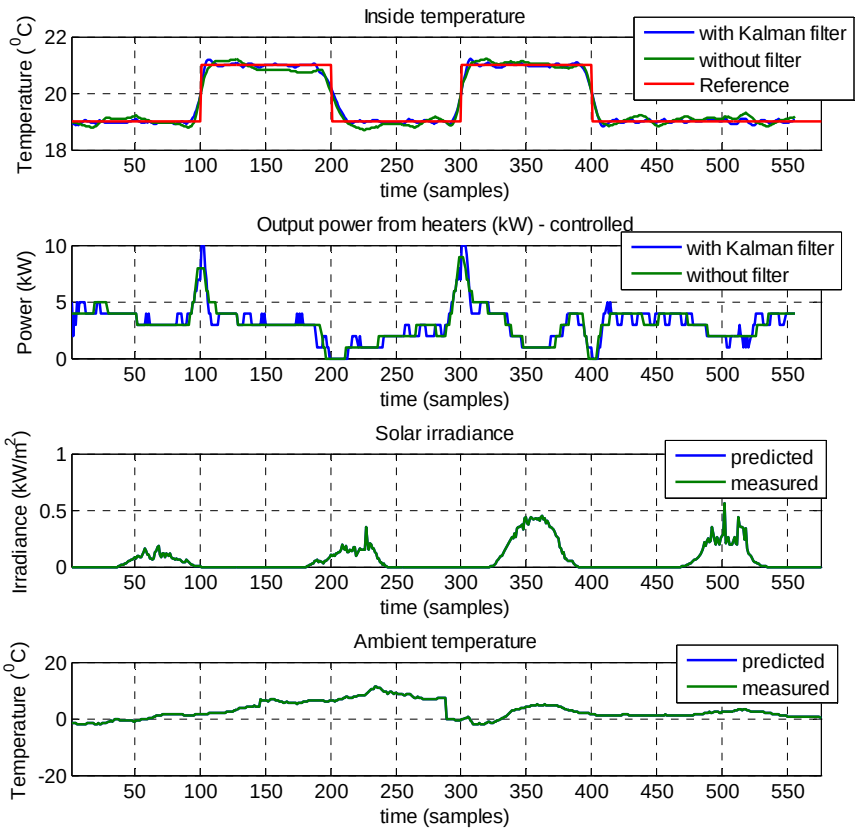

Fig. 4.6. Simulation Sim2 results ΦO0= 0.0229 ΦO1= 0.0168

Figure 4.6 presents the results for **Sim2** when the heaters are considered, like in the real experiment, as having two operation states: on or off, so the manipulated variables can take only integer numbers as viable values. Under these considerations the performance of the two MPC diminishes to Φ_{O0}= 0.0229 Φ_{O1}= 0.0168, a larger drop of performance being seen in the case where no state observer is used.

Figure 4.7 shows the simulation results of **Sim4**, when for the weather prediction were used data from the local weather station with a 24 hours ahead prediction. The process is considered perfect modelled and the heaters are controlled in 1 kW step change. The weather prediction accuracy can vary in accuracy from one day to another, so the error of the disturbance, modelled by the additional state in the augmented state-space system used for the offset free MPC in equation 4.50

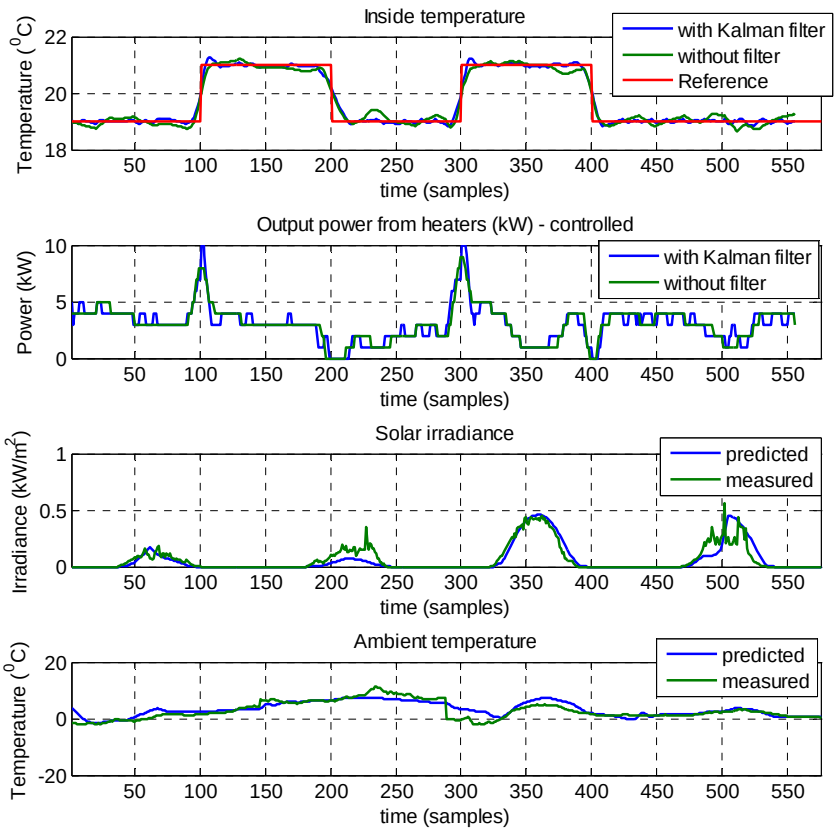

Fig. 4.7. Simulation Sim4 results Φ_{O0}= 0.0252 Φ_{O1}= 0.0174

, can have different effect. Even if the performance is lower for both MPC solutions, the usage of the observer can be well justified starting with this simulation as Φ_{O0}= 0.0252 and Φ_{O1}= 0.0174 and will be more meaningful in the future simulations, as they approach the realistic operation regime.

In figure 4.8 is presented the case of **Sim6**, when no weather station is available and no predicted data on the disturbance of the system, the ambient temperature and solar irradiance.

In this case, however historical data can be used, and were used for the simulation; that is for the ambient temperature one can use the historical average temperature for that area for the day, week or month depending on the data available, and for the solar irradiance one can compute the maximum solar irradiance shape of the current day, given the latitude, longitude and time of day, as presented in Chapter 2 for calculating the PV output power based on measurements taken at the horizontal plane. If for the augmented state-space MPC the

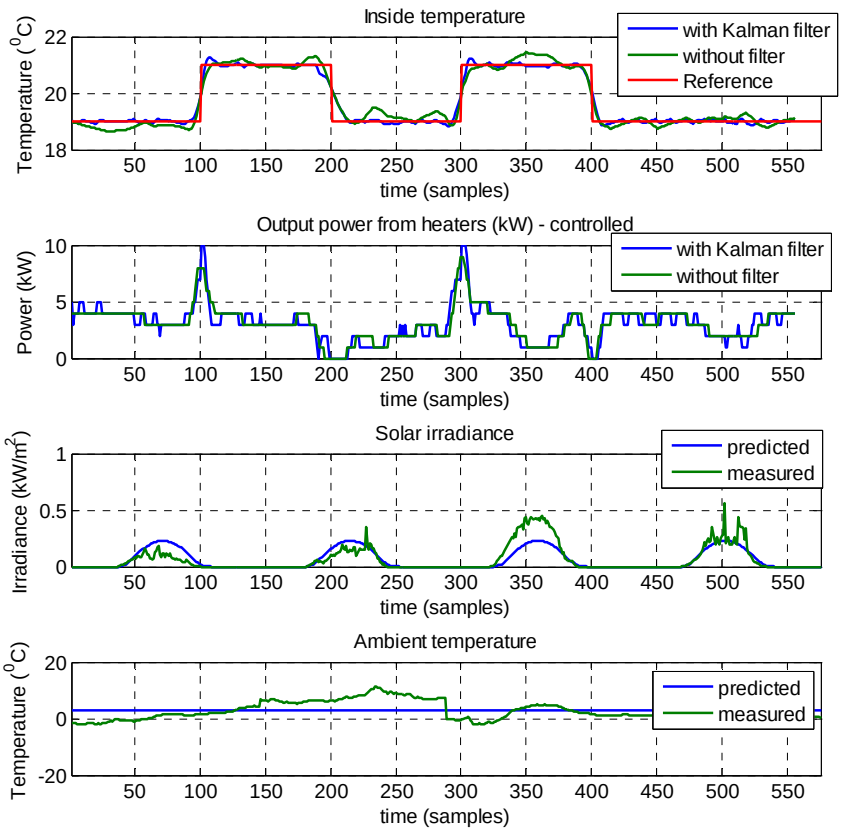

Fig. 4.8. Simulation Sim6 results Φ_{O0}= 0.0312 Φ_{O1}= 0.0173

performance cost function is not notably influenced by this approximation, Φ_{O1}= 0.0173 being, for this simulation, even smaller than in the case of a weather forecast usage, the classical MPC presents a worst result compared to the last simulation, and a large difference from the augmented MPC for this simulation scenario with Φ_{O0}= 0.0312.

Starting from **Sim10**, presented in figure 4.9, the simulated process has the three state-variables system from equation 4.3, and the MPC uses, as before, the one state model augmented with disturbance states. As it can be seen from the first plot, the difference between the process output and the output of the model used by the MPC is the largest at the moment of the rising step reference. Due to the model difference, there is an oscillatory evolution of the controller until the difference is included in the disturbance error state of the augmented MPC. The differences between using the classic MPC and using an observer for the initial state

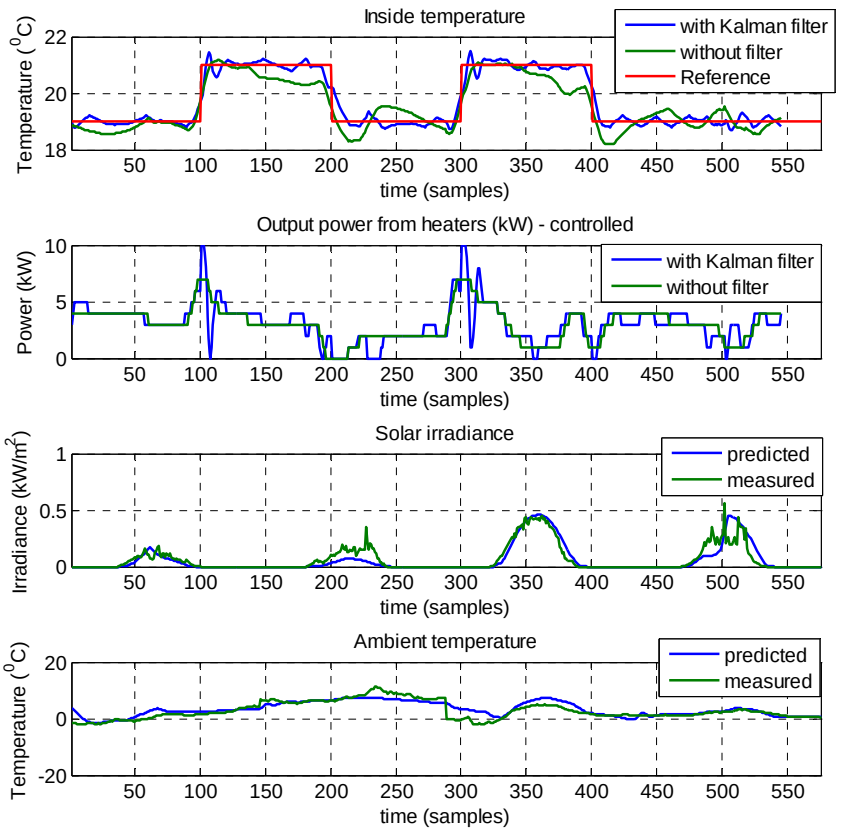

Fig. 4.9. Simulation Sim10 results Φ_{O0}= 0.0938 Φ_{O1}= 0.0264

are reflected in the performance cost functions of the two for this simulation case: Φ_{O0}= 0.0938 and Φ_{O1}= 0.0264.

Figure 4.10 presents the results of **Sim12**, for the case when the process has a different state space model than the one considered by the MPC algorithm to project the future state over the prediction horizon, real heaters that can be turned on and off which translate into 1kW steps of the manipulated variable and unavailable weather forecast. The performance of the offset free MPC is Φ_{O1}= 0.0262 while the performance of the classic MPC is rising to higher values of Φ_{O0}= 0.0992.

Another assumption that can be changed is the presence of white noise disturbances into the process internal states or in the output of the process due to measurement noise. The state and output noise is introduced in future simulations for researching the effect on the controller's performance under simulation scenarios presented so far.

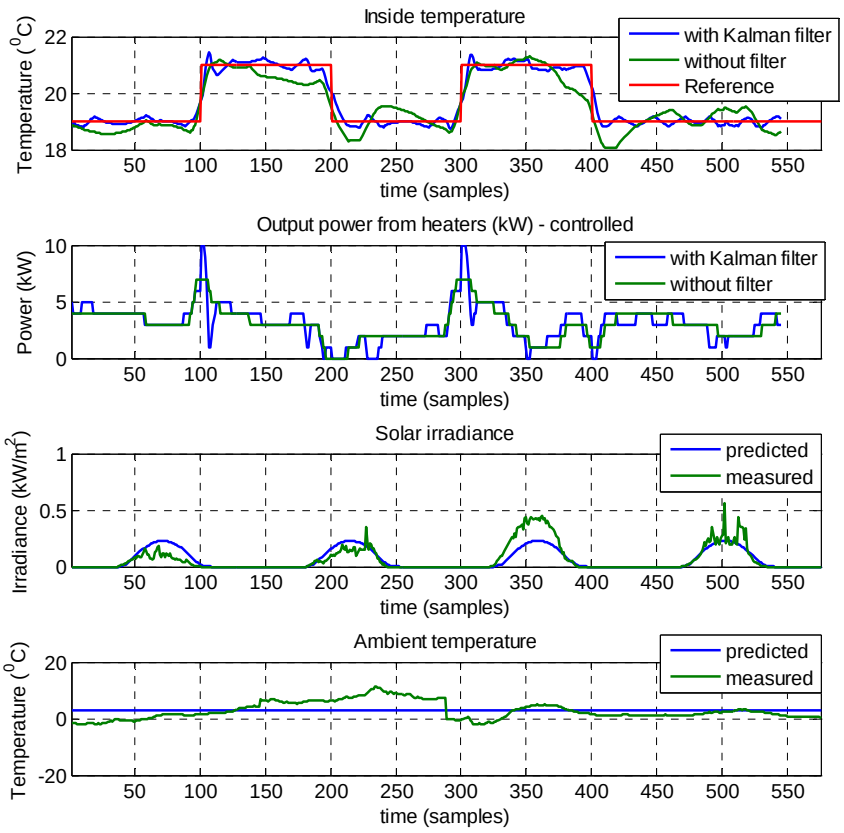

Fig. 4.10. Simulation Sim12 results Φ_{O0}= 0.0992 Φ_{O1}= 0.0262

Figure 4.11 presents the simulation case study **Sim16** where the process and system model differ, the heaters are 1kW, the weather from the local weather station is available with a 24 hours ahead prediction, and white noise on the states and output.

This simulation case is constructed from the simulation case Sim10, on which the white noise was added. From the performance cost of the two MPC strategies Φ_{O0}= 0.0805 and Φ_{O1}= 0.0337 one can conclude that the classic MPC is operating with a better result than the same algorithm in the case of Sim10; however, this is true only for this simulation, as the consistency of the result is not proved and will depend on the two white noise sequences affecting the states and the system output

The augmented variation based MPC will perform with more close results on different white noise sequences than the classic MPC, as it results from the comparison chart at the end of the section.

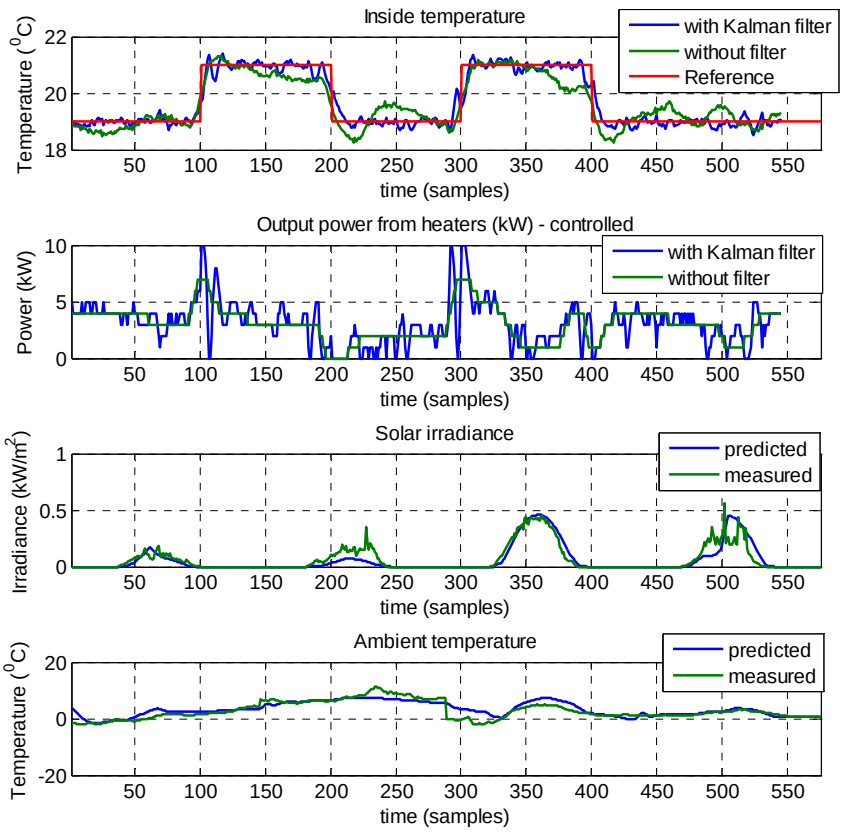

Fig. 4.11. Simulation Sim16 results Φ_{O0}= 0.0805 Φ_{O1}= 0.0337

The simulation case study **Sim18** presented in figure 4.12 represents the worst case scenario for the MPC for controlling the inside temperature of a building:

- The process and the model used by the controller are different
- There is no weather prediction, and the values are considered constant (for the temperature) as the local average for that period and the solar irradiance is considered half of the maximum irradiance available for that particular day, in order to approach both the case of sunny weather – when the actual solar irradiance will get close to the maximum available irradiance and the case of cloud cover – when the irradiance will be closer to zero
- The heaters have 1kW step change
- There is noise both on the state of the process and on the output measurements

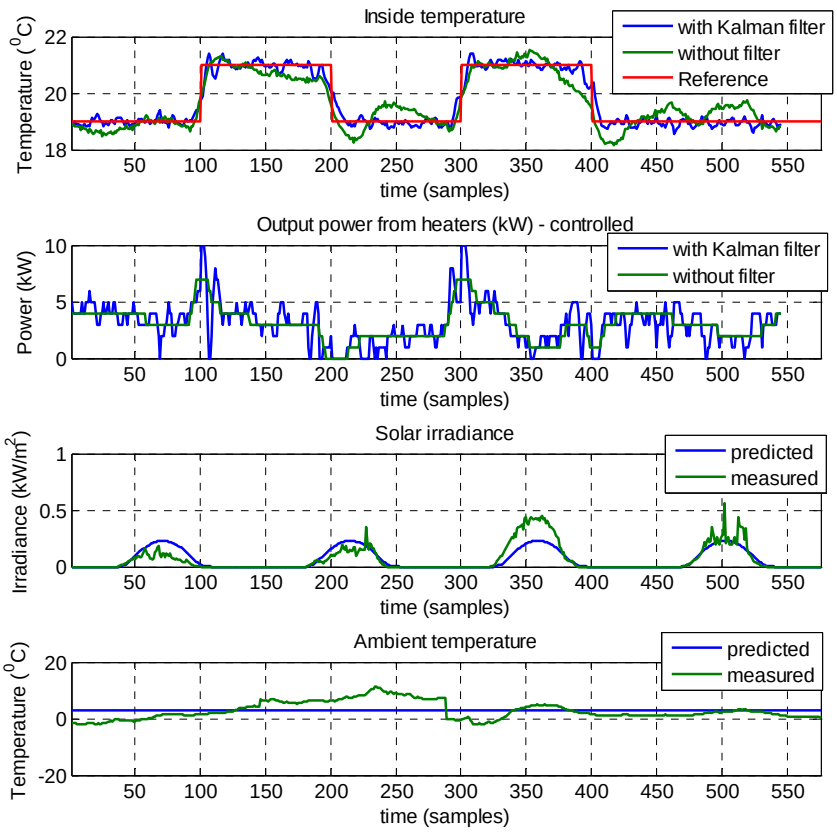

Fig. 4.12. Simulation Sim18 results Φ_{O0}= 0.0893 Φ_{O1}= 0.0315

The performance results are given by the cost Φ_{O0}= 0.0893 and Φ_{O1}= 0.0315.

However, as stated before, the classical MPC is not consistent, as the performance varies over large intervals, due to the lack of adaptability to disturbances and modelling errors. As shown in simulation case study **Sim18b**, presented in figure 4.13, with different disturbance prediction – which can represent, for this case a different calendar day, for which the historical annual average is different from the study case of Sim18. As results the performances values of the two MPCs are Φ_{O0}= 0.1138 and Φ_{O1}= 0.0313. The performance of the augmented state variation based MPC is changed only by 0.0002 which is insignificant, while the classic MPC is subject to a decrease of 0.0345.

A graphical overview of the simulated case studies considered here is presented in figure 4.14.

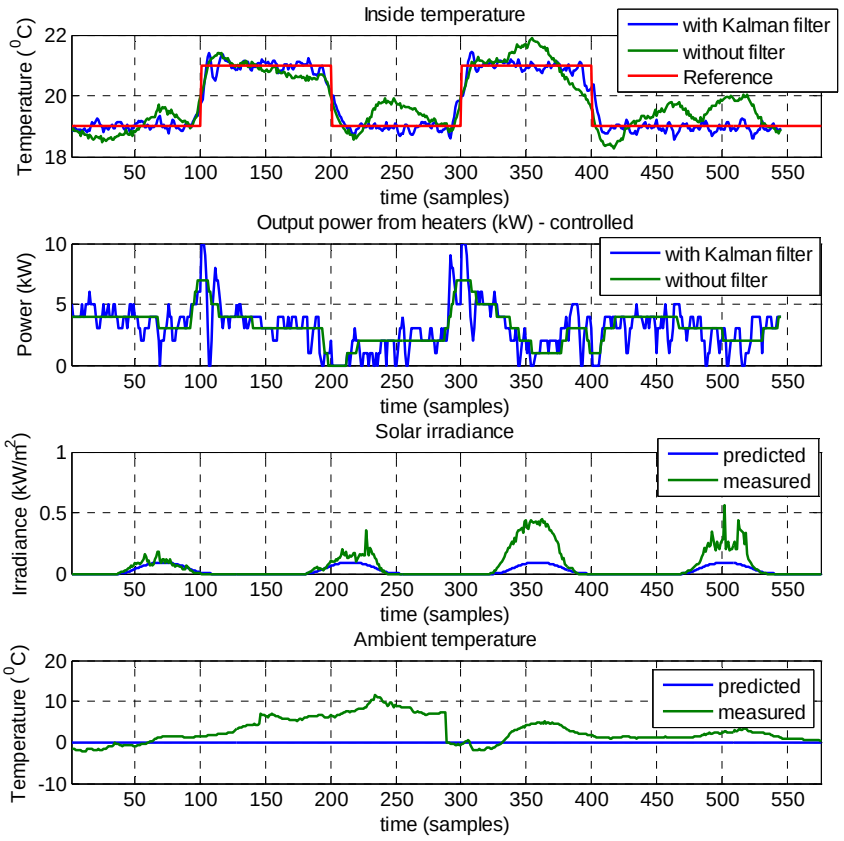

Fig. 4.13. Simulation Sim18b results Φ_{O0}= 0.1138 Φ_{O1}= 0.0313

One can see from this representation of the performance cost of the considered study cases that the use of state observer enhances the performance and gives consistent results over simulation scenarios.

The first simulation is considered the bench mark, as it runs under ideal conditions, with perfect predicted disturbances and a perfect model of the system.

A large variation, especially on the classic MPC, is clearly seen beginning with simulation number 10, where the process and used model are different.

From simulation number 16 noise is added on the states and on the output.

Although the MPC using the Kalman filter for state estimation is constant in performance under same type of assumptions, as seen for groups of simulations {1,2,4,6}, {10,12} – when the process differs from the model and {16,18,18b} – where white noise is added, the classical MPC, with no observer has large variations in the performance index, influenced by the model errors and disturbances in an unpredictable way.

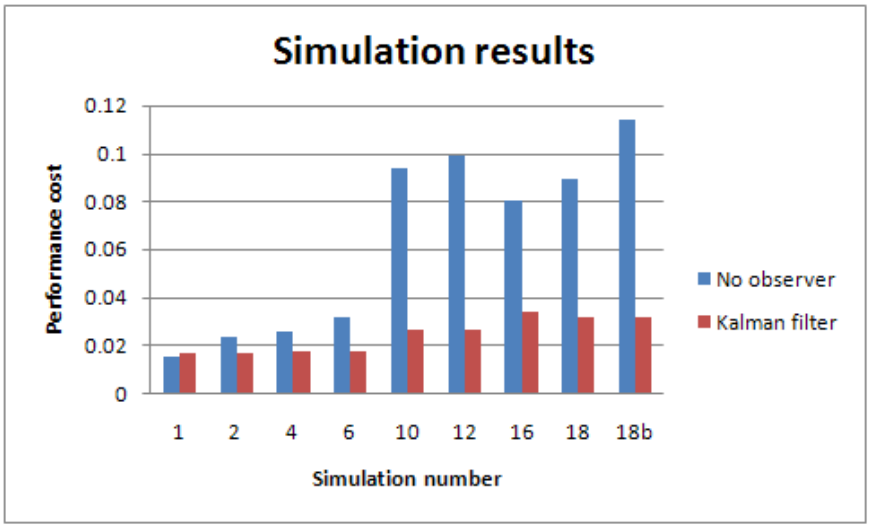

Fig. 4.14. Performance cost of the simulated study cases

Table 4.1 presents the simulation results when using the two model predictive control algorithms developed in this chapter. There were 19 simulation scenarios considered for validating the algorithms, each having different initial assumptions regarding the system model, the stochastic noise, the weather forecast, and the electrical heaters, as described at the beginning of section 4.4.4. The first column of the table represents the simulation index, the most relevant of these simulation results being shown in the above presented figures.

Table 4.1. Performance cost function values for different simulation scenarios

Sim.	System model	Stochastic noise	Weather forecast	Electrical heaters	Initial state	$\bar{\Phi}$
1	M1	S0	W1	H0	O0	0.0148
					O1	0.0163
2	M1	S0	W1	H1	O0	0.0229
					O1	0.0168
3	M1	S0	W2	H0	O0	0.0195
					O1	0.0166
4	M1	S0	W2	H1	O0	0.0252
					O1	0.0174
5	M1	S0	W3	H0	O0	0.0267
					O1	0.0165
6	M1	S0	W3	H1	O0	0.0312
					O1	0.0173
7	M3	S0	W1	H0	O0	0.0716
					O1	0.0185
8	M3	S0	W1	H1	O0	0.0848
					O1	0.0252
9	M3	S0	W2	H0	O0	0.0754
					O1	0.0204
10	M3	S0	W2	H1	O0	0.0938
					O1	0.0264
11	M3	S0	W3	H0	O0	0.0744

					O1	0.0190
12	M3	S0	W3	H1	O0	0.0992
					O1	0.0262
13	M3	S1	W1	H0	O0	0.0581
					O1	0.0272
14	M3	S1	W1	H1	O0	0.0861
					O1	0.0311
15	M3	S1	W2	H0	O0	0.0604
					O1	0.0285
16	M3	S1	W2	H1	O0	0.0805
					O1	0.0337
17	M3	S1	W3	H0	O0	0.0633
					O1	0.0290
18	M3	S1	W3	H1	O0	0.0893
					O1	0.0315
18b	M3	S1	W3	H1	O0	0.1138
					O1	0.0313

4.4.5. Experimental results

Experiments were conducted in order to test and validate the developed MPC strategy on the SYSLAB infrastructure from DTU Elektro at RISØ campus, as presented in chapter 2 and Appendix 1 of this thesis.

The MPC was running in Matlab, on a computer connected to the network node of the FlexHouse (the energy efficient building used as the process for this experiment).

The MPC solution – the command u_k representing the number of heaters to turn on – was used to call a Java code which is connected to the main computer serving the FlaxHouse interface, responsible for controlling all the switches in the house – the heaters, the lights, the oven, and other appliances.

For turning the heaters on and off a vector was defined having the dimension 10 by 1 containing the address of each of the 10 heaters and as the MPC was commanding a certain number of heaters u_k to be turned on, a function would turn on the first u_k heaters from the vector and turn off all the others.

Using the same interface, the controller reads the inside temperature of the house, representing the process output on which the observer is used for the state estimation step. The experiments are running with a time sample of 10 minutes, and the x axis of the plots represent the time (in sample) of the day; for example, the day starts at sample 0 and end at sample 144 – representing midnight.

The results plots from the experiment are arranged similar to the ones presenting the simulation results:

- The first plot presents the prescribed reference and the measured inside temperature in the building (FlexHouse)
- The second plot presents the number of heaters running at each time interval
- The third presents the predicted (blue) and measured (red) solar irradiance
- The fourth plot presents the predicted (blue) and measured (red) ambient temperature

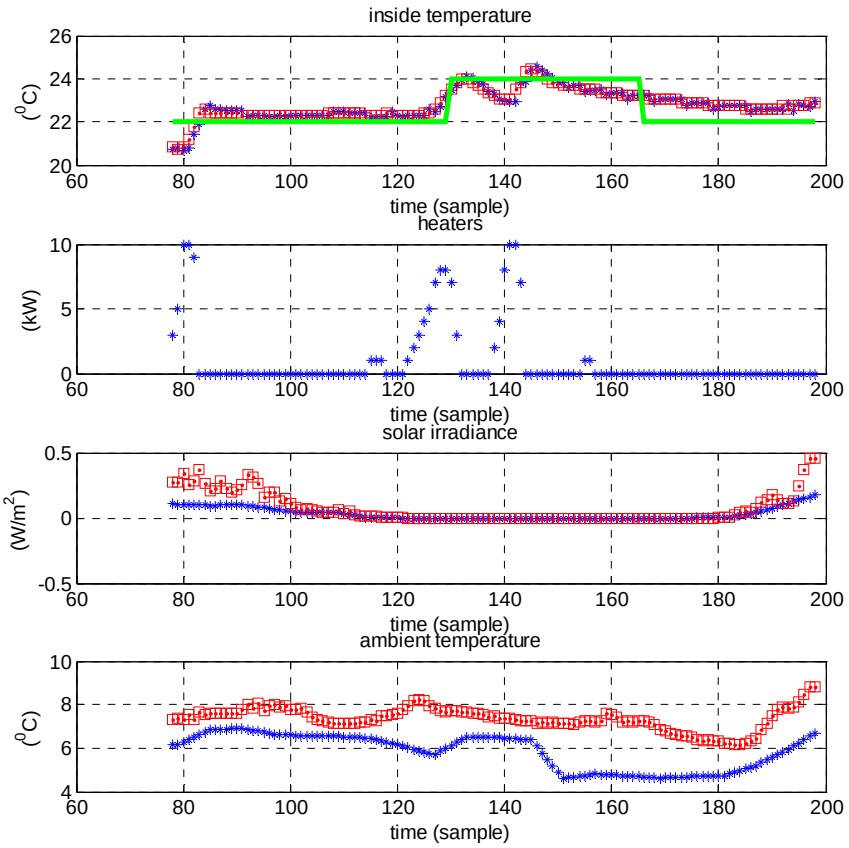

Fig. 4.15. Experimental results 1

After running the first experiment, with the results presented in figure 4.15, two undesired effects were observed:

- Oscillations at the step increase in the reference
- The temperature offset present from the second part of the experiment

Having this in mind, after the first experiment, additional considerations and changes had to be made:

- The inside temperature had to be calculated as the average temperature of the eight rooms, as for this experiment only one temperature was measured, the one from the main hall, room 0
- The communication interface had to be enforced with additional function calls because it was observed that the heaters were not

responding to the MPC command; for example, in the morning, time between 160-180, the controller was requesting 0 heaters and there were two heaters turned on; this was seriously affecting the experiment

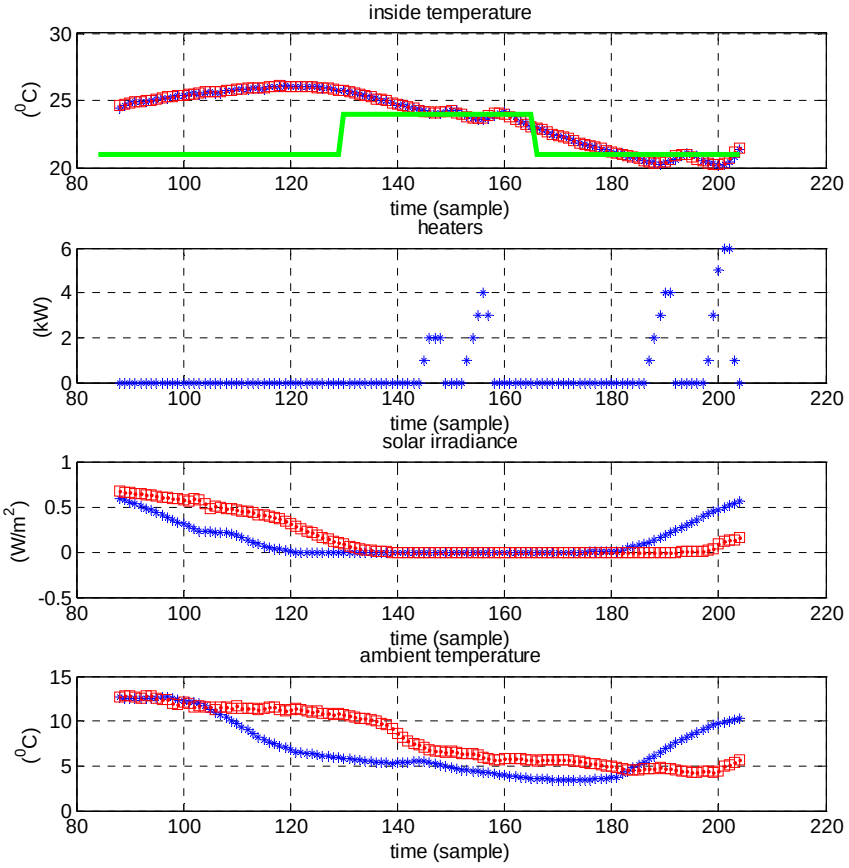

Fig. 4.16. Experimental results 2

The assumption on which the MPC was based that all the heaters have 1kW output power and the same effect on the inside temperature if a one room building model is used in a real life experiment are introducing additional modelling errors.

The second experiment was using the average inside temperature of all the eight rooms and the modified communication interface in order to get better results, as seen in figure 4.16.

The MPC was developed and ready for field tests at the end of April, when the weather started to become sunny and the temperatures rose as it can be seen

in the plots from experiment 1 and 2. During the day no heaters were necessary for the inside temperature to reach the prescribed values.

All the electrical heaters were physically limited by a thermocouple which turns off the heaters when the temperature reaches 30 degrees Celsius. As the model considers one large room (with one temperature) and the real system consists of eight rooms (each with its own temperature) although all the inside doors are open, due to the building's geometry, the rooms can have a large difference in temperature. Because the heaters are used in the same sequence by the MPC, starting from the low index of the vector defining the addresses of the heaters, the reference was not set to higher values closer to 30 degrees; in this case it is likely that in some rooms (which have their heaters set at the beginning of the vector and are started first) the inside temperature could reach 30 degrees and automatically shut down the heaters, altering the operation of the MPC.

As it can be seen from figure 4.16, at the end of the day (sample 126 is 9 PM), the temperature inside the house is 26 degrees and the MPC can operate only during the night to track the prescribed values.

The controller of this process can affect only one direction of the system, that is the MPC cab only increase the temperature by turning heaters on and cannot take any action in lowering it. The decrease in temperature must come naturally, and the MPC can only set all the heaters to off.

4.5. Conclusions

The model predictive control is a well suited algorithm to be used for inside temperature control of a building. Due to the nature of the process which has large time constants, this advanced control algorithm can be used at time samples of minutes or tens of minutes, that overcomes the MPC's shortcoming of requiring computation effort to solve a multivariable optimization problem.

This MPC formulation presented in the first part of the chapter presents offset from the reference due to model errors and unknown disturbances as seen in the simulations case studies. The performance cost, defined to measure the systems offset, increase its value as the simulation scenarios are considering more difficult cases, showing a decay of performance.

These unknown errors can be integrated into the model by augmenting the state-space model with additional disturbance states and using an observer to estimate the new states. As presented in the comparison results, by using this augmented model for the MPC formulation, the performance cost has better and consistent values over the simulation scenarios compared to the initial MPC and relatively close to the bench mark scenario that considers perfect simulation conditions.

The MPC implementation for the experimental setup revealed the necessity of additional considerations and modifications: an average inside temperature based on measurements from all eight rooms of the building was used.

Another onsite observation was that all the heaters have a thermostatic controller that disconnects the power if the temperature exceeds 30 degrees Celsius. This physical limitation, corroborated with the use of the average inside temperature as the controlled variable and the fact that the heaters were always switched in the same order, increased the probability that, even dough all the doors were open inside the house, in some rooms the temperature would exceed the 30

degrees limit; this would lead the heaters to be automatically switched off, disregarding the command from the controller, even if the house average temperature would not be achieved.

The simulation results show that the MPC is operating with very good results even in the case when no data is available from a weather station for the predicted solar irradiance and outside ambient temperature. As the MPC needs the weather prediction in order to calculate future states over the prediction horizon, in this case, the controller is considering a constant outside temperature like the annual average temperature of the geographic location or the best approximation based on available data; for the solar irradiance the same can be done: a solar irradiance evolution during a sunny day can be generated considering the particularities of the location. The errors between the real and the roughly predicted values of the disturbance are integrated by the additional states of the system, and offset free control is achieved.

As a Kalman filer is used to estimate the system's states, the controlled process achieves good results, with low performance cost, when white noise is affecting the states and the process output. However, the information about the noise covariance has to be known, which itself, is a separate system identification problem.

During simulations considering white noise disturbance, one could see that the evolution of the performance cost of the process controlled by the first MPC algorithm manifested large variations from one white noise sequence to another compared to the constancy of the second offset free MPC that presented very similar values.

5. Optimizing Energy Consumption by using Economic MPC

5.1. Introduction

On the objective of the MPC criteria, the literature concerning energy efficient buildings can be divided into two groups: controlling the inside comfort parameters, like the inside temperature to track a prescribed reference [Chen2002] [Henze2004] [Koch2012a] [Kolokotsa2009] [Kumemrt2001] and second, to minimize the energy cost of maintaining the parameters inside a comfort zone; the energy cost optimization is also referred to as economic MPC [Grande2008] [Halvgaard2012] [Hazyuk2012b] [Houwing2008] [Koch2012b] [Hovgaard2011] [Winn1985] [Ma2009] [DiGiorgio2012]. Recently Economic MPC has emerged as a general methodology with efficient numerical implementations and provable stability properties [Hovgaard2012].

This control is seeking to incorporate predictions of weather, occupancy behavior, renewable energy availability, and price signals from the grid. The model predictive control (MPC) presents a methodology that can use all these predicted values in order to improve the energy efficiency consumption by load shifting and peak shaving, minimize the cost of operation by using low price energy, as shown in (Nagai, 2002) and in (Ma 2011), and maximizing the use of renewable energy.

This chapter proposes a MPC that minimizes the overall electrical energy cost of heating a building which also has a local PV installation. By using the building's ten 1 kW heaters, a price signal for electrical energy, a prediction of solar irradiation and of ambient temperature it is possible to coordinate the heaters consumption so that as much energy as possible is consumed from the locally produced PV.

In [Hazyuk2012b] a simulation study is presented where a cost function minimization is proposed for MPC which ensures the thermal comfort in the building with minimal energy consumption. The problem is formulated as a linear program, the optimization function being linear as well as the constraints.

In Norway an economic MPC was implemented on a small scale experiment as presented in [Grande2008], where market participation is involved in demand response. The paper presents a pilot study of distributed resources from household customers utilizing smart meters, remote load control and load shifting.

Another paper that deals with a floor heating system and a heat pump presented in [Halvgaard2012]. The system is represented by a state space model and the objective is to minimize the cost of maintaining the inside temperature inside the thermal comfort zone. By shifting the consumption of the heat pumps used by the floor heating systems to periods of time when the energy has a lower price. The objective function is defined as a linear program which minimizes the cost of the problem – hence the usage of the name 'economic MPC'.

Another example of economic MPC is in [Hovgaard2011] where the simulation study of MPC implementation for supermarket refrigeration is presented. Models validated from real supermarkets as well as real weather data and energy prices from the Nordic power market are used. The paper considers the fluctuations of price in the real power market that are available for industrial consumers which can change within a time interval of 2 to 15 minutes. According to the movement of price due to the relation between production and consumption, this effect is named

up regulating price as primary reserve, when the production exceeds consumption, or down regulating as primary reserve, when the consumption is larger. As a cost objective function, the problem is regarded as a linear program.

A system of a building equipped with a water tank used for storing cold water produced by chillers is presented in [Ma2009]. Predictive knowledge of building loads and weather conditions is available. A model predictive control algorithm for optimally store thermal energy in the tank is developed. Terminal constraints are introduced for ensuring stability of the optimization problem. Historical consumption patterns are considered that provide the predictor with an envelope for computing the future values into the prediction horizon.

In [Ma2011] economic MPC with a linear programing problem is implemented. The problem is formulated as a single floor multi-zone commercial building equipped with a variable air volume cooling system. The MPC is implemented in Matlab and a virtual building is simulated in EnergyPlus. Matlab is also used to identify the model's parameters by generating a set of inputs. The models for temperature and power consumption of the building are identified. The identification models are autoregressive exogenous (ARX) and the identification is realized by using a sequence of pseudorandom binary sequence (PRBS) inputs to each zone of the floor. It is showed that in a smart-grid environment the MPC can make cost savings by pre-cooling and load shifting at low-price energy tariffs.

In [DiGiorgio2012] an economic MPC was used for load shifting of different house loads smart appliances, energy storage units and smart meters. The loads are categorized in plannable loads, which can be shifted from the set start time without a discomfort for the user, this is mainly true for the smart appliances, and the non plannable loads, represented by the loads that are required to operate at the time the consumer sets the start time, for example the lights and the TV set. This solution is implemented by using Matlab and the optimization function is solved using the commercial software package CPLEX [CPLEX].

The subject of this chapter is minimizing the cost of maintaining the inside temperature of the house between set limits, by using the electric heaters when the energy price from the grid is lower. Unlike the tracking MPC described in the last subchapter when the objective was to control the inside temperature to follow the reference in the presence of disturbances and model and prediction errors, in the case of economic MPC formulation, the thermal model of the house is used as a storage device which has the possibility to store thermal energy when the price is low, by reaching an upper comfort limit of the temperature and to use that excess heat in order to operate during high price of the grid energy periods by using as little grid energy as possible.

5.2. Optimizing grid energy cost

The economic MPC algorithm development in this work relies on the algorithm presented in section 4.4 as it is developed in Matlab using the *quadprog* solver from the Optimization Toolbox.

An additional term was added to the optimization function which represents the grid energy price (C_G) at each moment k, with the assumption that the energy price from the grid is accurately predicted. As the optimization algorithm relies on future values of the price, these price values must be known in order for the system

to react properly and to store low price energy into the inside environment of the building. This is one assumption made in this chapter, as the price is changing in real time.

The optimization function is represented by Equation 5.1:

$$\min_{u} \Phi = \frac{1}{2}\sum_{k=0}^{N} \|z_k - r_k\|_Q^2 + \frac{1}{2}\sum_{k=0}^{N-1} \|\Delta u_k\|_S^2 + Q_{cost} \sum_{k=0}^{N} C_{G,k} u_k \quad (5.1)$$

The grid energy cost also has a weight factor Q_{cost}, which enables a tradeoff between tracking the desired inside temperature and minimizing the consumption cost of the overall operation.

For the simulation scenarios the setup presented in figure 5.1 was used. The household is connected to the grid which provides the house loads with electric power. The price of the grid electric power is known over the entire optimization horizon and the controller shifts the load power consumption to the time intervals when the price is lower.

In all the simulations the MPC controller uses the formulation described in Equation 4.50 which relies on the process mode, equation 4.2, with two additional space variables for considered disturbances: solar irradiance and ambient temperature. These two additional state variables are estimated by the observer in order to achieve offset free control in the presence of deviations from the predicted values of the two disturbances.

The MPC controller has hard limitations on the controlled variable – the inside temperature, that has to be inside [20...23] °C interval and on the manipulated variable – power supplied to the heaters, that has to be in the [0...10] kW interval, and can have only integer values as power consumption steps.

The MPC controller starts with offline predicted values for solar irradiance, temperature, and grid price and for the third simulation case presented in this chapter, the predicted PV power output.

The sample time of the simulations is 10 minutes, and the prediction horizon is 50 time steps.

In addition to the power consumed from the grid, (represented by $P_{Grid2Load}$ in figure 5.1) the household can be supplied with green power produced by a local PV plant mounted, for example, on the roof of the house. This scenario, considering the presence of the PV plant, is used both in this section and in section 5.3, as the thesis presents the study of renewable energy resources integration in the low voltage distribution grids.

In the case that the household is equipped with a PV installation, the PV it produces power independently of the heaters' (load) consumption, according to the weather conditions; however, the power source of the heaters can be prioritized: it is considered that the load first consumes the necessary power form the PV ($P_{PV2Load}$) and the remaining produced and locally unconsumed power is injected to the grid ($P_{PV2Grid}$).

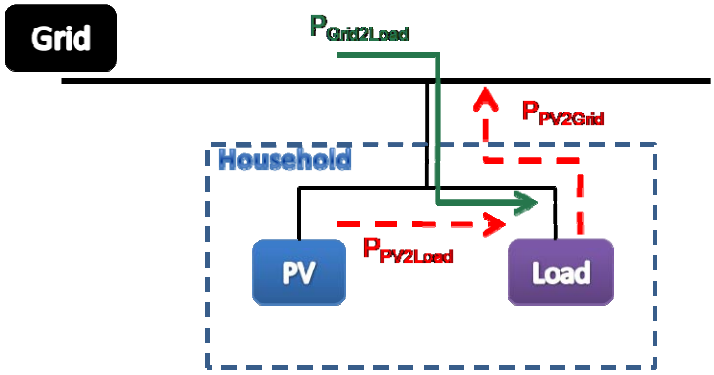

Fig. 5.1. Energy consumption setup for a household

For expressing the different study cases, an index was defined, based on the classification from section 4.4.4. In addition, for this section were considered only the cases when the heaters are controlled by on/off bases, hence only steps of 1kW are permitted; also, only the augmented state-space model with state observer is used. The case study index is defined as:

M*a*M*b*W*c*S*d*

where:

a – state-space model for the MPC
(**1** for the one state space model; **3** for the three states space model)

b – state-space model for the process
(**1** for the one state space model; **3** for the three states space model)

c – weather data source and availability
(**1** for perfect prediction; **2** for weather station forecast; **3** for no data available)

d – stochastic disturbance
(**0** – no stochastic disturbance; **1** – stochastic disturbance present)

From the simulations it can be seen, as expected, that by minimizing the operation cost, the controller will keep the inside temperature at lower values, using as little energy as possible, with respect to the lower temperature constraint. The effect of the economic MPC can be seen prior to a peak in grid price, when the heaters are turned on and the inside temperature rises near to the upper temperature limit. During the peak energy price, the heaters are turned off and the inside temperature drops due to the ambient outside temperature. This can be seen in the two simulation scenarios presented in the following.

In figure 5.2 the results of a simulation over a week is presented, when the economic MPC is used to minimize the cost of energy consumed to keep the inside temperature inside the comfort zone, between 20 and 23 degrees Celsius. The first plot represents this inside temperature in the time interval considered, where the x axis represents hours.

The second plot represents the electric heaters' output power, controlled by the MPC, with the additional representation of the power generated by a 10 kW PV plant installation mounted near the house to provide green energy. The sources of the power consumed by the heaters are prioritized as mention before: first the

energy is consumed from the PV plant and second from the grid; the sources are also represented with red (PV) and green dotted lines (Grid). In this way both the cases when the household is provided with a PV plant and the case when the household has the grid as the single power source are described.

In the third plot, one can see the energy price from the grid in Euro/MWh. These values were taken from Nord Pool spot market [NordPool].

The effect of economic MPC is clearer when the difference in the price is higher, as it is around the peak price at 30 hours and 130 hours.

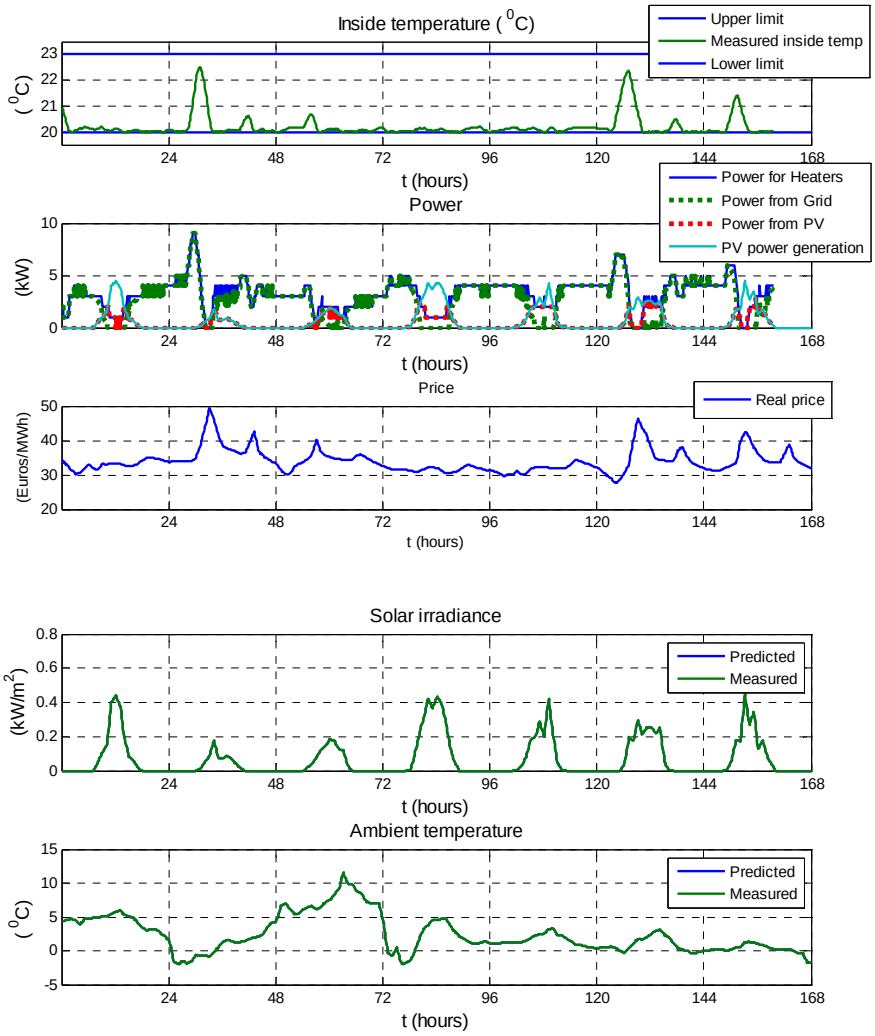

Fig. 5.2 . Economic MPC simulation results for the study case M1M1W1S0

Plots four and five show the weather conditions: in this study case, the solar irradiance and the ambient outside temperature are perfect predicted. In addition,

the MPC uses a perfect thermal model of the house. This case can be considered a benchmark case for further comparison of the performance of different algorithms.

In figure 5.3 a study case of more realistic operation is simulated:

- The economic MPC uses the one state-space model as for the plant model the three state-space model was used
- There are weather prediction errors; the weather prediction was taken from a web resource, a weather station [WeatherRISO] and the real data was measured with onsite devices
- White noise was considered on the input and output of the system – representing measurement errors and unknown stochastic evolution of the inside temperature

The same plot representations as described above were used to illustrate the results in this case.

One can see that the overall evolution is very similar to the first study case, in the sense that prior to the price peaks the controller stores thermal energy around 30 hours and 130 hours. However, the heaters are switched more often in order to cope with the disturbances and prediction errors.

In some moments the lower limit is slightly breached due to the stochastic perturbation. This breach can be avoided by using the so called stochastic MPC, which considers the cumulative dispersion of the white noise over the optimization (prediction) horizon and includes this cumulus in the constraints definition at each computation step; This has the role of tightening the constraints, or the limits, on the controlled variable, in this case the inside temperature, and when the stochastic perturbation occurs, the imposed limit is not reached due to this extra 'space' that the tighten limit provided.

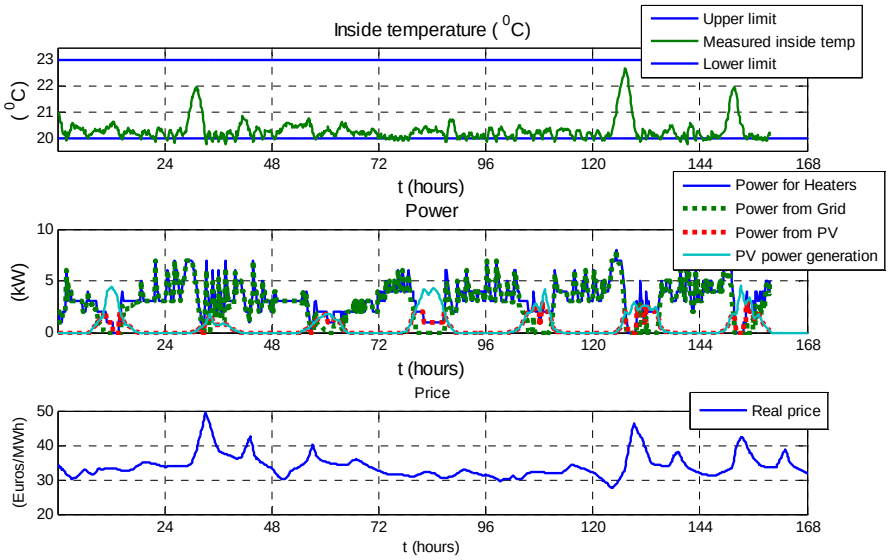

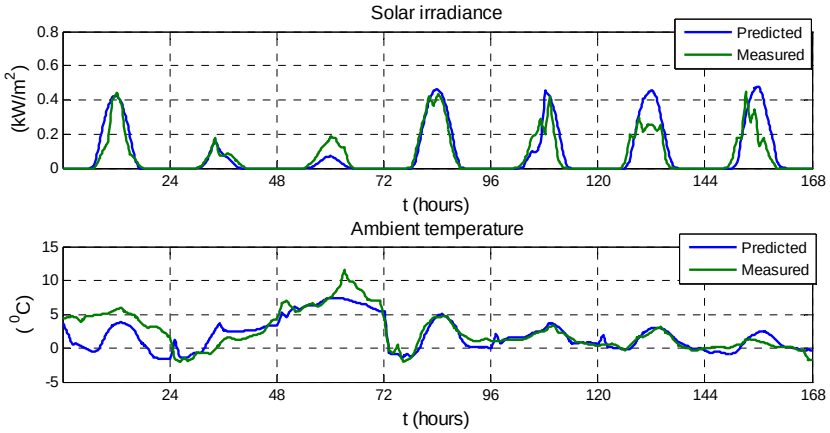

Fig. 5.3. Economic MPC simulation results for the study case M1M3W2S1

In order to emphasize the effect of the economic MPC on the minimization of the overall operation cost for different study cases, the results by using the economic MPC were compared with the operation results by using the tracking MPC presented in section 4.4. For each study case, for the tracking MPC the prescribed reference is constant over the operation interval and is equal to the average inside temperature resulting from the simulation with the economic MPC. This consideration was intended to eliminate the differences in the consumed energy for the two cases and to be able to compare the effect of load shifting both from a qualitative and quantitative perspective.

Figure 5.4 presents the operation results when the tracking MPC was used for the study case of M1M3W2S1; the same study case which is represented in figure 5.3 when the economic MPC is used.

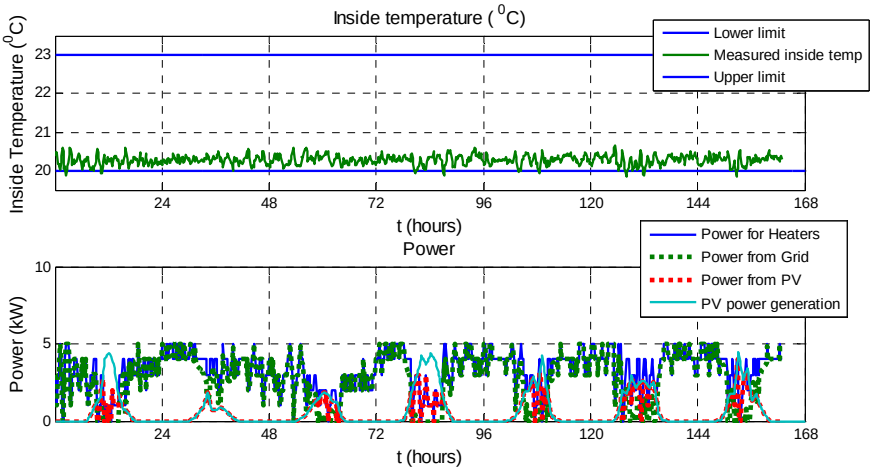

Fig. 5.4. Simulation results by using tracking MPC set at a constant value for the study case of M1M3W2S1

A number of six simulation study cases were chosen to compare the results of using the Economic MPC, presented in table 5.1, and the results by using the tracking MPC, presented in table 5.2, which does not take into account the price of energy. The simulations were realized under similar conditions, having the same weather data and the same models were used. Also the average inside temperature was chosen to be similar in order to make the comparison possible.

Table 5.1. Economic MPC simulation results for different operation study cases

Study Case	E_H	E_{PV2H}	E_{G2H}	E_{PV2G}	C_{PV2H}	C_{G2H}	$C_{G2HnoPV}$	T_{avg}
	(kWh)	(kWh)	(kWh)	(kWh)	(Euro)	(Euro)	(Euro)	(°C)
M1M1W1S0	510.66	72.84	437.82	45.08	1.457	14.498	17.01	20.20
M1M3W1S0	516.33	74.40	441.93	43.52	1.488	14.672	17.26	20.22
M1M3W2S0	517.33	72.31	445.02	45.61	1.446	14.759	17.28	20.25
M1M3W3S0	516.50	76.34	440.16	41.58	1.526	14.622	17.27	20.23
M1M3W2S1	516.00	69.64	446.36	48.28	1.39	14.80	17.23	20.29
M1M3W3S1	515.33	74.38	440.94	43.53	1.487	14.628	17.21	20.28

Table 5.2. Tracking MPC simulation results for different operation study cases

Study Case	E_H	E_{PV2H}	E_{G2H}	E_{PV2G}	C_{PV2H}	C_{G2H}	$C_{G2HnoPV}$	T_{avg}
	(kWh)	(kWh)	(kWh)	(kWh)	(Euro)	(Euro)	(Euro)	(°C)
M1M1W1S0	526.33	83.47	442.86	34.48	1.67	14.82	17.79	20.20
M1M3W1S0	531.16	84.21	446.96	33.74	1.68	14.97	17.96	20.18
M1M3W2S0	533.83	81.85	451.98	36.09	1.64	15.15	18.07	20.25
M1M3W3S0	533.00	82.21	450.79	35.74	1.64	15.10	18.20	20.23
M1M3W2S1	531.66	79.36	452.30	38.58	1.58	15.15	17.98	20.27
M1M3W3S1	531.83	80.25	451.57	37.69	1.60	15.13	17.98	20.28

For the results presented in table 5.1 and table 5.2, the following notations have been used:

Study case – simulation identifier

E_H – the total energy consumed by the heaters during simulation interval

E_{PV2H} – the amount of energy consumed by the heaters from the local produced PV energy

E_{G2H} – the amount of energy consumed by the heaters from the grid

E_{PV2G} – the amount of energy produced by the PV to be sold to the grid

C_{PV2H} – cost of E_{PV2H} in Euros

C_{G2H} – cost of E_{G2H} in Euros

$C_{G2HnoPV}$ – cost of E_H in Euros, in the case that no PV panels are present and the entire energy is taken from the grid, at the grid set price

Avg. Ti – average inside temperature over the simulated time horizon

For a more clear view over the benefits of the economic MPC regarding the cost minimization, the obtained results for the cost of energy used during operation are presented in figure 5.5.

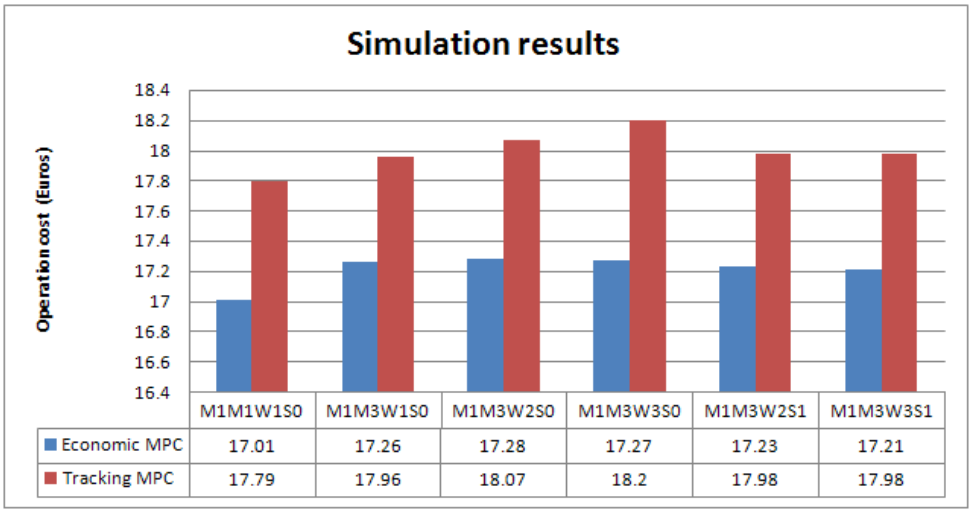

Fig. 5.5. Comparative results between using a cost optimization MPC and a constant reference tracking MPC

These results show a cost reduction of the energy bill for each study case over a time interval of one week, emphasizing the effect of the economic MPC. This is due to the fact that the tracking MPC keeps the inside temperature using a rather continuous energy consumption of the heaters while the economic MPC uses more low price energy and decreases consumption on the high price intervals.

However, for single household, the savings are rather modest in a time interval of one week as presented in these simulations. The consumption optimization's effect is seen better on large scale local grids when a large number of consumers are optimizing their consumption.

5.3. Economic MPC with local PV production

One of the most rapidly growing types of distributed generation is in household PV plants; this increased penetration adds to the complexity of distribution grid operation as stated in [Madureira2009].

In this section an approach was made to include in the economic MPC formulation the locally produced PV power availability. The purpose of this is to give high priority for consumption to the local green energy. In other words to integrate the PV resource installed by the consumer near the house, in the low voltage distribution network as presented in figure 5.1.

By using the local produced energy, the amount of energy that flows between the grid and the consumer diminishes and the grid is less used as a storage device as it is nowadays, hence the consumer is more energy independently and the grid is less congested.

During each simulation, two different cases can be studied:

- The first, when the house does not have any PV installation – the heaters are consuming power entirely from the grid
- The second, when the house has a PV installation – the heaters are consuming power both from the PV plant and from the grid. The higher priority is to

consume from the local PV plant and the remaining required power is taken from the grid. The amount of unused PV energy is sold to the grid.

The MPC controller tracks the inside temperature with minimal overall energy cost, also considering the power production of the installed PV panels. The controller calculates a virtual price on which the available PV power, that has a lower cost for the user (C_{PV}) of 0.02 Euros, is considered to alter, with a weight factor, the market imposed price.

$$U = P_{Grid} + P_{PV} \tag{5.2}$$

where

U – is the heaters' consumed power

P_{grid} – is the amount of power consumed by the heaters from the grid

P_{PV} – is the amount of power consumed by the heaters from the local PV system.

The cost minimization function would be

$$\min_{P_{Grid}} \Phi = C_G P_{Grid} \tag{5.3}$$

Considering U as the optimization variable and replacing equation 5.2 in equation 5.3 the following relation is obtained:

$$\min_{U} \Phi = C_G U \left(1 - \frac{P_{PV}}{U}\right) \tag{5.4}$$

where

C_G – is the predicted price of the grid energy

U – represents the vector with the next N command values for the time horizon

P_{PV} – represents the predicted output power from the PV installation

The virtual price which considers both the grid price and the PV available output power is calculated with the following mathematical relation:

$$C_v U = C_G \left(1 - \alpha \frac{P_{PV}}{u_s}\right) U \tag{5.5}$$

Where additional assumptions were made:

- $\alpha = \frac{C_{pv}}{C_G}$ - a weight factor
- at each optimization step, u_s is taken as the last command value, u_{k-1}.

The optimization function is written as:

$$\min_{u} \Phi = \frac{1}{2}\sum_{k=0}^{N} \|z_k - r_k\|_Q^2 + \frac{1}{2}\sum_{k=0}^{N-1} \|\Delta u_k\|_S^2 + Q_{cost} \sum_{k=0}^{N} C_{v,k} u_k \tag{5.6}$$

The optimization function in the case of the economic MPC with PV integration contains three terms referring to temperature tracking, command variation, and command cost each with a set weight: Q, S and Q_{cost} respectively.

Figure 5.6 and figure 5.7 represent the result plots of two simulation study cases, under operation conditions explained in section 4.5 as coded in the case study index.

The simulations were realized in the same conditions as presented in section 4.5: the same models, the same available weather prediction data and time step. In this case however the economic MPC uses the objective function from equation 5.6 that maximizes the consumption of the local produced PV energy by applying a virtual price, equation 5.5, depicted in the second plot of the next two figures.

The plots illustrated here have the same represented values as described in section 4.5 which now have a different operation evolution according to the new objectives.

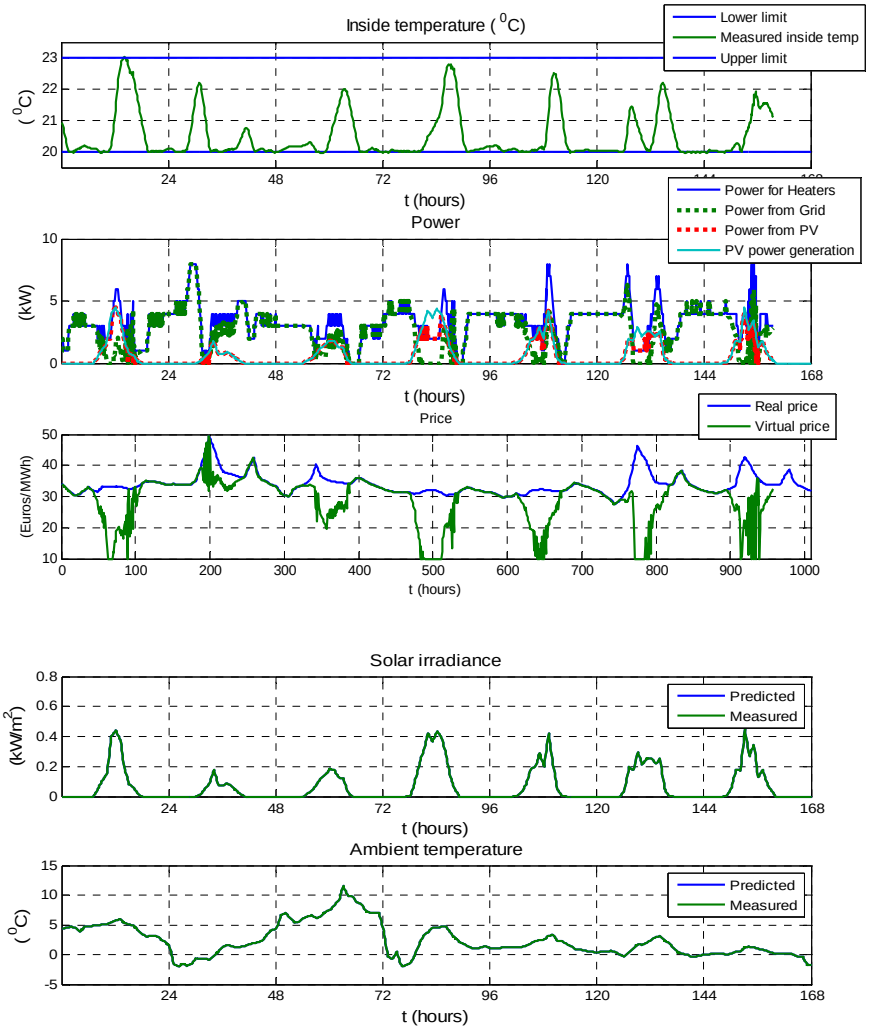

Fig. 5.6. Economic MPC with PV integration simulation results for the study case M1M1W1S0.

Figure 5.6 plots the results from the study case M1M1W1S0 which is the ideal case when both the model used by the MPC and the weather prediction are perfect; thus this is more a bench mark study case.

In figure 5.7 a more realistic case is presented where modelling errors, unknown disturbances and white noise are affecting the system.

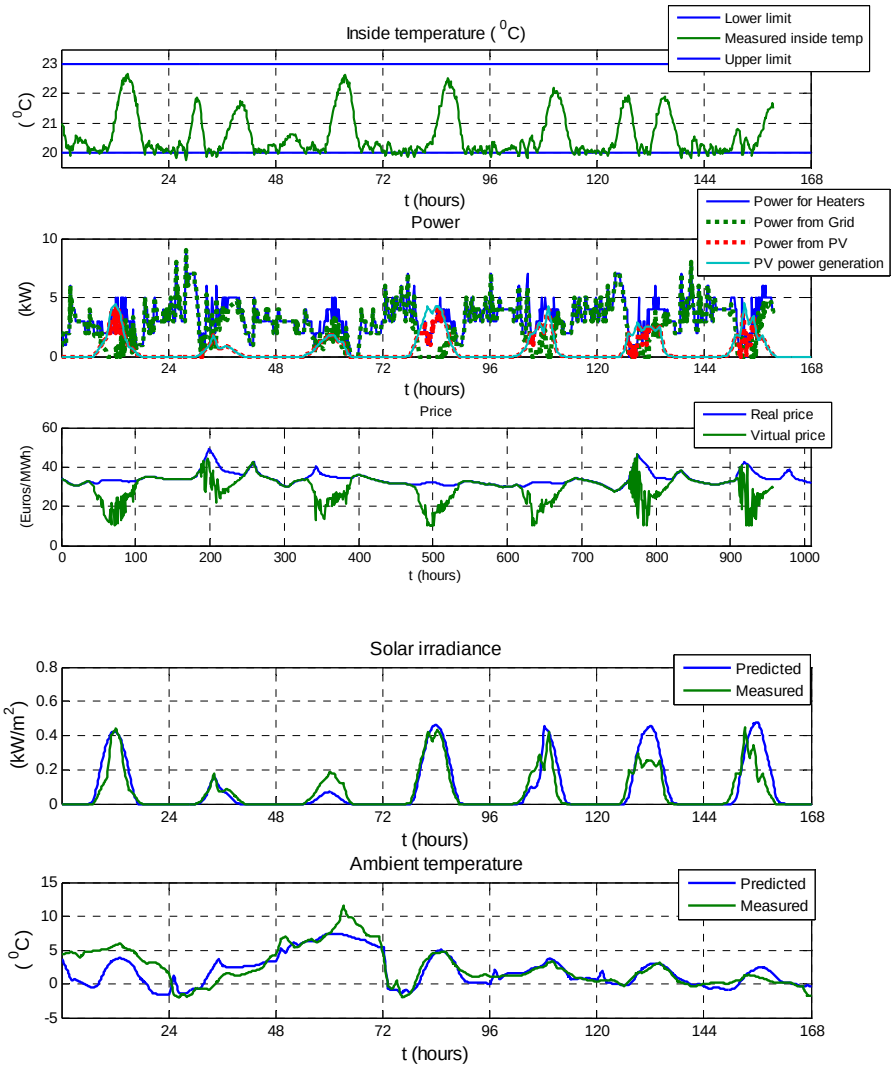

Fig. 5.7. Economic MPC with PV integration simulation results for the study case M1M3W2S1.

From the simulations one can see that the controller shifts the load (the electrical heaters) to the intervals when the virtual price is low, that is when the PV production is high. In the second plot it is shown that the PV output power (represented with teal line) is largely consumed by the heaters, represented with red dotted line.

For a quantitative perspective of the proposed economic MPC with PV integration, an extensive array of study cases were investigated for testing. The numeric results are presented in table 5.3 and a visual representation is shown in figure 5.8.

Table 5.3. Economic MPC with PV integration simulation results for different operation study cases

Study Case	E_H (kWh)	E_{PV2H} (kWh)	E_{G2H} (kWh)	E_{PV2G} (kWh)	C_{PV2H} (Euro)	C_{G2H} (Euro)	$C_{G2HnoPV}$ (Euro)	T_{avg} (°C)
M1M1W1S0	523.66	100.77	422.89	17.14	2.01	14.07	17.58	20.48
M1M3W1S0	528.33	102.98	425.35	14.93	2.05	14.18	17.77	20.49
M1M3W2S0	534.16	100.23	433.93	17.69	2.00	14.44	17.96	20.51
M1M3W3S0	530.67	100.04	430.62	17.88	2.00	14.35	17.82	20.51
M1M3W2S1	528.66	98.56	430.10	19.36	1.97	14.32	17.74	20.56

Figure 5.8 shows graphical representations of the amount of local produced PV power used by the heaters in fife different operation scenarios. For each scenario the consumed PV power by using the proposed economic MPC and the tracking MPC algorithm are compared to the total amount of available produced PV power.

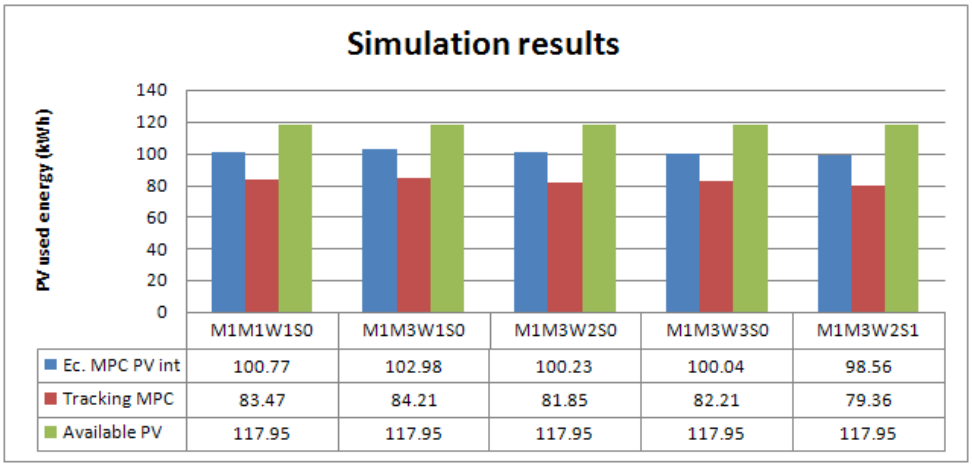

Fig. 5.8 Comparative results between using a cost optimization MPC with PV integration and a constant reference tracking MPC

It is shown that by using the proposed economic MPC algorithm with PV availability estimation the controllers manages to consume around 85% of the produced PV power

5.4. Comparison between traditional thermal control and proposed algorithms

In this section it is presented a comparison between the results obtained by using a traditional thermostatic controller and the algorithms proposed and developed in the last section. The purpose of this comparison is to highlight the advantages of using control algorithms in controlling the inside temperature of a building introducing optimization in the operation cost and maximizing the local produced green energy.

Making buildings energy efficient is an important task because, as presented in chapter 2, the building sector is responsible for an important percent of the total consumed power at the global scale.

As presented in the simulation results from the last section, by using advanced control algorithms for cost optimization the benefits for a single household are rather modest, just a few Euros per month. This small gain is due to small variations in the grid energy price from high and low price intervals and also for the relatively small consumption of a household.

Also this optimization consists in modifying the internal temperature set by the user on different time intervals, both for lowering and rising the temperature according to grid energy price and PV availability. This has been discussed by researchers and green energy sceptics like in [Vaclav2012] that considers that in real life the user will not be willing to give up the total comfort (in this case a constant temperature set by himself) for such a small amount of economic gain.

However, even if for an individual the economic savings are not high and the advanced controllers could alter with the thermal comfort of a person, if these controllers are implemented on large scale some important benefits can be drown:

- the savings are accumulating from a large number of households
- considering the grid energy price, the consumption can be shifted to time intervals when energy is cheaper (that is the plants connected to the grid are producing more energy that is consumed) and thus fewer large energy storage devices are needed at the grid level
- considering the local produced green energy for renewable resources the buildings can become more energy independent
- the case when the consumer is becoming an energy producer and energy is transported into the grid in both ways is avoided

This section will present comparisons from the perspective of the grid energy and grid energy cost used for the heating system in the case a 10 kW PV plant is installed near the household, as shown in figure 5.1 as well as the amount of available local produced PV energy is consumed by using different control algorithms.

The four control algorithms are:

- thermostatic control
- tracking MPC
- economic MPC with grid energy cot optimization
- economic MPC with grid energy cot optimization and local PV availability

5.4.1. Control algorithm 1 - Thermostatic controller

The simplest controller for the inside temperature of a building is the thermostatic controller, which is an on/off controller: for its operation an upper and

a lower temperature limit are set; during operation, when the upper temperature limit is reached, the electric heaters are turned off and when the lower limit is reached, the heaters are turned on.

For the simulation a thermostatic controller is implemented to maintain the inside temperature of the building between given limits: [19...21.5]. For comparison reasons, the limits in this simulation scenario differ from the other scenarios in order that the average temperature in the house, for the simulation time interval, to be the same. This has the purpose to accurately reflect the MPC controller's effect in similar operation conditions.

Figure 5.9 represents the operation results of using this controller. In the first plot is represented the inside temperature during the operation. One can see that it oscillates between the imposed limits, having a slower descent during daytime, when the solar irradiance heats the inside temperature of the building and slows its decay due to the low outside temperature.

The second plot represents the power consumed by the heaters, which for this controller are all turned on or off in the same time, and the two energy sources consumed by these heaters, the PV and the grid, the local PV having higher priority. Also with teal is represented the available PV power, which in this case is largely unused by the heating system and is injected into the grid.

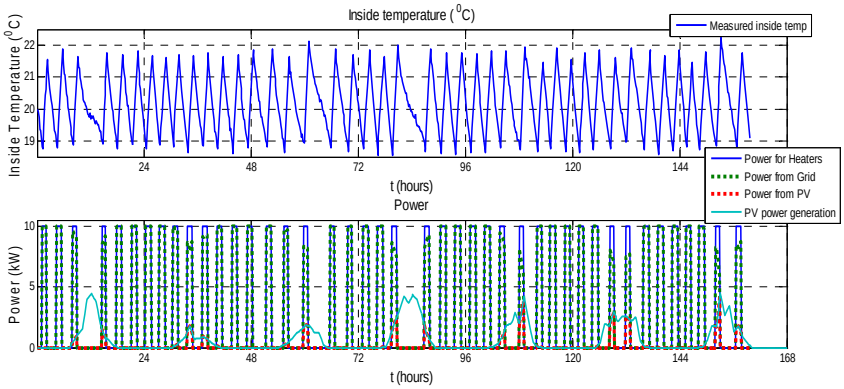

Fig. 5.9: Thermostatic control simulation.

From the simulation results two conclusions can be drawn regarding the thermostatic control:

- this type of controller commands high power consumption on short time intervals (tens of minutes)
- due to the solar irradiance heating effect on the inside temperature, the heaters are more likely to be switched off during sunny time intervals.

5.4.2. Control algorithm 2 - Tracking MPC

For the next three control algorithms the graphical illustrated study cases are the same and the operation considerations are for the worst case scenario, when modelling errors, unknown disturbances, and white noise on the input and output of the process are present.

The proposed tracking PMC minimizes the difference between a preset reference and the inside temperature under modelling errors and unknown disturbances as was explained in section 4.4.

The results when using this algorithm are shown in figure 5.10. the first plot shows the inside temperature which is maintained inside the comfort limit.

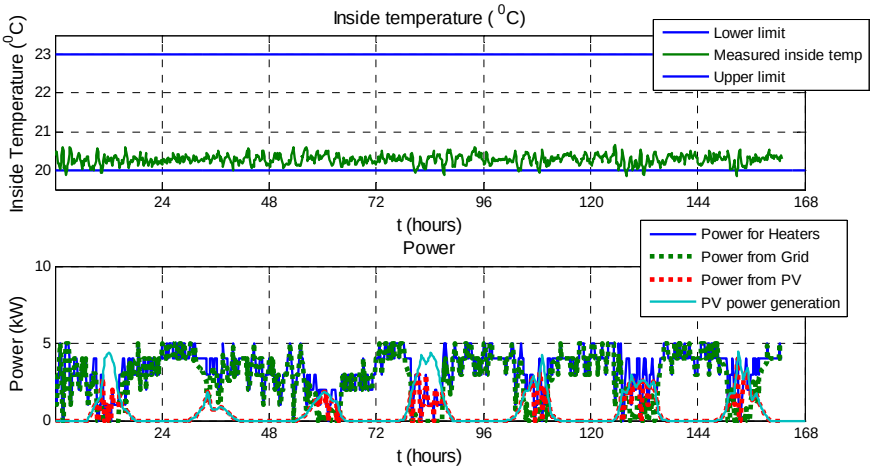

Fig. 5.10: Tracking MPC simulation.

5.4.3. Control algorithm 3 - Economic MPC with grid energy cost optimization

The economic MPC was formulated by adding a term to the optimization function which minimizes the operation cost of the heating system. This implies that the heaters will consume more energy at low price intervals and store thermal energy into the house internal environment. The tendency for the controller is to store energy prior to high peak prices as seen in figure 5.3.

Although the operation cost is minimized in the case when the energy is consumed from the grid, as shown in the results from section 4.5 in figure 5.5, in the case of using a household configuration with an installed PV plant as in figure 5.1, the amount of PV used is rather smaller than using the tracking algorithm.

Also one can note that in the use of control algorithm 2 and 3, the energy consumed from the local PV plant has a fluctuating percentage of the total PV production, because the controllers are not directly correlated to the PV power availability.

5.4.4. Control algorithm 4 - Economic MPC with grid energy cost optimization and local PV availability

By defining a virtual energy price, as in equation 5-5, considering the grid energy price, the predicted available PV power and the necessary power for the electrical heaters a new economic MPC was proposed, developed and tested through simulations as explained in section 4.6.

The results during the worst case scenario simulation are represented in figure 5.7 and present the effect of the control which stores thermal energy both when solar energy is available and prior to the peak energy price in the grid.

5.4.5. Results

As the purpose of this study is to highlight the benefits of using the locally produced green energy, with a high priority over the energy taken from the grid, the discussions will focus on the amount of PV energy used by the heating system and the cost of consumed grid energy in each simulation study case.

From the knowledge of the author, to this day, the national governments are subsidizing the individual renewable energy resources installation and production; this translates into policies in which the grid is buying energy from the consumer with a higher price than it is selling. In this case, it would be more economical convenient for the consumer to sell all the green energy that his PV is producing to the grid. As the RES are entering the low distribution grid in rising numbers and consumers are including them in the household setup even into the architectural design of the buildings, the policy on green energy price will change.

This work considers the case when the selling price of the green energy from the consumer to the grid is lower than the grid energy price; this would encourage the consumer to use the locally production which is cheaper than buying energy from the grid.

Comparative results between the four control algorithms developed in this section are presented in table 5.4 and in figures 5.11 to 5.13, for the simulation conditions defined by M1M3W2S1. For table 5.4 the following notations have been used:

Controller type – one of the four controllers investigated in this study

E_{G2H} – the amount of energy consumed by the heaters from the grid

C_{G2H} – cost of E_{G2H} in Euros

E_{PV2H} – the amount of energy consumed by the heaters from the local produced PV energy

E_{PV2G} – the amount of energy produced by the PV to be sold to the grid

C_{PV2G} – cost of E_{PV2H} in Euros

Table 5.4. Comparative results for the four control algorithms

Controller type	E_{G2H} (kWh)	C_{G2H} (Euros)	E_{PV2H} (kWh)	E_{PV2G} (kWh)	C_{PV2G} (Euros)
Thermostatic	498.37	16.78	24.96	92.99	1.86
Tracking MPC	451.57	15.13	80.25	37.70	0.75
Economic MPC	440.94	14.63	74.38	43.57	0.87
Ec. MPC PV	430.10	14.32	98.56	19.39	0.39

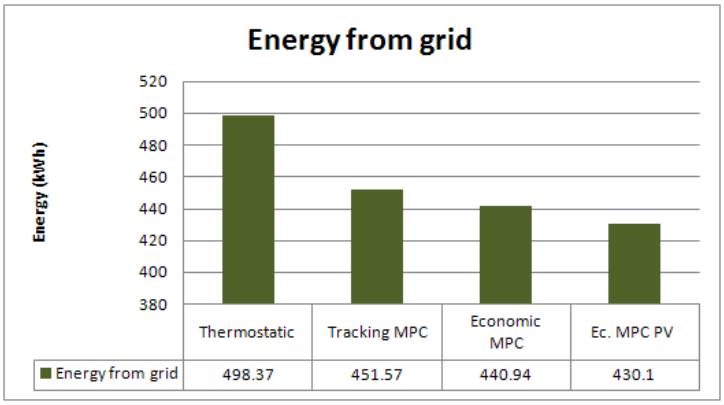

Fig. 5.11: Graphical representation of the energy consumed from the grid.

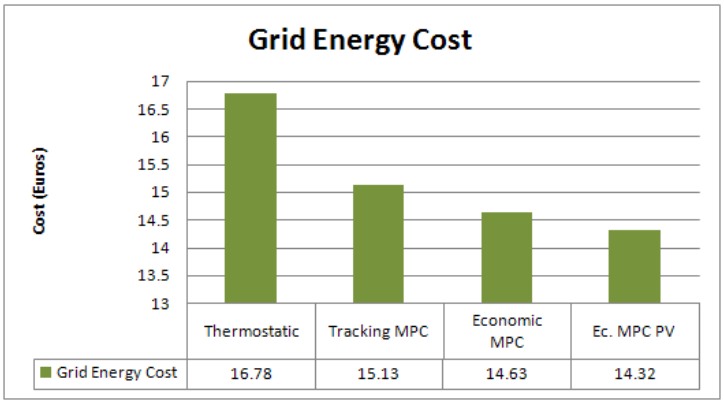

Fig. 5.12: Graphical representation of the cost of the energy consumed from the grid.

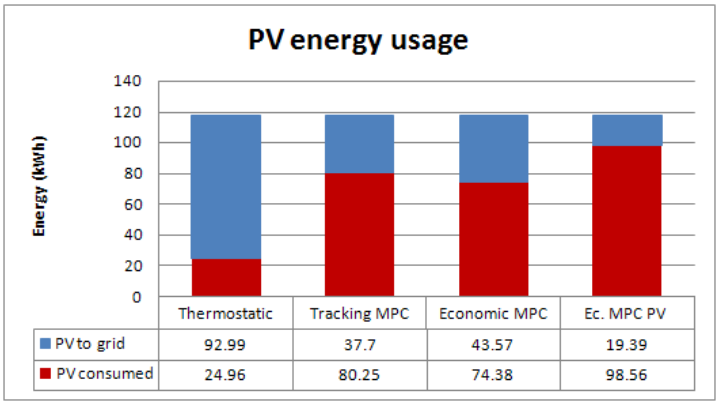

Fig. 5.13: Graphical representation of the energy consumed from the local PV plant.

When interpreting the three figures presenting the simulation results, one needs to keep in mind the initial assumption on the household setup stating that the

heating system is supplied from two energy sources. The PV system has the high priority, the electric heaters consuming the energy from the PV, and the remaining energy deficit is taken from the grid.

Another observation is that all the simulation study cases consider the same weather conditions and the same average inside temperature. This means that both the energy from the sun and the total energy consumed by the heaters, that are responsible for the inside temperature are the same for the four simulations.

Figure 5.11 shows the evolution of the grid energy consumption when using the four algorithms. By using the thermostatic controller, the heaters will be turned off most of the time when the PVs are producing and hence, they will consume the largest amount of grid energy compared to the other controllers.

The tracking MPC algorithm controls the electric heaters at a more constant consumption profile, operating also during the day and thus using more energy from the PV system; as a consequence, the energy consumed from the grid is less than in the first case.

The economic MPC optimizes the energy consumption by minimizing the grid energy cost and so, the grid energy price will determine the amount of energy taken from the grid as the consumption is shifted to low price time interval. This does not assure a decrease in the grid energy consumption and, consequently, an increase of PV energy consumption.

When using the economic MPC with maximizing the consumption of locally produced PV energy a decrease in the energy taken from the grid is obtained. This has an economic advantage for the consumer and also a stability advantage for the grid as it is less subject to congestions.

The results plotted in figure 5.12 are in direct link to the results from the previous figure as it presents the economic cost of operation for the four algorithms.

As the first two algorithms are running without any knowledge of grid price, their operation will achieve great economic costs.

The economic MPC is formulated to achieve the minimum cost as if it would consume energy exclusively from the grid. This algorithm achieves lower operation costs than the first two.

The last algorithm minimizes the operation cost considering also the consumption of PV output power. This economic MPC controller is able to achieve the best operation cost compared to the others.

5.5. Conclusions

The results presented in this chapter emphasize the benefits of using model predictive control for houses as a dynamic thermal energy storage.

By formulating the optimization problems and feeding the controller with predictions on the system's variables, the MPC is able to achieve cost reduction on the electrical energy consumption from the grid.

As demonstrated through simulations in this chapter, the MPC formulation can consider the presence of an installed PV plant maximizing the usage of locally produced renewable energy. The consumption of locally produced energy has a major benefit both for the user, by lowering the overall cost of energy and also for the operation of distribution grids with a high penetration of renewable energy generation.

This chapter presented an algorithm that deals with the two problems: minimizing the operating cost of the house heating system and maximizing the use of local produced energy and thus, lowering the burden on the distribution grid.

From the source of power consumption perspective, the algorithm can be extended to use the energy from other types of local renewable energy sources. It can be extended also from the perspective of the types of loads that are shifted, not focusing only on the heat system but also on different household appliances.

The proposed algorithm can be used to manage energy produced by other types of renewable energy generation, such as wind turbines and combined heat and power plants. The algorithm can also be modified for other types of consumption that has the ability to be shifted in time, such as water heaters, air conditioning units and refrigeration systems.

6. Conclusions

6.1. Results and conclusions

The work presented in this thesis is contributing to solve current problems affecting the microgrids due to renewable energy resources (RES) penetration on the low voltage distribution grid, by proposing and testing algorithms for voltage control and for optimizing the load consumption according to the grid energy price and RES availability.

The main body of the thesis is structured on chapters around the five major objectives of the work:

- Development of mathematical models for microgrid components and their validation based on measurements at the SYSLAB facility from Elektro DTU at RISØ campus
- Development, implementation, and validation of voltage control algorithms at a local consumer level, having no information about the configuration or parameters grid except the measured voltage at the local busbar
- Development, implementation, and validation of an advanced control algorithm for controlling the inside temperature of an energy efficient building
- Development, implementation, and validation of an model predictive control that optimizes the energy consumption of the heating system of the efficient building regarding the grid energy price
- Development, implementation, and validation of an model predictive control algorithm that maximizes the consumption of locally produced energy

Based on solving the problems raised by these objectives, as it was presented in the thesis, the main conclusions can be drawn:

- At the SYSLAB facility there was only one weather station that measured the solar irradiance on a horizontal plane at a height of a few meters. In order to estimate the values of the solar irradiance and the temperature of the PV panels, having different tilt angles and orientations, a correction module was needed to be developed to estimate these weather values. Comparisons between electrical measurements taken from the real PV panels and the model output power when using the measured weather data and the correction module emphasized the role of panel orientation on the power output profile and also the effect of both solar irradiance and wind speed on the PC cells temperature.
- For the photovoltaic panels two mathematical models were used: the one diode equivalent model and a model that relies on coefficients stated by the PV manufacturer on the technical data sheet on calculating the output power given certain weather conditions. From simulations and comparisons with electrical measurements from the real PV panels, it is concluded that both the models achieve good performances and can be used in power grid simulations; however the model based of the coefficients given by the producer is much easier to use since it uses simple arithmetic operations and can be easily implemented in a software or on a microprocessor application.
- The developed and validated models for the PV panels, the vanadium redox battery, and the thermodynamic model of the house were implemented in

specialized software which facilitates simulations and experiments regarding power grid research topics.

- The proposed thermostatic controller developed for the inside temperature control of a house has additional states as to the classical bang-bang control. This algorithm is commanding a more constant power consumption of the heating system that the classical one, with benefits to the low voltage grid stability.
- The proposed voltage control algorithm implemented as a finite state machine uses the controllable electric heaters of the heating system to consume energy when the voltage is reaching high values. This operation, however, cannot be always used due to the inside temperature constraints, as a comfort temperature zone needs to be assured for the people inside the house.
- The study presented in the thesis presents a comparison between different load shifting algorithms used to achieve voltage control by commanding the electric heaters. For these load shifting algorithms, the house is used as an energy storage device that stores it in the form of thermal energy. This energy can be stored also in chemical form into batteries, with additional economic cost.
- The above mentioned algorithm concerns both busbar voltage and inside temperature constraints which are dealt with in separate states. The shortcomings of these algorithms are the lack of correlation between the two constrains and the inability to use predictions about the operation states of the process. An advanced control algorithm was needed to cope with these problems.
- A strong candidate algorithm for dealing with constraints on the inside temperature and on the consumed power was identified in the model predictive control (MPC). Its ability to formulate an optimization problem with respect to constraints and predicted values over a moving time horizon made it suited for the inside temperature control application.
- After a thorough investigation on the up to day specialized literature, a MPC formulation was developed, implemented and validated. An augmented state-space model, for integrating the unpredicted errors, was used for a second MPC that was presenting offset free control when operating during hard simulation conditions, in the presence of modelling errors, unknown disturbances and white noise. The comparison of simulation results considering scenarios with different operation conditions showed that the developed MPC presents good performances which are consistent and closer to the bench mark scenario performance than the classical MPC implementation with no additional disturbance states.
- The MPC can be formulated in order to optimize the cost of grid energy consumption by adding a term to the optimization function that considers the real value of the grid energy price over the scenario horizon. The controller shifts the electric load of the heating system to time intervals when the price is lower, thus storing ‘cheap’ energy into the building’s thermal capacity, and turns off the heaters when the price is high.
- The model predictive control can be used, as presented in the algorithm developed and validated in this thesis, to maximize the consumption of locally produced green energy, by defining a virtual price that includes the grid energy price, the predicted PV availability and the current power consumption of the heating system.

6.2. Personal contributions

The present thesis includes, from the author's point of view, the following major contributions:

- Development of a simulation model for a specific photovoltaic (PV) plant based on local measurements and experimental validation
- Development of a correction module that enables the estimation of the solar irradiance on the PV panels and the PV cells temperature based on measurements taken from the local weather station
- Development of a simulation model for a specific vanadium redox battery (VRB) based on measurements and experimental validation
- Implementation of both microgrid components models in specialized software Matlab/Simulink and PowerFactory
- Development and implementation of a finite states machine for a proposed three states thermostatic controller
- Development and implementation of a finite states machine for thermal control that include over- and under- voltage states for dealing with voltage fluctuations at the local bus bar due to power flow in the microgrid
- Experimental validation of the proposed finite states machine on SYSLAB microgrid setup
- Development and implementation of a model predictive control (MPC) algorithm for controlling the house's inside temperature to track the prescribed temperature reference
- Implement an offset free solution of the tracking MPC that operates during modelling uncertainties, unknown disturbances, and white noise presence
- Experimental validation of the proposed tracking MPC by experiments conducted on the SYSLAB microgrid
- Development, implementation and validation of an economic MPC for optimizing the energy cost according to the grid energy price
- Definition of a new virtual price that considers the grid energy price, the predicted available PV production, and the current power consumption of the house's heating system
- Development, implementation and validation of a new economic MPC based on the defined virtual price that will maximize the consumption of the local produced PV power

6.3. Future research generated by the present work

The present thesis includes, from the author's point of view, the following major contributions:

- Experimentally test the economic MPC that regards maximization of locally produced PV power consumption
- Formulate the economic MPC as a linear program and implement it on Java; this has the advantages that it can run for long time on the house's designated computer and it consumes less memory that running Matlab for days
- Investigate the explicit MPC algorithms and the possibility of using it for this type of process
- Extend the MPC formulation to include more loads inside the house: the washing machine, the air conditioning unit, the fridge and the water boiler
- Extend the MPC formulation to include other microgrid components as the storage devices and diesel generators

Appendix A

The SYSLAB is a laboratory for research in distributed control and smart grids with a high share of renewable energy production. Its experimental facility is a Wind/PV/Diesel Hybrid Mini-Grid with local storage and a novel control infrastructure. The facility is spread across three sites located several hundred meters apart, as can be seen in figure A.1.

The facility includes two wind turbines (11kW and 55kW), a PV-plant (7.8 kW), a diesel generator-set (48kW/60kVA), an intelligent office building with controllable loads (20kW), a number of loads (75kW, 3*36kW) and a Vanadium Battery of 15 kW/120 kWh. At each of the three sites there is a switchboard that allows the components installed at the site to be connected to either of two bus bars. The two bus bars at each site are connected to a crossbar switchboard allowing the flexible setup of the system(s) to be studied. The bus bars can be either connected to the national grid or can be part of an isolated system. It allows components and systems to be in grid connected operation, island operation, or operation in parallel with wind turbine or PV-plant.

The components are all connected in one distributed control and measurement system that enables very flexible setup with respect to experimental configuration.

All units on the grid – generators, loads, storage systems, switchgear – are automates and remote-controllable. Each unit is supervised locally by a dedicated controller node. The node design combines an industrial PC, data storage, measurement and I/O interfaces, backup power and an Ethernet switch inside a compact, portable container. All nodes are interconnected via redundant high speed Ethernet, in a flexible setup permitting on-line changes of topology and the simulation of communication faults.

A. PV Panels and Inverter

48th PV panels of around 8 kWp are connected to the SYSLAB grid through a three-phase PV inverter (SMA Sunny Tripower).

The PV inverter has the ability to provide active and reactive power regulation. PV controller can be programmed to automatically regulate the active power at frequency deviations and the reactive power at line voltage deviations when SYSLAB is operated in isolated mode and also grid connected mode.

B. Data Acquisition and Control System

The data acquisition and control system (hardware and software) is responsible for the supervision and control of the research platform for distributed intelligent energy systems with a high penetration of renewable energy. The supervisory software code was written in Java and is able to manage the data acquisition, processes the data and executes the control loop and outputs the control variables. The sensors outputs are connected to a signal conditioning board, which in turn is connected to the data acquisition (DAQ) board based on a PC (SCADA System).

Some loads can be controlled by the central building controller which receives data and events from wireless switches and sensors. In one room, a small touch-screen user interface can be used to influence the controller policy (figure A.2). Through its own grid control node, the building controller can get information on the status of the power grid, and adapt its control strategy accordingly. Active policies, measurement data and user settings can be communicated back to the grid.

a) Aerial view of the SYSLAB facility

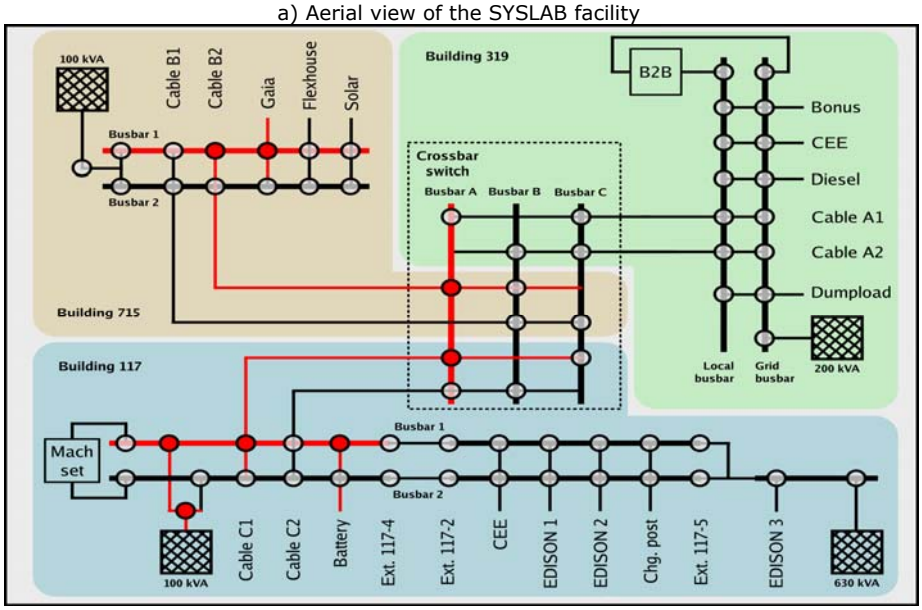

b) wire diagram of the SYSLAB facility

Fig. A.1. SYSLAB facility from Elektro DTU at Risø campus

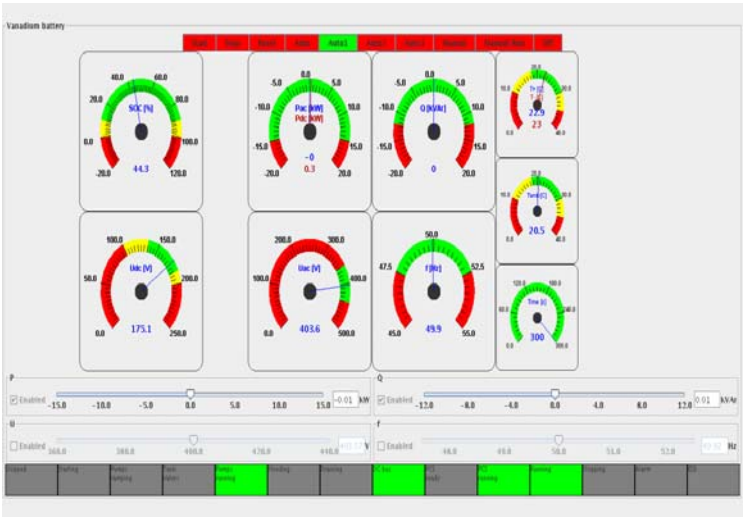

Fig. A.2. Graphical user interface for control system.

A dedicated controller node is collocated with each of the components. The nodes combined an X86-based computer, local disk storage, analogue measurement hardware, field-bus interfaces, status display backup power and an Ethernet switch inside a portable rack.

Appendix B

The Kalman filter is used as a state observer in systems presenting white noise perturbation. It is able to estimate the value of a signal by processing the noisy measurements.

A state space form of a system containing noise on both the internal states and on the measurement is:

$$\begin{cases} x(k+1) = Ax(k) + Bu(k) + w(k) \\ y(k) = Cx(k) + v(k) \end{cases} \quad \text{B-1}$$

As starting assumption we consider:

$$E\{w(k)\} = 0 \quad \text{B-2a}$$
$$E\{v(k)\} = 0 \quad \text{B-2b}$$
$$E\{w(k)v(k)\} = 0 \quad \text{B-2c}$$
$$E\{w(k)w^T(k)\} = Q \quad \text{B-2d}$$
$$E\{v(k)v^T(k)\} = R \quad \text{B-2e}$$

The state observer has the following form:

$$\hat{x}(k+1) = A\hat{x}(k) + Bu(k) + L\big(y(k) - C\hat{x}(k)\big) \quad \text{B-3}$$

Considering the error between the real state and the estimated state, B-1 and B-3, that is:

$$\underbrace{x(k+1) - \hat{x}(k+1)}_{=\varepsilon(k+1)} \quad \text{B-4}$$
$$= A\left(\underbrace{x(k) - \hat{x}(k)}_{=\varepsilon(k+1)}\right) - L\big(Cx(k) + v(k) - C\hat{x}(k)\big) + w(k)$$

Or, in a condensed form:

$$\varepsilon(k+1) = (A - LC)\varepsilon(k) - Lv(k) + w(k) \quad \text{B-5}$$

P is defined as being the error covariance:

$$P(k) = E\{\varepsilon(k)\varepsilon^T(k)\} \quad \text{B-6}$$

That is

$$E\{\varepsilon(k+1)\varepsilon^T(k+1)\} \quad \text{B-7}$$
$$= E\{(A - LC)\varepsilon(k)[(A - LC)\varepsilon(k)]^T\} + E\{Lv(k)[Lv(k)]^T\} + E\{w(k)w^T(k)\}$$

Or. In a condensed form:

$$P(k+1) = E\{(A - LC)\varepsilon(k)\varepsilon^T(k)(A - LC)^T\} + E\{Lv(k)v^T(k)L^T\} + Q \quad \text{B-8}$$

$$P(k+1) = (A - LC)E\{\varepsilon(k)\varepsilon^T(k)\}(A - LC)^T + LE\{v(k)v^T(k)\}L^T + Q \quad \text{B-9}$$

$$P(k+1) = (A - LC)P(k)(A - LC)^T + LRL^T + Q \quad \text{B-10}$$

The observer's objective is to minimize the error between the state and its estimate. The Kalman filter is minimizing the trace of the error variance, a measure of minimizing the overall error of all the estimated states:

$$tr\big(P(k+1)\big) = tr\big((A-LC)P(k)(A-LC)^T\big) + tr(LRL^T) + trQ \qquad \text{B-11}$$

Minimizing equation B.11 implies that the derivative over the controlled variable L, the filter gain, has to be zero:

$$\frac{\partial tr\big(P(k+1)\big)}{\partial L} = \frac{\partial tr\big((A-LC)P(k)(A-LC)^T\big)}{\partial L} + \frac{\partial tr(LRL^T)}{\partial L} + \frac{\partial trQ}{\partial L} \qquad \text{B-12}$$

Or

$$tr\left(\frac{\partial P(k+1)}{\partial L}\right) = tr\left(\frac{\partial (A-LC)P(k)(A-LC)^T}{\partial L}\right) + tr\left(\frac{\partial (LRL^T)}{\partial L}\right) + tr\frac{\partial Q}{\partial L} \qquad \text{B-13}$$

Equation B.13 can be solved using relations from linear algebra:

$$tr\left(\frac{\partial ABA^TC}{\partial A}\right) = C^TAB^T + CAB \qquad \text{B-14}$$

$$tr\left(\frac{\partial AB}{\partial A}\right) = B^T \qquad \text{B-15}$$

$$tr(AB) = tr(BA) \qquad \text{B-16}$$

The first term of equation B.13 develops into:

$$tr\left(\frac{\partial (A-LC)P(k)(A-LC)^T}{\partial L}\right) = tr\left(\frac{\partial\big((A-LC)P(-C^TL^T+A^T)\big)}{\partial L}\right) \qquad \text{B-17}$$
$$= tr\left(\frac{\partial(-APC^TL^T + APA^T + LCPC^TL^T - LCPA^T)}{\partial L}\right)$$

Applying equations B.14 to B.16, and considering that P = P^T for individual terms of B.17, the following results are obtained:

$$\frac{\partial tr(APC^TL^T)}{\partial L} = \frac{\partial tr(LCP^TA^T)}{\partial L} = APC^T \qquad \text{B-18}$$

$$\frac{\partial tr(APA^T)}{\partial L} = 0 \qquad \text{B-19}$$

$$\frac{\partial tr(LCPA^T)}{\partial L} = AP^TC^T \qquad \text{B-20}$$

$$\frac{\partial tr\left(L\underbrace{CPC^T}L^T\right)}{\partial L} = LCPC^T + LCP^TC^T = 2LCPC^T \quad \text{B-21}$$

Equation B.13 becomes

$$tr\left(\frac{\partial P(k+1)}{\partial L}\right) = -2APC^T + 2LCPC^T + 2LR \quad \text{B-22}$$

For solving equation B.22 considering the unknown variable L, for minimum values of P

$$LCPC^T - APC^T + LR = 0 \quad \text{B-23}$$

The solution for the Kalman filter coefficient is given in equation B.23

$$L = (CPC^T + R)^{-1}APC^T \quad \text{B-23}$$

Appendix C

```
function [Ad,Bd,Cd,Dd,Ed] = MPC_ModelInit()
% System parameters
CiA = 3.42;   % for a time interval of 1 hour
RiaA = 4.87; %
AwA = 5.53; %
% State-space formulation
AA = -1/(CiA*RiaA);
BA =  1/(CiA);
CA = 1;
EA = [1/(CiA*RiaA)  AwA/CiA];
DA = [0 0 0];
% Discrete time state space formulation
delta = 1/6; % time step of 10 minutes (1/6 of an hour)
Ad = eye(1)+delta*AA;
Bd = delta*BA;
Cd = CA;
Ed = delta*EA;
Dd = DA;

function [A3d,B3d,C3d,D3d,E3d] = MPC_3SM()
% Augmented 3 states system model
Ci = 2.66;
Cm = 3.08;
Ch = 0.00384;
Ria = 4.82;
Rim = 3.45;
Rih = 33.3;
Aw = 5.53;
 % State-space formulation
 A3 = [-(1/(Ci*Ria)+1/(Ci*Rim)+1/(Ci*Rih))       1/(Ci*Rim)      1/(Ci*Rih);
                1/(Cm*Rim)               -1/(Cm*Rim)         0;
                1/(Ch*Rih)                  0         -1/(Ch*Rih)];
B3 = [0 0 1/Ch]';
C3 = [1 0 0];
E3 = [1/(Ci*Ria)    Aw/Ci;
       0            0;
       0            0];
D3 = 0;
% Discrete time state space formulation
delta = 1/6;% time step of 10 minutes (1/6 of an hour)
A3d = eye(3)+delta*A3;
B3d = delta*B3;
C3d = C3;
E3d = delta*E3;
D3d = D3;

function [Kf, Ae,Be,Ce,Ee] = MPC_AugmentedSystem(A,B,C,E,qw,qxi,rv)
```

```
% The function builds the matrix for the augmented model of the system and
% determines the Kalman filter gain
[nA,mA] = size(A);
[nB,mB] = size(B);
[nC,mC] = size(C);
[nE,mE] = size(E);
% Noise matrix formulation based on the noise covariances
Qw = qw * eye(nA,mA); % responsable for the process noise
Qxi = qxi * eye(mE,mE); % responsable for the disturbance noise
Rv = rv * eye(mC,mC); % responsable for the output noise
% Design the augmented system
Ad = eye(mE,mE);
Ae = [A E; zeros(mE,mA) Ad];
Be = [B; zeros(mE,mB)];
Ee = [E; zeros(mE,mE)];  %!!!!
Ce = [C zeros(nC,mE)];
Qe = [Qw          zeros(nA,mE);...
      zeros(mE,mA)  Qxi];
% Kalman filter
P = dare(Ae',Ce',Qe,Rv); % solution of the discrete Riccati equation
Re = Ce*P*Ce'+Rv;  % the inovation covariance
Kf = P*Ce'/Re;  % Kalman filter gain

function [phi, gama, gamad, MPC] = MPC_HorizonFormulation(A,B,C,E,Nc,S,Qz)
%%% phi generation
%    phi = [CA
%         CA^2
%         CA^3
%
%         CA^Np]
[nA,mA] = size(A);
[nB,mB] = size(B);
[nC,mC] = size(C);
Ap = A;
for i=1:Nc
  phi((i-1)*nC+1:i*nC, 1:mA)= C*Ap;
  Ap = Ap * A;
end
%%% gama, gamad generation
% gama (Np,Nc)
% gama = [       CB           0          ...         0
%                CAB          CB         ...         0
%               CA^2B         CAB        ...         0]
%        ...
%            CA^(Np-1)B    CA^(Np-2)B ..... CA^(Np-Nc-1)B]
 [nE,mE] = size(E);
v = zeros(nB,mB*Nc);
vTa = zeros(nE,mE*Nc);
Phi=zeros(nC*Nc,mB*Nc);
PhiTa = zeros(nC*Nc,mE*Nc);
for i=1:Nc
```

```
   Bv = zeros(nB,Nc);
   Tav = zeros(nE,mE*Nc);
   if i<=Nc
      Bv(1:nB,i) = B;
      Tav(1:nE,(i-1)*mE+1:i*mE) = E;
   end
   v = A * v + Bv;
   vTa = A * vTa + Tav;
   Phi(i,:)= C * v;
   PhiTa(i,:) = C * vTa;
end
gama = Phi; %
gamad = PhiTa;
Hs = zeros(Nc,Nc);
Hs(1,1:Nc) = [2*S,-S,zeros(1,Nc-2)];
for i=2:Nc-1
    Hs(i,1:Nc)=[zeros(1,i-2),-S,2*S,-S,zeros(1,Nc-i-1)];
end
Hs(Nc,1:Nc) = [zeros(1,Nc-2),-S,S];
% generating the matrix for MPC formulation as a convex optimization
% function
H = gama' * Qz * gama + Hs;
Mx0 = gama' * Qz * phi;
MR = -gama'*Qz;
Mu = -[S, zeros(1,Nc-1)]';
Md = gama' * Qz * gamad;
% MPC formulation including H, Hs, Mx0, MR, Mu, Md
MPC.H = H;
MPC.Hs = Hs;
MPC.Mx0 = Mx0;
MPC.MR = MR;
MPC.Mu = Mu;
MPC.Md = Md;
MPC.Nc = Nc;

function [x,fval,exitflag,output,lambda] = MPC_Solver(MPC, xk, u_1,dTaG, R, Ulim)
% the function calls the Matlab solver after the optimization problem was written in
the standard form
AMPC = [eye(MPC.Nc,MPC.Nc); -eye(MPC.Nc,MPC.Nc)];
g = MPC.Mx0*xk+MPC.MR*R+MPC.Md*dTaG+MPC.Mu*u_1;
 [x,fval,exitflag,output,lambda] = quadprog(MPC.H,g, AMPC, Ulim);
```

Main program

```
% % MPC offline
Np = 30;
Nc = 30;
% model initialization
[Ad,Bd,Cd,Dd,Ed] = MPC_ModelInit();
% weights initialization and noise covariance
```

```
Qz = 0.5;
S = 0.3;
qw = 0.01;
qxi =  0.5 ;
rv =  0.001;
% augmented model generation and Kalman filter gain calculation
[Kf, Ae,Be,Ce,Ee] = MPC_AugmentedSystem(Ad,Bd,Cd,Ed,qw,qxi,rv);
% the MPC prediction horizon matrix generation
[phi, gama, gamaTa, MPC] = MPC_HorizonFormulation(Ae,Be,Ce,Ee,Nc,S,Qz);
% real plant - 3 states model
[A3d,B3d,C3d,D3d,E3d] = MPC_3SM();
% initializing the vectors of MPC available known data :
% R2 - the reference vector [N,1] vector
% dTaG - the predicted ambient temperature and solar irradiance [2N,1]
% vector
 % initializing the vector of measurements taken online
% dTaGreal - the measured ambient temperature and solar irradiance [2N,1]
% vector

 % % MPC online
for i= 1:Horizon-Nc
    ys = Tin; % the current system output - measured inside temperature
    rs = r(i); % the current prescribed reference
    dy = rs - ys; % the difference between the reference and the output
    dum1 = uk_1-us ; % the command variation at the last step
% the reference and predicted disturbance for the next prediction horizon:
    dR = reshape(r(:,i+1:i+Nc)-repmat(ys,1,Nc), Nc*nz,1);
    dD = reshape(d(:,(i-1)*2+1:(i-1)*2+mE*Nc)-repmat(ds,1,Nc), Nc*nd,1);
% the difference between the current and last step predicted disturbance:
    dd = d(1,(i-1)*nd+1:i*nd)'-ds';
% the Kalman filter correction step
    e = -dy  - Ce * (xp); % inovation calculation
    xf = xp + Kf * e; % the best available estimation of the augmented states - the
% inside temperature and the unknown perturbation errors setting the constrain
% limits for the prediction horizon considering the current step
    Umin = ones(MPC.Nc,1)*us;
    Umax = ones(MPC.Nc,1)*(10-us);
    Ulim = [Umax;Umin];
% solving the optimization problem considering the prediction horizon future states
%based on the one state-space model of the system, predicted disturbances and
%prescribed reference and constraints on the inside temperature (controlled
%variable) and electrical heaters output power (manipulated variable)
    [x,fval,exitflag,output,lambda] = MPC_Solver(MPC, xf, dum1, dD, dR, Ulim);
    x(1)=round(x(1)); % used for calculating the 1 kW step of the electrical heaters

% the next state is calculated by the MPC according to the 1 state space model used
%in the MPC formulation
    xp = Ae * xf + Be * x(1) + Ee * dd;
    yk = Ce*xp;
% the last command for the next step is the current command:
    uk_1 = us;
```

```
% and the command that is applyed to the building's heaters
   us  = uk_1 + x(1);
% the last predicted disturbances for the next step are:
   ds = [dTaG((i-1)*2+1,1) dTaG(i*2,1)];

   % THE PROCESS
% the one state-space model of the process
%     Tin = Ad * ys + Bd * (us) + Ed * [dTaGreal((i-1)*2+1,1) dTaGreal(i*2,1)]';
%     Tinsidereal(i,1) = Tin;
% the three state-space model of the process
   xplant = A3d * xplant + B3d * us+ E3d * [dTaGreal((i-1)*2+1,1)
dTaGreal(i*2,1)]';
   Tin = xplant(1,1);
   Tinsidereal(i,1) = Tin;
End
```

References

[Alexis2011] K. Alexis and G. Nikolakopoulos and A. Tzes, "Model Predictive Control Scheme for the Autonomous Flight of an Unmanned Quadrotor," *IEEE International Symposium On Industrial Electronics* (ISIE), pp. 2243 - 2248, 2011

[Amjad2010] A. Abu-Rmileh and W. Garcia-Gabin, "A Gain-Scheduling Model Predictive Controller for Blood Glucose Control in Type 1 Diabetes," *IEEE Transactions On Biomedical Engineering*, Volume 57, Issue 10, pp. 2478-2484, 2010

[Angeli2011] D. Angeli, R. Amrit and J.B. Rawlings, "On average performance and stability of economic model predictive control," *IEEE Transactions on Automatic Control*, Volume 57 , Issue 7, pp. 1615 – 1626, 2011

[Bacher2010] P. Bacher, A. Thavlov and H. Madsen, "Models for Energy Performance Analysis", Informatics and Mathematical Modelling Technical University of Denmark, IMM-Technical Report-2010-02, 2010

[Balan2009] R. Bălan, S.D. Stan and C. Lăpușan, "A Model Based Predictive Control Algorithm for Building Temperature Control", *3rd IEEE International Conference on Digital Ecosystems and Technologies*, pp 540-545, 2009

[Barote2010] L. Barote, C. Marinescu "Storage Analysis for Stand-Alone Wind Energy Applications," *12th International Conference on Optimization of Electrical and Electronic Equipment*, pp.1180-1185, September 2010, Brasov, Romania.

[Beccuti2007]A. Beccuti, T. Demiray, M. Zima, G. Andersson and M. Morari, "Comparative assessment of prediction models in voltage control," *In PowerTech Conference*. Lausanne, Switzerland. pp. 1021 – 1026, 2007

[Beccuti2009]A.G. Beccuti, S. Mariéthoz, S. Cliquennois, S. Wang and M. Morari, "Explicit Model Predictive Control of DC–DC Switched-Mode Power Supplies With Extended Kalman Filtering," *IEEE Transactions On Industrial Electronics*, VOL. 56, No. 6, June 2009

[Begovich2007]O. Begovich, V.M. Ruiz, G. Besancon, C.I. Aldana and D. Georges , "Predictive control with constraints of a multi-pool irrigation canal prototype," *Journal of Latin American Applied research*, no. 37, pp. 177-185, 2007

[Bemporad2002]A. Bemporad, F. Borrelli, and M.Morari, "Model predictive control based on linear programming—The explicit solution," *IEEE Trans. Autom. Control*, vol. 47, no. 12, pp. 1974–1985, Dec. 2002

[Bemporad2011]A. Bemporad and C. Rocchi, "Decentralized linear time-varying model predictive control of a formation of unmanned aerial vehicles," *IEEE CONFERENCE ON DECISION & CONTROL (CDC),* pp. 7488-7493, 2011

[berkley] *https://sites.google.com/site/mpclaboratory/research/predictive-networked-building-control-1*

[Bernardini2009]D. Bernardini, S. Di Cairanoz, A. Bemporad and H.E. Tsengz, "Drive-by-wire vehicle stabilization and yaw regulation: a hybrid Model Predictive Control design," *Proceedings Of The IEEE Conference On Decision & Control, Including The Symposium On Adaptive Processes*, pp. 7621-7626, 2009

[Bindner2011] [RISOVRB] H. Bindner, C. Ekman, O. Gehrke and F. Isleifsson, "Characterization of Vanadium Flow Battery", Technical Report Risoe-R-1753, Feb 2011

[Boraci2012]R. Boraci, O. Prostean, N. Budisan and **C. Koch-Ciobotaru**, "Pragmatic Method to Obtain Optimal Control Laws for Small Windgenerators", In R.-E. Precup, S. Kovács, S. Preitl, and E.M. Petriu, Eds., *Applied Computational*

Intelligence in Engineering and Information Technology Topics in Intelligent Engineering and Informatics, Volume 1, pp 239-248, Springer Press, 2012.

[Borhan2010]H. A. Borhan and A. Vahidi, "Model Predictive Control of a Power-split Hybrid Electric Vehicle with Combined Battery and Ultracapacitor Energy Storage," *American Control Conference*, pp. 5031-5036, 2010.

[Borreli2011]F. Borrelli, A. Bemporad, and M. Morari, "Predictive Control for linear and hybrid systems," *Model Predictive Control Lab @ UC-Berkeley*, February 23, 2011, available: http://www.mpc.berkeley.edu/mpc-course-material.

[Bououden2012]S. Bououden, M. Chadli, S. Filali and A. El Hajjaji, "Fuzzy model based multivariable predictive control of a variable speed wind turbine: LMI approach," *Journal of Renewable Energy*, Volume 37, Issue 1, pp. 434-439, 2012.

[Braun1990]J.E. Braun, "Reducing energy costs and peak electrical demand through optimal control of building thermal mass," *ASHRAE Trans*. 96 (2) pp. 876–888, 1990.

[Budisan2010]N. Budisan, N. Muntean, R. Boraci, O. Cornea, **C. Koch-Ciobotaru** and D. Petrila, "Electronic Conversion System and Speed-Control Strategy for Small Wind Generators," *Proc. IEEE International Joint Conferences on Computational Cybernetics and Technical Informatics*, ICC-CONTI, pp. 455-458, May 2010, Timişoara, România.

[Campbell2007] R.C. Campbell, "A circuit-based photovoltaic Array model for Power System Studies", *Power Symposium NAPS'07*, pp 97-101, 2007

[Chan1987] D.S.H. Chan and J.C.H. Phang, "Analytical methods for the extraction of solar-cell single- and double-diode model parameters from I-V characteristics," *IEEE Transactions On Electron Devices*, Volume 34, Issue 2, pp. 286-293, 1987

[Chen T.Y.] T.Y. Chen and A.K. Athienitis, "Ambient temperature and solar irradiance prediction for predictive control of HVAC systems and a methodology for optimal building heating dynamic operation", *ASRAE Trans*. vol. 102, no. 1, pp 26-36, 1996

[Chen2001]T.Y. Chen, "Real-time predictive supervisory operation of building thermal systems with thermal mass," *Journal of Energy and Buildings*, vol. 33 pp. 141–150, 2001.

[Chen2002] T.Y. Chen, "Application of adaptive predictive control to a floor heating system with a large thermal lag", *Journal of Energy and Buildings*, vol. 34, no. 1, pp. 45–51, 2002.

[Chowdhury2009]S. Chowdhury, S.P. Chowdhury and P. Crossley*, Microgrids and active distribution networks*, IET renewable energy series 6, London: IET; 2009.

[CPLEX] "IBM ILOG CPLEX Optimizer, High-performance mathematical programming solver for linear programming, mixed integer programming, and quadratic programming", http://www-01.ibm.com/software/integration/optimization/cplex-optimizer/

[Cutler1979] C.R. Cutler and B.L. Ramaker, "Dynamic matrix control–a computer control algorithm," In *AIChE Meeting*, Houston, 1979

[DiGiorgio2012] A. Di Giorgio, L. Pimpinella and F. Liberati, "A Model Predictive Control Approach to the Load Shifting Problem in a Household Equipped with an Energy Storage Unit," *20th Mediterranean Conference on Control & Automation (MED)*, pp. 1491- 1498, July 3-6, 2012

[Doughty2010] D. H. Doughty, P. C. Butler, A. A. Akhil, N. H. Clark, and J. D. Boyes, "Batteries for Large-Scale Stationary Electrical Energy Storage," *The Electrochemical Society Interface*, pp. 49-53, 2010

[Eicker2003] U. Eicker, *Solar Technologies for Buildings*, Wiley, Chichester, 2003

[ENER] Energy efficiency and energy consumption in the household sector (ENER 022) - Assessment published Sep 2010 (http://www.eea.europa.eu/legal/ copyright). Copyright holder: European Environment Agency

[EnergyPlus] EnergyPlus Energy Simulation Software, http://apps1.eere.energy.gov/buildings/energyplus/

[EnStor2003] S. Eckroad , *EPRI-DOE Handbook of Energy Storage for Transmission and Distribution Applications*; Electrical Power Research Institute, Palo Alto, CA, and Department of Energy: Washington, DC, final report, 2003.

[eurostat] "European commission, Eurostat - energy consumption statistics", http://epp.eurostat.ec.europa.eu/statistics_explained/index.php/Consumption_of _energy

[eurostat2011] "Europe in figures Eurostat yearbook 2011", http://epp. eurostat.ec.europa.eu/cache/ITY_OFFPUB/KS-CD-11-001/EN/KS-CD-11-001-EN.PDF

[Fuller2011] J.C. Fuller, K.P. Schneider and D. Chassin, "Analysis of Residential Demand Response and double-auction markets", *IEEE Power & Energy Society General Meeting*, pp. 1-7, 2011

[Gehrke2010]O. Gehrke and F. Isleifsson, "An Aggregation Friendly Information Model for Demand Side Resources", *IEEE 35th Conference on Local Computer Networks (LCN),* pp. 1019 - 1023, 2010,

[Georgescu2010] M. Georgescu, L. Barote, C. Marinescu and L. Clotea, "Smart Electrical Energy Storage System for Small Power Wind Turbines," In *Proceedings of the International Conference on Optimization of Electrical and Electronic Equipments, OPTIM*, pp. 1192-1197, 2010,

[Geyer2008]T. Geyer, G. Papafotiou and M. Morari, "Hybrid Model Predictive Control of the Step-Down DC–DC Converter," IEEE Transactions On Control Systems Technology, vol. 16, no. 6, pp. 1112-1124, 2008

[Geyer2009]T. Geyer, G. Papafotiou and M. Morari, "Model Predictive Direct Torque Control – Part I: Algorithm, Concept & Analysis," *IEEE Trans. on Industrial Electronics*, vol. 56, no. 6, pp. 1894 - 1905, June 2009

[Goswami1999] Y. Goswami, F. Kreith, and J. Kreder, *Principles of solar engineering*, Philadelphia, PA: Taylor & Francis, 1999.

[Goswami2000] D.Y. Goswami, F. Kreith, J.F. Kreider, *Principles of Solar Engineering*, Second ed., Taylor Francis, Philadelphia, 2000

[Grande2008]O. S. Grande, H. Sæle, and I. Graabak, SINTEF Energy Research, Market based demand response. Research project summary 2008 [Online]. Available: http://www.energy.sintef.no/prosjekt/mabfot/uk/, TR A6775

[Grigsby2007] L. Grigsby, *Electric Power Engineering handbook*, *second edition*, CRC press, 2007

[Guerrero 2007] J. M. Guerrero, L. Garcia de Vicuna and J. Uceda, "Uninterruptible power supply systems provide protection," *IEEE Industrial Electronics Magazine*, no. 1, 2007, pp. 28-38.

[Guerrero2010] J. M. Guerrero, J. C. Vasquez, J. Matas, L. García de Vicuña, and M. Castilla, "Hierarchical Control of Droop-Controlled AC and DC Microgrids – A General Approach Towards Standardization," *IEEE Trans Ind Electronics*, vol. 58, no. 1, pp. 158-172, 2011.

[Hagedorn1984] [NASA] N. H. Hagedorn, "NASA Redox Storage System Development", Project Final Report," DOE/NASA/12726-24, NASA TM-83677 (1984)

[Halvgaard2012] R. Halvgaard, N.K. Poulsen, H. Madsen, J. B. Jørgensen, "Economic Model Predictive Control for Building Climate Control in a Smart Grid", *IEEE PES*

Innovative Smart Grid Technologies (ISGT) , pp. 1 - 6 , 2012.

[Hansen2000] [RISØ 2000] A.D. Hansen, P. Sørensen, L. H. Hansen and H. Bindner, "Models for a Stand-Alone PV System", Technical report, Risø-R-1219(EN) / SEC-R-12, 2000

[Hazyuk2012a] I. Hazyuk, C. Ghiaus, D. Penhouet, "Optimal temperature control of intermittently heated buildings using Model Predictive Control: Part I – Building modelling", *Journal of Building and Environment,* vol.51, pp. 379-387, 2012

[Hazyuk2012b] I. Hazyuk, C. Ghiaus and D. Penhouet, "Optimal temperature control of intermittently heated buildings using Model Predictive Control: Part II – Control Algorithm", *Journal of Building and Environment,* vol. 51, pp. 388-394, 2012

[Hennessy2006] [13] T. Hennessy, *DOE Energy Storage Systems Research Program*, Annual Peer Review, Washington DC, 3 November 2006

[Henze2004] G.P. Henze, C. Felsmann and G. Knabe, "Evaluation of optimal control for active and passive building thermal storage," *International Journal of Thermal Sciences*, vol. 43, no. 2, pp. 173-183, 2004

[Hovgaard2012] T. Hovgaard, L. Larsen, J. Jørgensen and B. Stephen, "Nonconvex Model Predictive Control for Commercial Refrigeration", *Preprints of 4th IFAC Nonlinear Model Predictive Control Conference*, pp. 514-521, June, 2012

[Huusom2010] J.K. Huusom, N.K. Poulsen, S.B. Jørgensen and J. Jørgensen, "ARX-Model based Model Predictive Control with Offset-Free Tracking", *20th European Symposium On Computer Aided Process Engineering*, vol. 28, pp. 601-606, 2010

[Huusom2010]J.K. Huusom, N.K. Poulsen, S.B. Jørgensen and J.B. Jørgensen, "Tuning of Methods for Offset Free MPC based on ARX Model Representations," In *American Control Conference, ACC 2010*, pp. 2255-2360 ,30 June -02 July 2010

[Huusom2011] J.K. Huusom, N.K. Poulsen, S.B. Jørgensen and J.B. Jørgensen, "Adaptive Disturbance Estimation for Offset-Free SISO Model Predictive Control," in *Proceedings of the American Control Conference*, pp. 2417-2422, 2011

[IEA 2009] "Overcoming PV grid issues in the urban areas" Technical report , IEA PVPS Task 10, Activity 3.3 Report IEA-PVPS T10-06, October 2009

[Jang2008]J. Jaehwi, "System design and dynamic signature identification for intelligent energy management in residential buildings." Ph.D. dissertation, Univ. California, Berkeley, 2008. Available online: http:// escholarship.org/uc/item/0v83w3kw.pdf

[Jiavi2008] H. Jiayi, J. Chuanwen, and X. Rong, "A review on distributed energy resources and microgrid," Renewable Sustainable Energy Rev., vol. 12, no. 9, pp. 2472–2483, 2008.

[Joosten2008] D. Joosten, T.J.J. Van Den Boom and T. Lombaerts, "Fault-tolerant control using dynamic inversion and model predictive control applied to an aerospace," *IFAC Proceedings Volumes*, vol. 17, no. 1, pp. 12030- 12035, 2008

[Jossen2004] J. Andreas, G. Juergen and U.S. Dirk," Operation conditions of batteries in PV applications", *SOLAR ENERGY Journal*, vol. 76, no. 6, pp. 759-769, 2004

[Junsangsri2010] P. Junsangsri and F. Lombardi, "Double diode modelling of time/temperature induced degradation of solar cells", *53rd IEEE International Midwest Symposium on Circuits and Systems (MWSCAS 2010)*, pp. 1005 – 1008, 2010

[Kacira2004] M. Kacira, M. Simsek,Y. Babur and S. Demirkol, "Determining optimum tilt angles and orientations of photovoltaic panels in Sanliurfa, Turkey," *Journal of Renewable Energy,* vol. 29, no. 8, pp. 1265-1275, 2004

[Koch2010] **C Koch Ciobotaru**, R Boraci, I Filip, C Vasar, G Prostean, "Control Strategy for a Variable-Speed Wind Turbine Using DC Bus Measurements, "*8th*

International Symposium on Intelligent Systems and Informatics, SISY 2010, pp. 329-335, September 2010, Subotica, Serbia.

[Koch2011]**C. Koch-Ciobotaru**, R. Boraci, O. Prostean and C. Vasar, "Managing The Energy Distribution Of An Energy Conversion System In A Standalone Application", *7th International Conference on the Management of Technological Changes*, 1-3 September 2011, pp. 393-396,Alexandroupoli, Greece

[Koch2012a] **C. Koch-Ciobotaru**, "Model Predictive Control for inside temperature of an energy efficient building, " in Janusz Kacprzyk, Eds., Advances in Intelligent and Soft Computing, Springer Press, pp.197 – 208, Proceedings of *5th International Workshop on soft computing applications*, Szeged, Hungary.

[Koch2012b]**C. Koch-Ciobotaru**, F. Isleifsson and O. Gehrke, "Optimizing Operation Costs of the Heating System of a Household using Model Predictive Control Considering a Local PV Installation", *2nd International Conference on Simulation and Modelling Methodologies, Technologies and Applications*, pp. 431-436, July 28–31, 2012

[Koch2012c]**C. Koch-Ciobotaru**, L. Mihet-Popa, F. Isleifsson and H. Bindner, "Simulation Model developed for a Small-Scale PV System in Distribution Networks," *7th IEEE International Symposium on Applied Computational Intelligence and Informatics*, pp 341-346, May 24–26, 2012

[Kolokotsa2009]D. Kolokotsa, A. Pouliezos, G. Stavrakakis and C. Lazos, "Predictive control techniques for energy and indoor environmental quality management in buildings", *Journal of Building and Environment,* vol. 44, 1850–1863, 2009

[Kreith 2007] F. Kreith and D.Y.Goswami*, Handbook of Energy efficiency and renewable energy*, CRC Press, Boca Raton, 2007

[Kummert2001] M. Kummert, P. André and J. Nicolas, "Optimal heating control in a passive solar commercial building," Journal of Solar Energy, vol. 69, pp. 103-116, 2001

[Kundur1994]P. Kundur, *Power System Stability and Control*, McGraw-Hill, Inc. 1994

[Lee2011]H.L. Jay, "Model Predictive Control: Review of the Three Decades of Development," *International Journal of Control, Automation, and Systems* , vol. 9, no. 3, pp. 415-424, 2011

[Li 2011] X. Li , H. Zhang , Z. Mai, H. Zhang and I. Vankelecom, "Ion exchange membranes for vanadium redox flow battery (VRB) applications," *Energy & Environmental Science journal*, vol. 4, pp. 1147-1160, 2011

[Lidula2011] N. W. A. Lidula and A.D. Rajapakse, "Microgrids research: A review of experimental microgrids and test systems," *Renewable & Sustainable Energy Reviews* Journal, vol. 15, no. 1, pp. 186-202, 2011

[Lind00] B. Lindgren. "A Power Converter for Photovoltaic Applications." PhD dissertation, Department of Electric Power Engineering, Chalmers University of Technology, Göteborg, Sweden, 2000.

[Liu2004]S. Liu and G.P. Henze, "Impact of modelling accuracy on predictive optimal control of active and passive building thermal storage inventory," *ASHRAE Transactions*, , no. 110, pp. 151-163, 2004

[Lopes2003] L.A.C. Lopes and A.M. Lienhardt, "A simplified nonlinear power source for simulating PV panels", *IEEE 34th Annual Conference on Power Electronics Specialist*, vol. 4, pp 1729-1734,2003

[Lu2011]S. Lu , M. A. Elizondo, N. Samaan, K. Kalsi, E. Mayhorn, D. Ruisheng, J. Chunlian and Z. Yu, "Control strategies for distributed energy resources to maximize the use of wind power in rural microgrids," *IEEE Power & Energy Society General Meeting,* pp. 1-8, 2011

[Ma 2011] Y. Ma, A. Kelman, A. Daly, and F. Borrelli "Predictive Control for Energy Efficient Buildings with Thermal Storage", *Control System magazine*, vol. 32 no. 1, pp. 44 - 64, Feb. 2012

[Ma Qin2011]J. Ma, S. J. Qin, B. Li and T. Salsbury, "Economic Model Predictive Control for Building Energy Systems", *Innovative Smart Grid Technologies (ISGT), IEEE PES*, pp. 1-6, 2011

[Ma2009] Y. Ma, F. Borrelli, B. Hencey, A. Packard and S. Bortoff, "Model Predictive Control of Thermal Energy Storage in Building Cooling Systems," *Joint 48th IEEE Conference on Decision and Control and 28th Chinese Control Conference*, pp. 392 - 397, December 16-18, 2009

[Ma2010] Y. Ma, F. Borrelli, B. Hencey, B. Coffey, S. Bengea and P. Haves, "Model Predictive Control for the Operation of Building Cooling Systems", *American Control Conference*, pp. 796 - 803 ,June 30-July 02, 2010

[Ma2011] Y. Ma, G. Anderson and F. Borrelli, "A Distributed Predictive Control Approach to Building Temperature Regulation," In *American Control Conference, ACC 2011*, pp. 2089 - 2094,29 June – 01 July, 2011.

[Maciejowski2002]J. M. Maciejowski, *Predictive Control with Constraints*, Prentice Hall, 2002

[Madureira2009] A.G. Madureira and J.A.P. Lopes, "Coordinated voltage support in distribution networks with distributed generation and microgrids," In *IET Renewable Power Generation*, vol. 3, no. 4, pp. 439–454, Dec. 2009.

[Magrab2010] E.B. Magrab, S. Azarm, B. Balachandran, J. Duncan, K. Herold and G. Walsh, *Engineers Guide to MATLAB*, 3rd edition, Prentice Hall, 2010

[Mariethoz2008]S. Mariethoz, A. G. Beccuti, G. Papafotiou, and M. Morari, "Sensorless explicit model predictive control of the DC–DC buck converter with inductor current limitation," in Proc. IEEE APEC, Austin, TX, pp. 1710–1715, Feb. 2008,.

[Marion2004] B. Marion, S. Rummel and A. Anderberg, "Current-voltage Curve Translation by Biliniar Interpolation," *Progress in Photovoltaics: Research and Applications*, vol. 12, pp. 593-607,2004

[Markakis2008] M.G. Markakis, G.D. Mitsis, G.P Papavassilopoulos and V.Z. Marmarelis, "Model Predictive Control of blood glucose in Type 1 diabetes: The Principal Dynamic Modes approach," *IEEE Engineering In Medicine And Biology Society Conference Proceedings*, pp. 5466-5469, 2008

[Mayne2003]D. Q. Mayne, J. B. Rawlings, C. V. Rao, P. O. M. Scokaert, "Constrained model predictive control: Stability and optimality", *Automatica*, vol. 36, pp. 789-814, 2000

[McDowell2006] [14] McDowell J. International Renewable Energy Storage Conference, IRES2006, Gelsenkirchen, Germany, 30–31 October 2006.

[Messenger2004] R. Messenger and G. Ventre, *Photovoltaic systems engineering. 2nd Ed*,. CRC Press, Boca Raton, 2004

[Mihet2012a]L. Mihet-Popa, **C. Koch-Ciobotaru**, F. Isleifsson, H. Bindner, "Development of Tools for Simulation Systems in a Distribution Network and Validated by Measurements,"*13th International Conference on Optimization Of Electrical And Electronic Equipment*, pp 1022-1031, May 24-26, 2012

[Mihet2012b] L. Mihet-Popa, **C. Koch-Ciobotaru**, F. Isleifsson and H. Bindner, "Development of Tools for DER Components in a Distribution Network," 20th International Conference on Electrical Machines, ICEM 2012, September 2012, Marsilia, Franta

[Mohamed08] Mohamed Faisal, "Microgrid Modelling And Online Management", PhD dissertation, University of Helsinki, 2008

[Muku99] R. Mukund, *Wind and solar power systems*, CRC Press LLC, 1999

[Nagai2002] T. Nagai, "Optimization Method for Minimizing Annual Energy, peak energy demand, and annual energy cost through use of building thermal storage," *ASHRAE Transactions*, vol. 108, no. 1, pp. 976-887, 2002.

[Nanayakkara] N. Nanayakkara, M. Nakamura and H. Hatazaki H. "Predictive control of wind turbines in small power systems at high turbulent wind speeds," *Journal of Control Engineer Practice*, vol.5, no. 8, pp. 063-1069, 1997

[NOAA] "Earth System Research Laboratory – NOAA Solar Calculator" http://www.esrl.noaa.gov/gmd/grad/solcalc/

[NordPool]The Nord Pool spot market , available: http://www.nordpoolspot.com/reports/systemprice

[Oldewurtel2010] F. Oldewurtel, A. Parisio, C.N. Jones, M. Morari, D. Gyalistras, M. Gwerder, V. Stauch, B. Lehmann and K. Wirth, "Energy efficient building climate control using Stochastic Model Predictive Control and weather predictions," *Proceedings of the American Control Conference*, pp. 5100-5105, 2010

[Oldewurtel2012] F. Oldewurtela, A. Parisio, C. N. Jones, D. Gyalistras, M. Gwerder, V. Stauch, B. Lehmann and M. Morari, "Use of model predictive control and weather forecasts for energy efficient building climate control," *Journal of Energy and Buildings*, vol. 45, pp. 15–27, 2012.

[OptiControl] "OptiControl use of weather and occupancy forecast for optimal building climate control", http://www.opticontrol.ethz.ch/index.html

[OptiControlRep] D. Gyalistras and The OptiControl Team, "Final report: Use of weather and occupancy forecasts for optimal building climate control (OptiControl).", Technical report, Terrestrial Systems Ecology ETH Zurich, Switzerland, 2010, 33pp. available: http://www.opticontrol.ethz.ch/Lit/ Gyal_10_Rep-OptiCtrlFinalRep.pdf

[Pannochia2003] G. Pannochia and J. Rawlings, "Disturbance Models for Offset-Free Model Predictive Control." *In AIChE Journa*l 2003, vol. 49, no. 2, pp. 426-437, 2003.

[Papafotiou2009]G. Papafotiou, J. Kley, K. Papadopoulos, P. Bohren and M. Morari, "Model Predictive Direct Torque Control – Part II: Implementation and Experimental Evaluation," *IEEE Trans. on Industrial Electronics*, vol. 56, no. 6, pp.1906- 1915, June 2009

[Park2004]M. Park and I.K. Yu, "A novel real-time simulation technique of photovoltaic generation systems using RTDS," *IEEE transaction on Energy Conversion*, vol. 19, pp 164-169, 2004

[Patrinos2011]P. Patrinos, S. Trimboli and A. Bemporad, "Stochastic MPC for real-time market-based optimal power dispatch," *IEEE Conference On Decision & Control,* pp. 7111-7116, 2011

[Petcut2012]F.M. Petcut, "Mathematical models for PV systems and their usage in automatic control", PhD dissertation, Politehnica University Timisoara, 2012

[Petreus2009] D.M. Petreus, I.C. Ciocan, A.R. Rusu and D.V. Cadar, "Maximum Power Point Tracking Simulator in Charging Photovoltaic Systems," *Acta Tehnica Napocensis - Electronics and Telecomunications*, vol. 50, no. 2, pp. 43 -48, 2009

[PowerFactory] PowerFactory Manual, Version 14.0, DIgSILENT GmbH, Gomaringen, Germany, July 2010

[Prasath2010] G. Prasath, B. Reckel, M. Chidambaram and J.B. Jorgensen, "Application of Soft Constrained MPC to a Cement Mill Circuit," *Proceedings of the 9th International Symposium on Dynamics and Control of Process Systems,* pp. 288-293, July 5-7, 2010

[Privara 2011] S. Prívara, J. Siroky, L. Ferkl and J. Cigler, "Model predictive control

of a building heating system: The first experience," *Journal of Energy and Buildings*, vol. 43, pp. 564–572, 2011

[Prodanovic2006]M. Prodanović and T. C. Green, "High-quality power generation through distributed control of a power park microgrid," *IEEE Trans. Ind. Electron.*, vol. 53, no. 5, pp. 1471–1482, Oct. 2006.

[Puglia2011] L. Puglia, D. Bernardini, A. Bemporad, "A multi-stage stochastic optimization approach to optimal bidding on energy markets," *IEEE CONFERENCE ON DECISION & CONTROL*, pp. 1509-1514, 2011

[Qin2003] S.J. Qin and T.A. Badgwell. "A survey of industrial model predictive control technology," *Control Engineering Practice*, vol. 11, pp. 733–764, 2003.

[Richalet1978] J. Richalet, A. Rault, J.L. Testud and J. Papon, "Model predictive heuristic control: Applications to industrial processes," *Automatica*, vol. 14, no. 5, pp. 413-428, 1978

[Ripaccioli2010] G. Ripaccioli, D. Bernardini, S. Di Cairano, A. Bemporad, I.V. Kolmanovsky, "A stochastic model predictive control approach for series hybrid electric vehicle power management," *Proceedings Of The American Control Conference*, pp. 5844-5849, 2010

[Saele2011]H. Saele and O. S. Grande, "Demand response from household customers: Experiences from a pilot study in Norway," *IEEE Transactions on Smart Grid*, vol. 2, no. 1, pp. 90–97, 2011.

[Sahin2009] A. Sahin, "Model Predictive Control for Large Scale Systems: Two Industrial Applications," PhD dissertation, ETH Zurich No. 18792, 2009

[Samarakoon2012] K. Samarakoon, J. Ekanayake, N. Jenkins, "Investigation of Domestic Load Control to Provide Primary Frequency Response Using Smart Meters," *IEEE Transactions on Smart Grid*, vol. 3, no. 1, pp. 282-292, 2012

[Sels2001] T. Sels, C. Dragu, T. Van Craenenbroeck and R. Belmans, "Electrical energy storage systems: existing systems versus newest systems—an overview," in Power Generation and Sustainable Development International Conference, pp. 215–220, 2001

[Seme2011] S. Seme, G. Stumberg and J. Vorsic, "Maximum Efficiency Trajectories of a Two-Axis Sun Tracking System Determined Considering Tracking System Consumption", *Power Electronics Transactions on*, vol. 26, no.4, pp. 1280 - 1290, April 2011

[Sera2007] D. Sera, R. Teodorescu and P. Rodriguez, "PV panel model based on datasheet values," *IEEE International Symposium on Industrial Electronics,* pp. 2392 - 2396, Jun 04-07, 2007

[Sera2008] D. Sera, R. Teodorescu and P. Rodriguez, "Photovoltaic module diagnostics by series resistance monitoring and temperature and rated power estimation," Industrial Electronics Conference, pp. 2195 - 2199, 2008

[Sera2009] D. Sera, "Real-time Modelling, Diagnostics and Optimised MPPT for Residential PV systems," PhD dissertation, Aalborg University Institute of Energy Technology, Denmark, January 2009

[Shibata1999] A. Shibata and K. Sato, "Development of vanadium redox flow battery for electricity storage," *Power Engineering Journal,* vol. 13, no. 3, pp. 130–135, 1999

[Shigematsu2010] T. Shigematsu, "RedoxFlow Battery for energy storage," *SEI Technical Review*, no. 73, pp. 4-13, Oct. 2011

[Skoplaki2008] E. Skoplaki, A.G. Boudouvis, J.A. Palyvos, "A simple correlation for the operating temperature of photovoltaic modules of arbitrary mounting," Journal of Sol Energy Mater Solar Cells, vol. 92, pp. 1393–1402, 2008.

[Skyllas,1988] M. Skyllas-Kazacos, M. Rychick and R. Robins, U.S. Patent, No.

4,786,567, 1988, "All-vanadium redox battery".

[Skyllas,1990] M. Skyllas-Kazacos, D. Kasherman, D. R. Hong and M. Kazacos, "Characteristics and performance of 1 kW UNSW vanadium redox battery," *Journal of Power Sources*, vol. 35, pp. 399-404, 1991

[Skyllas2010] M. Skyllas-Kazacos, G. Kazacos, G. Poon and H. Verseema, "Recent advances with UNSW vanadium-based redox flow batteries," *International Journal of Energy Research*, vol. 34, no. 2, pp. 182–189, Feb. 2010

[Song2010] D. Song, J. Qi, J Han and G Liu, "Active Model Based Predictive Control for Unmanned Helicopter in Full Flight Envelope" *International Conference On Intelligent Robots And Systems*, pp. 616-621, 2010

[Solomon2012] A.A. Solomon, D. Faiman, G. Meron, "Appropriate storage for high-penetration grid-connected photovoltaic plants," *Journal of Energy Policy*, vol. 40, pp. 335–344, Jan. 2012

[Spectrum] J. Kumagai, "A battery as big as the grid", *IEEE Spectrum*, Jan. 2012

[Tanaka1990]T. Tanaka, T. Sakamoto, N. Mori, K. Mizunami and T. Shigematsu, "Development of a Redox Flow Battery," SEI Technical Review, vol.137, pp.191, 1990

[Tang 2012] A. Tang, S. Ting, J. Bao and M Skyllas-Kazacos, "Thermal modelling and simulation of the all-vanadium redox flow battery", *Journal of Power Sources*, vol. 203, pp. 165-176, 2012

[Tavlov2008] A. Tavlov, "Dynamic optimization of power consumption", Master thesis, Denmark Technical University, 2008

[Tokuda2000] N. Tokuda, T. Kanno, T. Hara, T. Shigematsu, Y. Tsutsui, A. Ikeudhi, T. Itou, and T. Kumamoto, "Development of a Redox Flow Battery System", SEI Technical Review. No. 50, p. 88, 2000.

[Tsuno2009]Y. Tsuno, Y. Hishikawa and K. Kurokava, "Modelling of the I-V curves of the PV modules using linear interpolation/extrapolation," *Journal of Solar energy Materials&Solar cells*, vol. 93, pp 1070-1073, 2009

[Ueda2007] Y. Ueda, K. Kurokawa, T. Tanabe, K. Kitamura, K. Akanuma, M. Yokota and H. Sugihara, "Study On The Over Voltage Problem And Battery Operation For Grid-Connected Residential PV Systems," in *22nd European Photovoltaic Solar Energy Conference*, pp. 3094- 3097, 3-7 September 2007, Milan, Italy

[Vaclav2012]S. Vaclav, "A skeptic looks at alternative energy," IEEE Spectrum magazine, July 2012

[Vandoorn2011] T.L. Vandoorn, B. Renders, L. Degroote, B. Meersman and L Vandevelde, "Active Load Control in Islanded Microgrids Based on the Grid Voltage," in *IEEE Transactions on Smart Grid*, vol. 2, no. 1, pp. 139-151, 2011

[Wang 2011]Wang, P. • Huang, J.Y. • Ding, Y. • Loh, P. • Goel, L., Demand side load management of smart grids using intelligent trading/metering/ billing system 2011 IEEE PES Trondheim PowerTech: The Power of Technology for a Sustainable Society, POWERTECH 2011 — 2011, pp. 6019420

[weatherRISO] ftp://ftp.risoe.dk/pub/met/ahah/RisoeTS/

[WEO2010] "World Energy Outlook 2010", International Energy Agency: Paris, 2010, http://www.iea.org/Textbase/npsum/weo2010sum.pdf

[Winn1985] R.C. Winn and C.B. Winn, "Optimal control for auxiliary heating of passive-solar-heated buildings", *Journal of Solar Energy*, vol. 35, no. 5, pp 419-442, 1985

[Wu2008] Z. Wu, J. Stoustru and J.B. Jorgensen, "Moving Horizon Control and Estimation of Livestock Ventilation Systems and Indoor Climate," in *Proceedings of the 17th World Congress The International Federation of Automatic Control* , vol. 17, no. 1, pp 6039 - 6044, Seoul, Korea, July 6-11, 2008

[Xie2009] L. Xie and M.D. Ilic, "Model predictive economic/ environmental dispatch of power systems with intermittent resources." in Power and Energy Society (PES) General Meeting, pp. 1-6, Calgary, Canada, 2009

[Yang2011]Z. Yang, J. Zhang, M.C.W. Kintner-Meyer, X. Lu, D. Choi, J.P. Lemmon and J. Liu, "Electrochemical Energy Storage for Green Grid", *Chemical Review Journal*, vol. 111, no. 5, pp 3577–3613, 2011

[Zarkogianni2011] K. Zarkogianni, A. Vazeou, S.G. Mougiakakou, A. Prountzou and K.S. Nikita, "An Insulin Infusion Advisory System Based on Autotuning Nonlinear Model-Predictive Control", *IEEE Transactions on Biomedical Engineering*, vol. 58, no. 9, pp. 2467-2477, 2011

[Zavala2009] V. M. Zavala, E. M. Constantinescu, T. Krause and M. Anitescu, "Online economic optimization of energy systems using weather forecast information," *Journal of Process Control*, vol. 19, no. 10, pp. 1725–1736, 2009

[Zong2011] Y. Zong, D. Kullmann, A. Thavlov, O. Gehrke and H.W. Bindner, "Active load management in an intelligent building using model predictive control strategy," *IEEE PES Trondheim PowerTech: The Power of Technology for a Sustainable Society, POWERTECH 2011*, pp. 1-6, Trondheim, Norway.

[Zong2012] Y. Zong, D. Kullmann, A. Thavlov, O. Gehrke, H.W. Bindner, "Application of Model Predictive Control for Active Load Management in a Distributed Power System With High Wind Penetration," *IEEE Transactions on Smart Grid*, vol.3, no. 2, pp. 1055-1062, 2012